Influence of the axial anomaly on the chiral phase transition

Einfluss der axialen Anomalie auf den chiralen Phasenübergang
Zur Erlangung des Grades eines Doktors der Naturwissenschaften (Dr. rer. nat.)
Genehmigte Dissertation von Daniel Rosenblüh
Tag der Einreichung: 14.02.2025, Tag der Prüfung: 12.05.2025

1. Gutachten: Prof. Dr. Guy Moore
2. Gutachten: Priv. Doz. Dr. Michael Buballa
Darmstadt, Technische Universität Darmstadt

TECHNISCHE
UNIVERSITÄT
DARMSTADT

Fachbereich Physik
Institut für Kernphysik
Theoriezentrum

Influence of the axial anomaly on the chiral phase transition
Einfluss der axialen Anomalie auf den chiralen Phasenübergang

Accepted doctoral thesis by Daniel Rosenblüh

Date of submission: 14.02.2025
Date of thesis defense: 12.05.2025

Darmstadt, Technische Universität Darmstadt

Erklärungen laut Promotionsordnung

§ 8 Abs. 1 lit. c PromO

Ich versichere hiermit, dass die elektronische Version meiner Dissertation mit der schriftlichen Version übereinstimmt.

§ 8 Abs. 1 lit. d PromO

Ich versichere hiermit, dass zu einem vorherigen Zeitpunkt noch keine Promotion versucht wurde. In diesem Fall sind nähere Angaben über Zeitpunkt, Hochschule, Dissertationsthema und Ergebnis dieses Versuchs mitzuteilen.

§ 9 Abs. 1 PromO

Ich versichere hiermit, dass die vorliegende Dissertation selbstständig und nur unter Verwendung der angegebenen Quellen verfasst wurde.

§ 9 Abs. 2 PromO

Die Arbeit hat bisher noch nicht zu Prüfungszwecken gedient.

Darmstadt, 14.02.2025

D. Rosenblüh

Zusammenfassung

In dieser Dissertation werden zwei Aspekte des chiralen Phasenübergangs in QCD mit FRG Methoden untersucht. Zunächst werden Suszeptibilitäten und pseudokritische Temperaturen für abnehmende Pionmassen mithilfe eines Simulationspaketes berechnet, das auf einer Trunkierung der effektiven Wirkung basiert, mithilfe der schon in der Vergangenheit gute Resultate für das QCD Phasendiagramm erzielt werden konnten. Wir haben eine gute Übereinstimmung mit Gitter QCD Rechnungen und finden eine kritische Temperatur $T_c \approx 142$ MeV für den chiralen Phasenübergang. Dafür haben wir angenommen dass die $U_A(1)$ Symmetrie während des chiralen Übergangs gebrochen bleibt. Weiterhin werden mithilfe eines vereinfachten NJL Modells die Bedingungen untersucht die zu einer effektiven $U_A(1)$ Restauration im IR führen. Wir finden heraus dass für kleine $U_A(1)$ Verletzungen im UV die $U_A(1)$ Restaurationstemperatur und die chirale Übergangstemperatur fast übereinstimmen. Große $U_A(1)$ Verletzungen im UV führen zu deutlich verschiedenen Temperaturen, was zur Folge hat dass der chirale Phasenübergang in der $O(4)$ Universalitätsklasse liegt. Wir halten das zweite Szenario für plausibler.

Abstract

In this thesis two aspects of the chiral phase transition of QCD are studied with FRG methods. First susceptibilities and pseudo-critical temperatures are calculated for decreasing pion masses within a simulation framework employing a truncation of the effective average action, that has already given good results for the QCD phase diagram in the past. Our results compare well to results from lattice QCD calculations and we can find a critical temperature of $T_c \approx 142$ MeV for the chiral phase transition. For this it was assumed that the $U_A(1)$ symmetry stays broken at the chiral transition. Secondly, within a simplified NJL model, the conditions which lead to an effective $U_A(1)$ restoration in the IR were studied. It was found that for small $U_A(1)$ violations in the UV, the $U_A(1)$ restoration temperature and chiral transition temperature will almost coincide. A large $U_A(1)$ violation in the UV results in a gap between the temperatures, which implies that the chiral phase transition is in the $O(4)$ universality class. We consider the second scenario to be more plausible.

Contents

1. Introduction **1**

2. QCD **3**
2.1. Phenomenology . . . 4
2.1.1. Accelerator Experiments . . . 4
2.1.2. Neutron Stars . . . 4
2.2. Theoretical Foundations . . . 4
2.2.1. Path integral . . . 4
2.2.2. Construction of QCD . . . 6
2.2.3. Matsubara Formalism . . . 8
2.2.4. Chiral symmetry . . . 12
2.2.5. Axial anomaly . . . 13
2.2.6. Instantons . . . 15
2.3. Order of the chiral phase transition . . . 18
2.3.1. Phases of matter . . . 18
2.3.2. The chiral phase transition in QCD . . . 26
2.4. Low Energy Effective Models . . . 29
2.4.1. Why we need them . . . 29
2.4.2. Chiral Quark-Meson Model . . . 29

3. Functional Methods **31**
3.1. Flow Equation . . . 31
3.2. Regulators . . . 33
3.3. Truncations and technicalities . . . 34
3.4. The ϕ^4 theory as an example . . . 34
3.5. Dynamical bosonization . . . 37
3.5.1. Flow equations for the gauged NJL model without dynamical bosonization . . . 37
3.5.2. Dynamical bosonization via scale dependent fields . . . 38

4. Chiral Transition **41**
4.1. Inner workings of the eQCD code . . . 41
4.1.1. Truncation . . . 41
4.1.2. Flow equations . . . 42
4.1.3. Initial conditions . . . 53
4.2. Susceptibilities . . . 54
4.3. Data generation and analysis . . . 55
4.4. Results . . . 56

5. Four-Fermion Couplings **63**
5.1. Inner workings of the simulation code . . . 63
5.1.1. Truncation . . . 63
5.1.2. Flow equations . . . 64
5.2. Sumrules and effective $U_A(1)$ restoration . . . 66
5.3. Initial conditions . . . 67
5.4. Data generation and analysis . . . 68
5.5. Results . . . 70
5.5.1. Four-Fermion flows . . . 70
5.5.2. Sumrules and effective $U_A(1)$ restoration . . . 70

6. Conclusion **73**

A. Derivation of the Flow Equation **75**

B. Fierz-complete four-quark basis for $(2+1)$-flavor QCD **79**

C. Coupling flows of Fierz-complete $N_f = 2$ NJL model **83**

D. Threshold functions **97**
D.1. Threshold functions for the Litim regulator . . . 97
D.2. Threshold functions for the exponential regulator . . . 100

Bibliography **101**

1. Introduction

The motivation for this thesis comes from the wish to understand the laws that govern the physical world around us. For centuries physicists have come up with more and more evolved theories, from which many have been ruled out by experiments, yet a few survived all tests. With this method, we have arrived at the point that most physical phenomena are successfully explained by *matter* interacting via *forces*.

The forces are described very differently, depending on the scale on which we look at our surroundings. Gravity, which governs much of our everyday life and most physics on large scales, is described in the language of differential geometry, and modeled as the curvature of spacetime. In this picture the relationship between matter and the spacetime geometry is given by the Einstein Field Equations.

The other known forces which govern most processes on scales smaller than our everyday world, are described by quantum field theories. The first successful quantum field theory was QED which describes electromagnetic processes as charged fermions interchanging photons. Additionally, the weak and the strong force were discovered. They describe processes on atomic scales and are modeled in a similar fashion as QED, with force carriers that mediate interactions. The strong force describes how quarks, the building blocks of protons and neutrons, interact.

Although the strong force is described by a similar mathematical framework as QED, it behaves very differently. For example, the mediating force carriers interact with each other. This makes it notoriously hard to compute and accordingly to come up with reliable experimentally verifiable predictions.

The most commonly employed method to do computations is lattice QCD. There the *path integral* is discretized and long running simulations to solve it are performed on super computers. The results still suffer from artifacts due to the finite size of the lattice, as well as the lattice spacing.

The method which we want to employ in this work, that also can deal successfully with the strong coupling, is an approach based on the Functional Renormalization Group. Within that framework, *flow equations* can be derived that describe the evolution of a particular theory from a microscopic UV scale to a macroscopic IR scale. Here we benefit from the fact that the strong force actually becomes much simpler to compute in the UV,

where the initial conditions for the FRG flows are set.

Sometimes insights into the underlying mechanisms of physical models are gained from studying idealized versions where physical constants are set to different values than the naturally occurring ones. One example for this is chiral QCD where masses of the matter particles have been set to zero.

This model exhibits a phase transition at zero density for increasing temperature, the so-called chiral transition. It is not fully understood yet if it is of first or second order [1]. Here crucial features of QCD such as breaking the axial symmetry due to instanton configurations play a deciding role. To understand the nature of the transition computations are necessary that can take all contributing factors into account.

Lattice QCD simulations are even more computationally intensive or even impossible for low fermion masses and have produced different results with high uncertainties, so this phenomenon is an ideal candidate to be studied within the FRG framework. That is the objective of this thesis.

It is structured as follows: In Chapter 2 we present QCD, the theoretical description of the strong interaction. After that, in Chapter 3, an account of FRG is given, which enables us to gain insights into mechanisms of QFTs and perform calculations on comparatively cheap computing infrastructure. In Chapter 4, we inspect the chiral transition by studying susceptibilities for decreasing pion masses, and extrapolating to the chiral limit afterwards. Here we assume an $O(4)$ symmetry, which implies that the axial $U_A(1)$ symmetry is broken. We compare our results with the results from the HotQCD lattice QCD collaboration. In Chapter 5 we inspect the conditions under which the $U_A(1)$ restoration happens right at the chiral transition. For this we vary the strength of the $U_A(1)$ violation in the UV which ultimately arises from QCD instanton configurations. In Chapter 6 we draw our conclusions and give an outlook.

2. QCD

The strong interaction was found in the search for the building blocks of matter. After electrons were discovered by Thompson, Rutherford found out that there are hard positively charged nuclei. So there must be a strong force, stronger than electromagnetism, that holds the nucleus together and counters the electromagnetic repulsion. The finite range of the strong force suggested massive mediating particles. Yukawa called these mesons, derived from the Greek word for "intermediate" since they were heavier than electrons but lighter than nucleons.

In search for those mediators in cosmic rays, pions were found as a candidate. Also other particles appeared that didn't fit into the picture. Another force, the weak force needed to be introduced, to explain radioactive phenomena, parity violations, etc.

In the end, the *Standard Model* of particles physics emerged, that categorized the particle zoo according to underlying symmetries. The part of it concerned with the strong interaction is QCD, a $SU(3)$ gauge theory, which describes processes in the form of *quarks* interacting via *gluons*. In this picture baryons, such as protons or neutrons, and mesons, such as pions, are a consequence from the approximate $SU(3)$ flavor symmetry from the underlying quarks. This is the *Eightfold Way*[2]. For that only the lightest 3 quarks, namely the up, down and strange quark play a role. These quarks cannot be observed individually due to a mechanism that is named *confinement* and not yet fully understood. One important ingredient is *asymptotic freedom* [3], a possible feature of $SU(N)$ gauge theories. This causes the coupling constant of the strong interaction to become strong at small scales and weak at large scales, which is opposed to electromagnetism, for example, where the strength of interactions decreases with increasing distance. For a more extensive account on the history of QCD and the Standard Model the reader is referred to [4].

In this chapter the theoretical foundations for the construction of QCD are presented. Parts of it are taken from the authors Master thesis [5].

2.1. Phenomenology

2.1.1. Accelerator Experiments

Accelerator experiments are the main tool to infer properties of subatomic particles. If one wants to study collective phenomena, such as the quark-gluon plasma, one needs a very dense state of matter. This is produced in practice by the high speed collision of heavy ions, usually lead or gold. The phenomena typically happen at very short timescales and inferring properties about the intermediate states only works indirectly by analyzing different resulting observables of the out-coming particles. These can be, for example, their transverse momentum distribution, statistics of particle jets, etc.

2.1.2. Neutron Stars

Another method to infer properties of strongly interacting matter is to observe *neutron stars*. The *Tolman-Oppenheimer-Volkov* (TOV) equation describes the behavior of a static, ideal fluid with a non-negligible background spacetime curvature. Taking an equation of state as input, possibly occurring masses M and radii R of neutron stars can be calculated. This is a one-to-one correspondence: If we know the M-R curve of neutron stars, the underlying equation of state is uniquely determined [6]. The masses of neutron stars are most easily measured in binary systems, with the partner being a pulsar pointing towards us and serving as a "clock" in the system. The determination of radii is unfortunately much harder. Still, the observation of one neutron star with a high enough mass is already sufficient evidence to rule out equations of state that are incapable of producing it.

2.2. Theoretical Foundations

2.2.1. Path integral

Notation

In this part we have set $\hbar = c = k_B = 1$. The metric reads $g^{\mu\nu} = \eta^{\mu\nu} = \text{diag}(1, -1, -1, -1)$. Double appearing indices are summed over (Einstein summation convention).

QFT Basics

Here the basics of vacuum QFT will be briefly summarized. For details see e.g. [7]. Since for our work the functional approach is most relevant we will focus on that.

For a scalar quantum field ϕ with mass m and a four-point interaction, the action is defined as

$$S[\phi] = \int d^4x \mathcal{L}(x) = \int d^4x \left[\frac{1}{2}\partial_\mu\phi(x)\partial^\mu\phi(x) - \frac{1}{2}m^2\phi^2(x) - \frac{\lambda}{4!}\phi^4(x)\right]. \tag{2.1}$$

The path integral results from an infinitesimal discretization of the time evolution operator $U(t) = e^{-iHt}$ with time-independent Hamiltonian H and an identification of the vacuum $\big|\Omega\big\rangle$ at $t = -\infty$ and $t = +\infty$. It reads

$$\big\langle\Omega\big|\Omega\big\rangle = \int \mathcal{D}\phi e^{iS[\phi]} \tag{2.2}$$

where we integrate over all possible field configurations. A general time-ordered n-point correlation functions is defined as

$$\big\langle\Omega\big|T\phi(x_1)\cdots\phi(x_n)\big|\Omega\big\rangle = \frac{\int \mathcal{D}\phi\ \phi(x_1)\cdots\phi(x_n)e^{iS[\phi]}}{\int \mathcal{D}\phi e^{iS[\phi]}} \tag{2.3}$$

The arguments are automatically time-ordered by construction of the path integral. The generating functional is defined as

$$Z[J] = \int \mathcal{D}\phi e^{iS[\phi]+iJ\cdot\phi}, \tag{2.4}$$

where the dot means $J\cdot\phi = \int d^4x J(x)\phi(x)$. With this we can write the correlation functions as

$$\big\langle\Omega\big|T\phi(x_1)\cdots\phi(x_n)\big|\Omega\big\rangle = \frac{1}{Z[0]}\frac{\delta}{i\delta J(x_n)}\cdots\frac{\delta}{i\delta J(x_1)}Z[J]\bigg|_{J=0} \tag{2.5}$$

The two-point function is also called propagator. For a free theory it gives the transition amplitude for one particle from one point to the other. In an interacting theory possible intermediate interactions are included.

As it turned out, matter is fundamentally composed of fermions rather than bosons. The action for a free fermion with mass m reads

$$S[\bar{q},q] = \int d^4x \mathcal{L}(x) = \int d^4x \bar{q}(x)\left(i\not{\partial} - m\right)q(x). \tag{2.6}$$

Here q and $\bar{q}$ are anti-commuting Grassmann-valued fields and $\bar{q}$ is the conjugate of q. Both are integrated over separately in the path integral approach.

The concepts of propagator, spectral function, etc. carry over analogously. Now, we also know that matter interacts. For example electrons via photon exchange. This and other fundamental interactions can be derived from the concept of *local gauge invariance*:

We can never measure an absolute phase and therefore our theory should be invariant under the *gauge transformation*

$$q(x) \to e^{i\alpha(x)} q(x) \tag{2.7}$$

However, due to the derivative in Eq. (2.6) an additional term is created by the product rule. This can be compensated by making the derivative *covariant* with the help of a *connection*:

$$D_\mu q(x) = \partial_\mu q(x) + ieA_\mu(x). \tag{2.8}$$

The newly introduced field A_μ changes under the same gauge transformation as

$$A_\mu(x) \to A_\mu(x) - \frac{1}{e}\partial_\mu \alpha(x) \tag{2.9}$$

The net term added to the action due to making the derivative covariant reads $-e\bar{q}\gamma^\mu A_\mu q$ and describes interactions of the electrons with the photons of strength e. To give dynamics to the photons we add the gauge-invariant term $-\frac{1}{4}F_{\mu\nu}F^{\mu\nu}$ with $F_{\mu\nu} = -\frac{i}{e}\left[D_\mu, D_\nu\right] = \partial_\mu A_\nu - \partial_\nu A_\mu$. The full QED action then reads

$$S[\bar{q}, q, A_\mu] = \int d^4x \mathcal{L} = \int d^4x \left[\bar{q}\left(i\not{D} - m\right) q - \frac{1}{4}F_{\mu\nu}F^{\mu\nu}\right]. \tag{2.10}$$

2.2.2. Construction of QCD

Now we turn away from electrons and towards quarks, the elementary particles underlying protons, neutrons and various other observed hadrons. The spectrum of known hadrons suggests that each quark flavor comes in three distinct copies, called colors. To find the action of the interacting quarks, we again look at possible local gauge transformations

$$\begin{pmatrix} q_{\text{red}}(x) \\ q_{\text{green}}(x) \\ q_{\text{blue}}(x) \end{pmatrix} \longrightarrow e^{i\alpha(x)} \begin{pmatrix} q_{\text{red}}(x) \\ q_{\text{green}}(x) \\ q_{\text{blue}}(x) \end{pmatrix} \tag{2.11}$$

where now $e^{i\alpha(x)}$ is an $SU(3)$ matrix. Analogously to the electromagnetic case a connection is introduced

$$D_\mu = \partial_\mu - igA^a_\mu t^a \tag{2.12}$$

where the 8 matrices t^a are called the generators of $SU(3)$. This yields 8 *gluons* responsible for the interactions of quarks with each other. The gauge invariant term $-\frac{1}{4}F^a_{\mu\nu}F^{a\mu\nu}$ is added to introduce dynamics, where now

$$-igF^a_{\mu\nu}t^a = [D_\mu, D_\nu] \tag{2.13}$$

and

$$F^a_{\mu\nu} = \partial_\mu A^a_\nu - \partial_\nu A^a_\mu + g f^{abc} A^b_\mu A^c_\nu \tag{2.14}$$

with f^{abc} being the structure constants of $SU(3)$. The full gauge-invariant QCD action reads

$$S[\bar{q}, q, A^a_\mu] = \int d^4x\ \mathcal{L}[\bar{q}, q, A^a_\mu](x) = \int d^4x \left[\bar{q}\left(i\not{D} - m\right) q - \frac{1}{4}F^a_{\mu\nu}F^{a\mu\nu}\right] \tag{2.15}$$

Unlike the photons, the different gluons interact with each other. These interactions cause the coupling to become weak at large scales and strong at small scales. This *asymptotic freedom* [3] is believed to be the reason why we do not observe any color charge in nature. To quantize a gauge theory one has to take into account that one cannot simply integrate over the A^a_μ fields, like

$$\int \mathcal{D}A\ \exp\left[i\int d^4x \left(-\frac{1}{4}F^a_{\mu\nu}F^{a\mu\nu}\right)\right]. \tag{2.16}$$

Since they are only determined up to a gauge transformation the degrees of freedom would be over-counted. To solve this problem, a gauge-fixing prescription $G(A) = 0$ is adopted. To force it upon the path integration, the identity

$$1 = \int \mathcal{D}\alpha(x)\delta\left[G(A^\alpha)\right] \det\left(\frac{\delta G(A^\alpha)}{\delta\alpha}\right) \tag{2.17}$$

is used, where A^α denotes the gauge shifted field

$$(A^\alpha)^a_\mu\, t^a = e^{i\alpha^a t^a}\left[A^b_\mu t^b + \frac{i}{g}\partial_\mu\right] e^{-i\alpha^c t^c} \tag{2.18}$$

We choose the *Lorenz gauge* condition $G(A) = \partial^\mu A^a_\mu$, where

$$\frac{\delta G(A^\alpha)}{\delta\alpha} = \frac{1}{g}\partial^\mu D_\mu \tag{2.19}$$

is independent of α. Within the path integral all occurring A^α can be replaced by A:

$$\left(\int \mathcal{D}\alpha\right) \int \mathcal{D}A \, \exp\left[i \int d^4x \left(-\frac{1}{4} F^a_{\mu\nu} F^{a\mu\nu}\right)\right] \delta\left[G(A)\right] \det\left(\frac{\delta G(A^\alpha)}{\delta \alpha}\right) \tag{2.20}$$

The measure $\int \mathcal{D}\alpha$ factors and is absorbed into the normalization. To lift the determinant into the exponent, we introduce anti-commuting Grassmann variables $\bar{c}$ and c

$$\det\left(\partial^\mu D_\mu\right) = \int \mathcal{D}\bar{c}\mathcal{D}c \, \exp\left[i \int d^4x \, \bar{c}\left(-\partial^\mu D_\mu\right) c\right]. \tag{2.21}$$

The remaining $1/g$ factor is absorbed into the normalization. The path integral without quarks then reads

$$\int \mathcal{D}A\mathcal{D}\bar{c}\mathcal{D}c \, \left[i \int d^4x \left(-\frac{1}{4} F^a_{\mu\nu} F^{a\mu\nu} - \frac{1}{2\xi}\left(\partial^\mu A^a_\mu\right)^2 + \bar{c}\left(-\partial^\mu D_\mu\right) c\right)\right] \tag{2.22}$$

The Grassmann fields $\bar{c}$ and c are called *ghosts*. They are unphysical and cannot be measured. Nevertheless, their contribution has to be taken into account when calculations are done to obtain meaningful results. Even though they anti-commute, they behave as scalars under Lorentz transformations. Their introduction leads to a reformulation of the $SU(3)$ symmetry. It becomes the *BRST-symmetry*, which differentially acts as

$$\begin{aligned} \delta A^a_\mu &= -D_\mu c^a \\ \delta c^a &= -\frac{1}{2} f^{abc} c^b c^c \\ \delta \bar{c}^a &= \partial^\mu A^a_\mu. \end{aligned} \tag{2.23}$$

2.2.3. Matsubara Formalism

In this subsection we want to introduce the *Matsubara* (or *Imaginary Time*) formalism by which temperature dependence of observables can be computed. It was first introduced in [8] where it was applied to the description of an electron-phonon interaction, which is critical for the understanding of superconductivity in condensed matter physics.

For the concept of temperature to make sense, we have to talk about ensembles of particles in thermal equilibrium, rather than about single particles as in vacuum QFT. In general ensembles of quantum states are described by a density matrix ρ. For a system in thermal equilibrium i.e. with density matrix $\rho = e^{-\beta H}/Z$ the expectation value for any

operator $\mathcal{O}$ reads $\langle\mathcal{O}\rangle_\beta = \mathrm{Tr}\,[\rho\mathcal{O}]$. For a thermal correlation function of two Heisenberg operators $A_H(t)$ and $B_H(t')$ we have that

$$\begin{aligned}\left\langle A_H(t)B_H(t')\right\rangle_\beta &= \mathrm{Tr}\left[\rho A_H(t)B_H(t')\right]\\ &= \frac{1}{Z}\mathrm{Tr}\left[e^{-\beta H}A_H(t)B_H(t')\right]\\ &= \frac{1}{Z}\mathrm{Tr}\left[e^{-\beta H}A_H(t)e^{\beta H}e^{-\beta H}B_H(t')\right]\\ &= \frac{1}{Z}\mathrm{Tr}\left[A_H(t+i\beta)e^{-\beta H}B_H(t')\right]\\ &= \frac{1}{Z}\mathrm{Tr}\left[e^{-\beta H}B_H(t')A_H(t+i\beta)\right]\\ &= \left\langle B_H(t')A_H(t+i\beta)\right\rangle_\beta \end{aligned} \tag{2.24}$$

Where the definition of an Heisenberg operator $A_H(t) = e^{iHt}Ae^{-iHt}$ was used in the third step and the cyclicity of the trace in the fourth. Eq. (2.24) is known as the Kubo-Martin-Schwinger (KMS) condition. Note that the cyclicity of the trace does not hold in general, it can be violated e.g. for unbounded operators.

To be able to calculate correlation functions we do a path integral construction analogously to the vacuum case with time t traded for imaginary inverse temperature $i\beta$. However, there are some differences regarding the integration boundary conditions. These can be illustrated already by the simpler case of a zero-dimensional harmonic oscillator.

Bosonic zero-dimensional harmonic oscillator

We have

$$H = \frac{1}{2m}p + \frac{1}{2}m\omega^2x^2 = \omega\left(a^\dagger a + \frac{1}{2}\right) \qquad \text{with} \qquad [a,a] = 0, \quad \left[a^\dagger, a^\dagger\right] = 0, \quad \left[a, a^\dagger\right] = \mathbb{1} \tag{2.25}$$

and the identities for the position and momentum eigenstates

$$\langle x|p\rangle = e^{ipx}, \quad \int dx\,|x\rangle\langle x| = \mathbb{1}, \quad \int \frac{dp}{2\pi}\,|p\rangle\langle p| = \mathbb{1}. \tag{2.26}$$

We divide the partition function infinitesimally into

$$Z = \mathrm{Tr}e^{-\beta H} = \int dx \left\langle x|e^{-\beta H}|x\right\rangle = \int dx \left\langle x|e^{-\epsilon\beta H}\cdots e^{-\epsilon\beta H}|x\right\rangle \tag{2.27}$$

Into this we now repeatedly insert the identities Eq. (2.26) so that we end up evaluating the expressions

$$\left\langle x_{i+1}\middle|p_i\right\rangle \left\langle p_i\middle|e^{-\epsilon\beta H}\middle|x_i\right\rangle = \exp\left(-\epsilon\beta\left[\frac{p_i^2}{2m} - ip_i\frac{x_{i+1}-x_i}{\epsilon} + V(x_i)\right]\right) \tag{2.28}$$

The left- and rightmost x bra and ket still belong to the same eigenvalue and after doing the switch to the continuum and carrying out the momentum path integral, we arrive at

$$Z = \int\limits_{x(\beta)=x(0)} \mathcal{D}x \exp\left(-\int_0^\beta d\tau\left[\frac{m}{2}\dot{x}(\tau)^2 + V(x(\tau))\right]\right) \tag{2.29}$$

I.e. we have a periodic boundary condition on $x(\tau)$

Fermionic zero-dimensional harmonic oscillator

For the fermionic case we have

$$H = \omega\left(a^\dagger a - \frac{1}{2}\right) \qquad \text{with} \qquad \{a,a\} = 0, \quad \left\{a^\dagger, a^\dagger\right\} = 0, \quad \left\{a, a^\dagger\right\} = \mathbb{1} \tag{2.30}$$

As in vacuum QFT we use Grassmann variables to deal with the fermionic nature. For coherent states, eigenstates of the annihilation operator, we have

$$\begin{aligned}\int dc^*dc\, e^{-c^*c}\left|c\right\rangle\left\langle c\right| &= \int dc^*dc\,(1-c^*c)(1-ca^\dagger)\left|0\right\rangle\left\langle 0\right|(1-ac^*) \\ &= \left|0\right\rangle\left\langle 0\right| + \int dc^*dc\, ca^\dagger\left|0\right\rangle\left\langle 0\right|ac^* \\ &= \left|0\right\rangle\left\langle 0\right| + \left|1\right\rangle\left\langle 1\right| = \mathbb{1}\end{aligned} \tag{2.31}$$

$$\begin{aligned}\int dc^*dc\, e^{-c^*c}\left\langle -c\right|A\left|c\right\rangle &= \int dc^*dc\,(1-c^*c)\left\langle 0\right|(1+ac^*)A(1-ca^\dagger)\left|0\right\rangle \\ &= \left\langle 0\right|A\left|0\right\rangle - \int dc^*dc\;\left\langle 0\right|ac^*Aca^\dagger\left|0\right\rangle \\ &= \left\langle 0\right|A\left|0\right\rangle - \left\langle 1\right|\int dc^*dc\, c^*cA\left|1\right\rangle \\ &= \left\langle 0\right|A\left|0\right\rangle + \left\langle 1\right|A\left|1\right\rangle = \mathrm{Tr}\left[A\right]\end{aligned} \tag{2.32}$$

So the trace of a bosonic operator A is defined over antiperiodic states. With this we can now do the path integral construction by inserting Eq. (2.32) repeatedly into

$$Z = \mathrm{Tr}e^{-\beta H} = \int dc^*dc\, e^{-c^*c}\left\langle -c\right|e^{-\epsilon\beta H}\cdots e^{-\epsilon\beta H}\left|c\right\rangle, \tag{2.33}$$

however, the eigenvalues of the left- and rightmost states will always carry opposite sign. After the switch to the continuum we arrive at

$$Z = \int\limits_{\substack{c(\beta)=-c(0)\\ c^*(\beta)=-c^*(0)}} \mathcal{D}c^*(\tau)\mathcal{D}c(\tau)\ \exp\left(-\int_0^\beta d\tau\ \left[c^*(\tau)\dot{c}(\tau) + H(c^*(\tau), c(\tau))\right]\right) \tag{2.34}$$

I.e. we have anti-periodic boundary conditions on $c(\tau)$ and $c^*(\tau)$.

Three-dimensional path integral

The (anti-) periodicity carries over to the three-dimensional case where we have analogously

$$Z = \mathrm{Tr} e^{-\beta H} = \int\limits_{\substack{\varphi(x,\beta)=\varphi(x,0)\\ q(x,\beta)=-q(x,0)\\ \bar{q}(x,\beta)=-\bar{q}(x,0)}} \mathcal{D}\varphi\mathcal{D}q\mathcal{D}\bar{q}\ e^{-S_E[\varphi,q,\bar{q}]} \tag{2.35}$$

with the Euclidean action $S_E = \beta H = \int_0^\beta d\tau \int d^3x \mathcal{L}_E$. Propagators are defined as

$$G_\beta(\tau,\tau') = \left\langle \mathcal{P}_\tau \varphi_H(\tau)\varphi^\dagger(\tau')\right\rangle \tag{2.36}$$

with the τ-ordering operator $\mathcal{P}_\tau$. The Green function depends only on the difference $\tau - \tau'$. Due to the compactness of the τ interval, the Fourier transformed propagator only has discrete frequencies in the time direction

$$G_\beta(\tau) = T\sum_n e^{-i\omega_n\tau} G_\beta(\omega_n) \tag{2.37}$$

with $\omega_n = 2n\pi T$ for bosons and $\omega_n = (2n+1)\pi T$ for fermions. These are called Matsubara frequencies.

The Matsubara formalism is the one most widely used to study equilibrium systems. Slow time evolution can also be studied, but that requires an analytic continuation since there is no time variable anymore. There are two other formalisms which are commonly used to study temperature dependence, namely the *Real Time Formalism* and *Thermofield Dynamics*. For details the reader is referred to [9, 10].

2.2.4. Chiral symmetry

In QCD the up and down quark masses are small compared to the other scales involved. Assuming they are both equal to zero, the fermionic Lagrangian for $N_f = 2$ has a $U_L(N_f) \times U_R(N_f)$ symmetry and the left- and right-handed eigenstates of the γ_5 matrix decouple. To see this we define the projection operators

$$P_L = \frac{1-\gamma_5}{2}, \qquad P_R = \frac{1+\gamma_5}{2} \tag{2.38}$$

which satisfy

$$P_L^2 = P_L, \quad P_R^2 = P_R, \quad P_L P_R = P_R P_L = 0, \quad P_L + P_R = 1, \quad P_L^\dagger = P_L, \quad P_R^\dagger = P_R. \tag{2.39}$$

Also, since $\{\gamma_0, \gamma_5\} = 0$, we have

$$P_L \gamma_0 = \gamma_0 P_R, \qquad P_R \gamma_0 = \gamma_0 P_L. \tag{2.40}$$

The left- and right-handed components of the quark fields are defined as

$$q_L = P_L q, \qquad q_R = P_R q \qquad \text{with} \qquad q = q_L + q_R. \tag{2.41}$$

These are eigenstates of the γ_5 matrix

$$\gamma_5 q_L = (-1) q_L, \qquad \gamma_5 q_R = (+1) q_R. \tag{2.42}$$

By definition we have $\bar{q} = q^\dagger \gamma_0$ so that with Eq. (2.40)

$$\bar{q}_L = \bar{q} P_R, \qquad \bar{q}_R = \bar{q} P_L, \qquad \text{and} \qquad \bar{q}_R q_R = \bar{q}_L q_L = 0. \tag{2.43}$$

With this we can now write our fermionic Lagrangian as

$$\mathcal{L} = \bar{q} \left(i \not{D} - m \right) q = \bar{q}_L i \not{D} q_L + \bar{q}_R i \not{D} q_R - m \left(\bar{q}_R q_L + \bar{q}_L q_R \right) \tag{2.44}$$

Acting on this with infinitesimal $U_L(N_f)$ and $U_R(N_f)$ shifts, we have with the Pauli matrices σ^a

$$q_L \longrightarrow (1 + i\alpha + i\beta^a \sigma^a) q_L \tag{2.45}$$

$$q_R \longrightarrow (1 + i\gamma + i\delta^a \sigma^a) q_R \tag{2.46}$$

$$\mathcal{L} \longrightarrow \mathcal{L} - m \left[i(\alpha - \gamma) + i(\beta^a - \delta^a)\sigma^a \right] \left(\bar{q}_R q_L - \bar{q}_L q_R \right) \tag{2.47}$$

So for $m = 0$ the Lagrangian is $U_L(N_f) \times U_R(N_f)$ symmetric, which is why it is called *chiral symmetry*. For $m \neq 0$ it is only invariant if $\alpha = \gamma$ and $\beta^a = \delta^a$. This still leaves a residual $U_V(N_f)$ symmetry as can be seen when writing the shifts in the form

$$q_L \longrightarrow (1 + ia + ib\gamma_5 + ic^a\sigma^a + id^a\sigma^a\gamma_5)q_L \tag{2.48}$$

$$q_R \longrightarrow (1 + ia + ib\gamma_5 + ic^a\sigma^a + id^a\sigma^a\gamma_5)q_R \tag{2.49}$$

where the individual terms correspond to infinitesimal shifts of $U_V(1)$, $U_A(1)$, $SU_V(N_f)$ and $SU_A(N_f)$ respectively. The Lagrangian transforms as

$$\mathcal{L} \longrightarrow \mathcal{L} - m\left[ib + id^a\sigma^a\right](\bar{q}_R q_L - \bar{q}_L q_R) \tag{2.50}$$

So the mass term only violates the invariance under $U_A(1)$ and $SU_A(N_f)$ shifts. Here $SU_A(N_f)$ denotes the coset $(SU_L(N_f) \times SU_R(N_f))/U_V(N_f)$.

In nature the masses of the light quarks are small and chiral symmetry is realized approximately. However, it is spontaneously broken at low energies giving rise to a pseudo-Goldstone boson, the pion. This mechanism explains the small pion mass and was first postulated by Nambu [11].

Now, in the case when the chiral symmetry is restored we just argued that the Lagrangian is invariant also under $U_A(1)$ shifts. This turns out to be not true anymore on the quantum level, as shown in the next subsection.

2.2.5. Axial anomaly

The main topic of this thesis concerns the *axial anomaly* of chiral QCD. An anomaly is a symmetry of the classical Lagrangian that is violated in the quantized theory. In the case of chiral QCD it turns out that the $U_A(1)$ flavor symmetry of the classical Lagrangian is such an anomaly. This anomaly is present for any theory with N_f massless fermions coupled to a gauge field. It was first discovered (in electrodynamics) by Adler, Bell and Jackiw [12, 13] where it is responsible for the "anomalous" neutral pion decay rate.

In the classical case we have for massless fermions by Noether's theorem

$$\partial_\mu j_5^\mu(x) = 0 \tag{2.51}$$

with the axial vector current, i.e. the Noether current of the $U_A(1)$ symmetry

$$j_5^\mu = \bar{q}\gamma^\mu\gamma_5 q. \tag{2.52}$$

Too see how this is violated in the quantum case we follow the presentation of [14], i.e. we examine the change of the path integral under an $U_A(1)$ shift. We have

$$q(x) \longrightarrow \exp(i\alpha(x)\gamma_5)q(x), \qquad \bar{q}(x) \longrightarrow \bar{q}(x)\exp(i\alpha(x)\gamma_5) \tag{2.53}$$

giving rise to a shift in the Lagrangian

$$\mathcal{L} \longrightarrow \mathcal{L} - \partial_\mu \alpha(x) \bar{q} \gamma^\mu \gamma_5 q \tag{2.54}$$

The change in the measure is more intricate. To derive its exact value we must first define the functional integral properly. For that we expand the Fermion fields with respect to the complete set of eigenfunctions of the hermitian operator $i\not{D}$, i.e.

$$q(x) = \sum_n a_n \varphi_n(x) \qquad \bar{q}(x) = \sum_n \bar{b}_n \varphi_n^\dagger(x) \tag{2.55}$$

with a_n, b_n being elements of the Grassmann Algebra. The functional measure is then

$$\Pi_x \mathcal{D}A_\mu(x) \mathcal{D}\bar{q}(x) \mathcal{D}q(x) = \Pi_x \mathcal{D}A_\mu(x) \Pi_{n,m} d\bar{b}_m da_a \tag{2.56}$$

The $U_A(1)$ transformation

$$q(x) \longrightarrow q'(x) = \exp(i\alpha(x)\gamma_5) q(x) = \sum_n a'_n \varphi_n(x) \tag{2.57}$$

causes a change in the coefficients

$$a'_n \sum_m \int d^4x \; \varphi_n^\dagger(x) \exp(i\alpha(x)\gamma_5) \varphi_m(x) a_m = \sum_m C_{n,m} a_m. \tag{2.58}$$

The anti-commuting nature of the Grassmann variables causes the inverse determinant to appear as the Jacobian factor (opposed to just the determinant in the case of commuting numbers).

$$\det C_{n,m}^{-1} = (\exp(\mathrm{tr} \log C_{n,m}))^{-1} = \exp\left(-i \int d^4x \; \alpha(x) \sum_k \varphi_k^\dagger(x) \gamma_5 \varphi_k(x) \right) \tag{2.59}$$

Our theory has not been regularized until now, and a natural way to do this is by weighting each mode with a factor $\exp\left(-(\lambda_k/M)^2\right)$, where λ_k is the corresponding eigenvalue to

φ_k. Then by sending $M \to \infty$, we get for the sum

$$\begin{aligned}
\sum_k \varphi_k^\dagger(x)\gamma_5\varphi_k(x) &= \lim_{M\to\infty} \sum_k \varphi_k^\dagger(x)\gamma_5 \exp\left(-(\lambda_k/M)^2\right)\varphi_k(x) \\
&= \lim_{M\to\infty, x\to y} \operatorname{tr}\gamma_5 \exp(-(\not{D}/M)^2)\delta^4(x-y) \\
&= \lim_{M\to\infty, y\to x} \int \frac{d^4k}{(2\pi)^4} \operatorname{tr}\gamma_5 \exp\left(-\left\{D^\mu D_\mu + \frac{1}{4}\left[\gamma^\mu,\gamma^\nu\right](-ig)F_{\mu\nu}\right\}/M^2\right) e^{ik(x-y)} \\
&= \lim_{M\to\infty} \underbrace{\operatorname{tr}\gamma_5 \left(1 + \left\{\frac{1}{4}\left[\gamma^\mu,\gamma^\nu\right](-ig)F_{\mu\nu}/M^2\right\}\right.}_{\operatorname{tr}\gamma_5 = \operatorname{tr}\gamma_5\gamma^\mu\gamma^\nu = 0} \left. + \frac{1}{2}\left\{\frac{1}{4}\left[\gamma^\mu,\gamma^\nu\right](-ig)F_{\mu\nu}/M^2\right\}^2 + \dots\right) \\
&\qquad\qquad \times \int \frac{d^4k}{(2\pi)^4} \exp(-k^\mu k_\mu/M^2) \\
&= \lim_{M\to\infty} \frac{(-ig)^2}{16} \operatorname{tr}\gamma_5 \left(\left[\gamma^\mu,\gamma^\nu\right]F_{\mu\nu}\right)^2 \frac{1}{2M^4} \int \frac{d^4k}{(2\pi)^4} \exp(-k^\mu k_\mu/M^2) \\
&= \frac{g^2}{16\pi^2} \operatorname{tr} \widetilde{F}^{\mu\nu} F_{\mu\nu}
\end{aligned} \tag{2.60}$$

with $F_{\mu\nu} = F^a_{\mu\nu} t^a$ and the dual field strength tensor defined as $\widetilde{F}^{\mu\nu} = \frac{1}{2}\varepsilon^{\mu\nu\alpha\beta}F_{\alpha\beta}$. The integration over $\bar{q}$ gives the same contribution. So we get in total for the measure shift

$$\Pi_x \mathcal{D}A_\mu(x)\mathcal{D}\bar{q}(x)\mathcal{D}q(x) \longrightarrow \Pi_x \mathcal{D}A_\mu(x)\mathcal{D}\bar{q}(x)\mathcal{D}q(x) \exp\left(-iN_f \int d^4x\, \alpha(x)(g^2/8\pi^2) \operatorname{tr}\widetilde{F}^{\mu\nu}F_{\mu\nu}\right) \tag{2.61}$$

This measure shift is of course absent in the classical theory and it is the cause for the anomaly. By variation of the whole path integral with respect to $\alpha(x)$ we get

$$\partial_\mu \left\langle j_5^\mu(x)\right\rangle = \frac{N_f g^2}{8\pi^2} \left\langle \operatorname{tr}\widetilde{F}^{\mu\nu}F_{\mu\nu}(x)\right\rangle \tag{2.62}$$

Contrary to the purely classical theory the current is not always conserved.

2.2.6. Instantons

Instantons are classical solutions of the (Yang-Mills) field equations which are localized in space and (Euclidean) time. They play a central role in the solution of the $U(1)$ problem, the apparent symmetry of QCD that doesn't survive quantization and is responsible for an unexpectedly high mass for the η' meson. This solution was summarized in [15] and we reproduce the main steps here.

Winding number

First, we note that for any field configuration with a finite action the expression

$$\frac{g^2}{16\pi^2}\int d^4x\ \mathrm{tr}\,\widetilde{F}^{\mu\nu}F_{\mu\nu}=\nu \tag{2.63}$$

is integer valued. This follows from homotopy theory, i.e for the third homotopy group of $SU(N)$ for $N\geq 2$ we have $\pi_3\left(SU(N)\right)=\mathbb{Z}$, see [16]. The integer ν for a given field configuration is called its winding number.

Another way to see that Eq. (2.63) is integer valued is to inspect the eigenvalues of the Dirac operator (following the presentation in [17]). Since $i\not{D}$ is hermitian it has real eigenvalues

$$i\not{D}\varphi_n=\lambda_n\varphi_n. \tag{2.64}$$

Since $\gamma^\mu\gamma_5=-\gamma_5\gamma^\mu$, for every eigenfunction φ_n there is another eigenfunction $\gamma_5\varphi_n$ with eigenvalue $-\lambda_n$, because

$$i\not{D}\gamma_5\varphi_n=-i\gamma_5\not{D}\varphi_n=-\lambda_n\gamma_5\varphi_n. \tag{2.65}$$

So all non-zero eigenvalues come in pairs. For the remaining zero-eigenvalues of $i\not{D}$ we diagonalize $i\not{D}$ and γ_5 simultaneously and define n_+ to be the zero modes with γ_5 eigenvalue $+1$ and n_- the ones with γ_5 eigenvalue -1. We now take the integral on both sides of Eq. (2.60) and have

$$\frac{g^2}{16\pi^2}\int d^4x\ \mathrm{tr}\,\widetilde{F}^{\mu\nu}F_{\mu\nu}=\int d^4x\ \sum_k\varphi_k^\dagger\gamma_5\varphi_k=\sum_{\text{zero modes}}\int d^4x\ \varphi_k^\dagger\gamma_5\varphi_k=n_+-n_-. \tag{2.66}$$

This is a manifestation of the Atiyah-Singer index theorem.

Single instanton solution

With Eq. (2.63) above we can derive a lower bound for the action of an instanton with positive winding number ν. For pure Yang-Mills theory in Euclidean space we have

$$S_{YM}=\frac{1}{2}\int d^4x\ \mathrm{tr}\,F^{\mu\nu}F_{\mu\nu}=\frac{1}{4}\int d^4x\ \mathrm{tr}\left(F_{\mu\nu}-\widetilde{F}_{\mu\nu}\right)^2+\frac{1}{2}\int d^4x\ \mathrm{tr}\,\widetilde{F}^{\mu\nu}F_{\mu\nu}\geq\frac{8\pi^2}{g^2}\nu \tag{2.67}$$

The lower bound is actually realized for self-dual configurations $F_{\mu\nu}=\widetilde{F}_{\mu\nu}$. Similarly, for instantons with negative winding number the solutions are anti self-dual $F_{\mu\nu}=-\widetilde{F}_{\mu\nu}$. In

practice it is often easier to solve these equations rather than $D_\mu F^{\mu\nu} = 0$ [16]. In fact this method was used when the first instanton solution for winding number $\nu = 1$ was presented in [18] for $SU(2)$, the *BPST instanton*. It reads

$$A_\mu(x) = \frac{2}{\rho}\frac{\eta_{a\mu\nu}(x_\nu - z_\nu)t^a}{(x-z)^2+\rho^2}, \qquad F_{\mu\nu} = \frac{-4\rho^2}{g}\frac{\eta_{a\mu\nu}t^a}{((x-z)^2+\rho^2)^2} \tag{2.68}$$

where ρ denotes it size, z its center and $\eta_{a\mu\nu} = \delta_{a\mu}\delta_{4\nu} - \delta_{a\nu}\delta_{4\mu} + \varepsilon_{a\mu\nu}$ the t' Hooft symbol. To embed it into $SU(3)$ one can take Eq. (2.68) and set the other matrix elements to zero.

Effective $2N_f$ fermion interaction

We now show the steps how the influence of instantons leads to an effective $2N_f$ interaction as presented in [15].

Instantons are part of the field configurations of the gauge field integration in the path integral, i.e. the integration is separated into a part of instantons and a perturbative part $A = A_{\text{inst}} + \delta A$. Presence of an instanton located at x_1 affects the q integration. The covariant Dirac operator now contains a zero mode rendering the whole path integral zero. A fermionic source is necessary to shift the lowest eigenvalue away from zero and make the value of the integral finite. It now turns out that instead of integrating over

$$\kappa \int \mathcal{D}\bar{q}\mathcal{D}q \exp\left(S_{A,q} + J\bar{q}q\right) \tag{2.69}$$

one can equally well integrate over

$$\kappa \int \mathcal{D}\bar{q}\mathcal{D}q \exp\left(S_{0,q} + J\bar{q}q\right) \det_{st}\left[\bar{q}^s(x_1)(1+\gamma_5)q^t(x_1)\right], \tag{2.70}$$

with no instanton present and κ to be determined, to achieve the same effect [19]. Here the determinant runs over flavor space. We now assume that for ν_+ instantons located at x_i a declustering assumption holds and we have

$$\kappa^{\nu_+} \int \mathcal{D}\bar{q}\mathcal{D}q\; e^{S_q} \prod_{i=1}^{\nu_+} \det_{st}\left[\bar{q}^s(x_i)(1+\gamma_5)q^t(x_i)\right] \tag{2.71}$$

When integrating over all possible values for the gluon field in the path integral we have to take any number of instantons into account. So we have to integrate over all possible positions x_i and introduce a factor $1/(\nu_+!)$ due to the exchange symmetry. Similarly any

number ν_- of anti-instantons has to be included, but here we have a factor $1-\gamma_5$ instead of $1+\gamma_5$ in the determinant. So, in total we have

$$\sum_{\nu_+=0}^{\infty}\sum_{\nu_-=0}^{\infty}\frac{\kappa^{\nu_+\nu_-}}{\nu_+!\nu_-!}\left(\int d^4x\ \det_{st}\left[\bar{q}^s(x)(1+\gamma_5)q^t(x)\right]\right)^{\nu_+}\left(\int d^4x\det_{st}\left[\bar{q}^s(x)(1-\gamma_5)q^t(x)\right]\right)^{\nu_-} \tag{2.72}$$

The summation can be carried to out to arrive at

$$\exp\int d^4x\ \left(\kappa\det_{st}\left[\bar{q}^s(x)(1+\gamma_5)q^t(x)\right]+\kappa\det_{st}\left[\bar{q}^s(x)(1-\gamma_5)q^t(x)\right]\right) \tag{2.73}$$

This is how instantons give rise to an effective $U_A(1)$ violating $2N_f$ fermion interaction. Since $U_A(1)$ is now explicitly broken when

$$\mathcal{L}_{\text{t' Hooft}}=\kappa\det_{st}\left[\bar{q}^s(1+\gamma_5)q^t\right]+\kappa\det_{st}\left[\bar{q}^s(1-\gamma_5)q^t\right] \tag{2.74}$$

is included in the Lagrangian, η' cannot be considered a pseudo-Goldstone boson any more. This, at least qualitatively, explains why it is much heavier than the other mesons which solves the $U(1)$ puzzle.

2.3. Order of the chiral phase transition

2.3.1. Phases of matter

As is known from thermodynamics matter assumes different phases in different environments. For example water can exist in liquid or in solid form depending on the surrounding temperature and pressure. The transition of one phase to the other by tuning these external parameters can induce rapid or even discontinuous changes in properties of the respective substance. An example for a first order phase transition is the melting of ice. There, at the transition temperature latent heat effects come into play and heat flowing into the system does not necessarily increase the temperature anymore. Instead the energy goes into breaking the crystal structures of the ice and only when all of them are broken up, the temperature increases again. An example for a second order phase transition is the heating of a magnet above the Curie temperature, the ferromagnetic transition. Above it the magnetization is lost. Second order transitions have no latent heat phenomena. A pedagogical introduction to the topic is given in [20]. In this subsection a summary of the points most relevant for us is given.

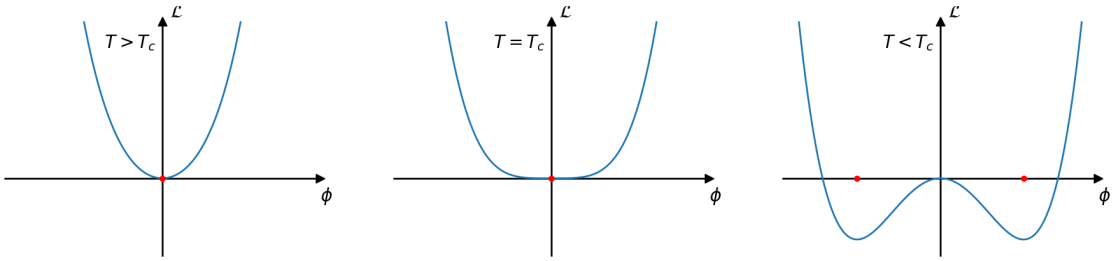

Figure 2.1.: A second order phase transition: The order parameter ϕ changes continuously to minimize the free energy.

Second order phase transitions in Landau theory

To get a quantitative grip of the situation one can introduce the *Landau Free Energy* functional $L(\phi)$ which depends on the *order parameter* ϕ. For example let

$$L(\phi) = V\mathcal{L}(\phi), \qquad \mathcal{L}(\phi) = at\phi^2 + \frac{1}{2}b\phi^4 \tag{2.75}$$

with V the volume of the system, ϕ assumed to be homogeneous, $b > 0$ and $t = (T - T_c)/T_c$ the distance from the critical temperature. Higher order terms in ϕ are neglected since ϕ is assumed to be small close to the transition. The physically realized state is where the order parameter assumes the value that minimizes the free energy. Above T_c the minimum is at the origin, below T_c new minima appear at finite values. The order parameter ϕ therefore obtains a finite expectation value below T_c and the change happens continuously when crossing T_c. The situation is depicted in Fig. 2.1.

Calculating the correlation length (its squared inverse appears as a "mass" term in the Greens function when the order parameter is allowed to be inhomogeneous) yields the behavior $\xi \sim |t|^{-1/2}$. The exponent $\frac{1}{2}$ characterizing the divergence is an example of a critical exponent, calculated in the mean-field approximation. The mean-field exponents are the same for all physical systems, irrespective of symmetries. There are more critical exponents but only two are independent. The relations among the various critical exponents are known as scaling laws, which can be proven via the renormalization group.

First order phase transitions in Landau theory

If a cubic term is allowed by the symmetries, the Landau functional assumes the following form

$$\mathcal{L}(\phi) = at\phi^2 + \frac{1}{2}b\phi^4 + C\phi^3 \tag{2.76}$$

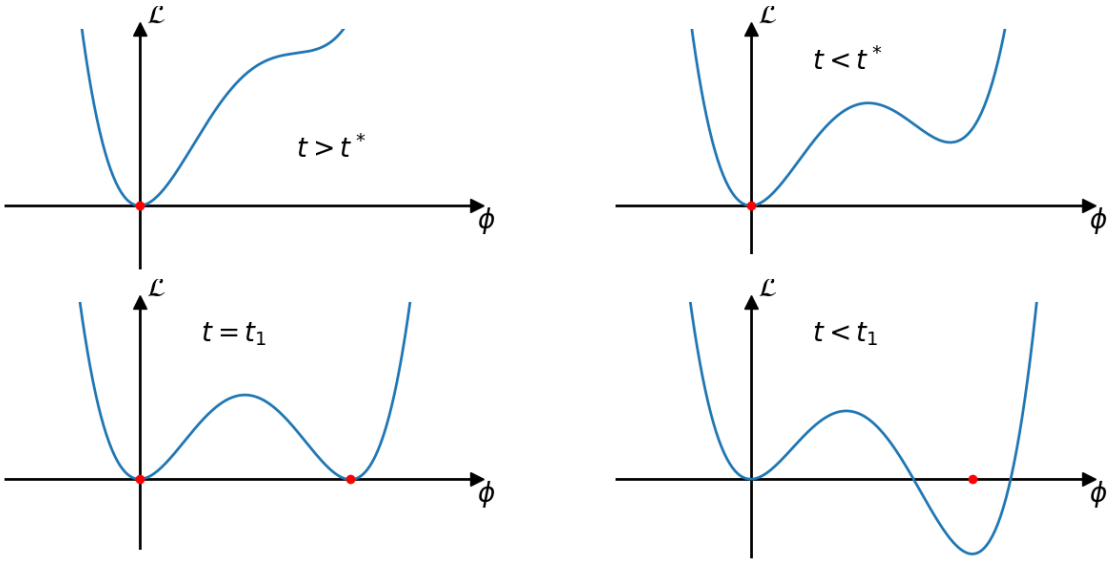

Figure 2.2.: A first order phase transition: The order parameter ϕ does a discontinuous jump to minimize the free energy as the temperature is lowered.

for $t < t^* = bc^2/a$ with $c = 3C/4b$ a second minium develops. For $t = t_1$ this second minimum becomes the global minimum and a first order phase transition occurs. The situation is depicted in Fig. 2.2. The latent heat effects characteristic for a first order transition are explained by the finite amount of energy that is necessary to change the value of the order parameter when the transition temperature is crossed by an infinitesimally small temperature step. Notably, when approaching the first order transition from below, ϕ is not arbitrarily small anymore and the assumption that higher order terms in the Landau functional can be neglected is not valid anymore.

Renormalization group

It turns out that the critical exponents predicted by mean-field theory are incorrect very close to the critical point. They contradict precise measurements from experiments and e.g. Onsager's exact solution of the two-dimensional Ising model [21]. The problem is that as the system approaches the critical temperature thermal fluctuations from all scales down to the lattice spacing need to be taken into account. To properly deal with this the renormalization group is needed.

Analogously in particle physics one needs to take into account quantum fluctuations over

a large range of scales. This was first done in QED for precise computations of the lamb shift and anomalous magnetic moment of the electron that matched the experimentally observed values.

In the RG framework a transformation is introduced that rescales the system, yielding a different Hamiltonian further away from criticality. If a system is described by the Hamiltonian

$$\mathcal{H} = \sum_n K_n \Theta_n \tag{2.77}$$

where K_n are coupling constants and Θ_n local operators, a renormalization group transformation R_ℓ maps the set of coupling constants to a different one and rescales the correlation length

$$\boldsymbol{K} \xrightarrow{R_\ell} \boldsymbol{K}' \tag{2.78}$$

$$\xi \xrightarrow{R_\ell} \xi' = \frac{\xi}{\ell} \tag{2.79}$$

Iterating this procedure can translate a system into a region of coupling space where it becomes computationally accessible again. So the renormalization method enables us to make statements about the original system very close to criticality. In particular critical exponents matching the experimentally observed values can be calculated.

Fixed points

The fixed points $\boldsymbol{K}^*$ of a given transformation R_ℓ are mapped to themselves

$$\boldsymbol{K}^* \xrightarrow{R_\ell} \boldsymbol{K}^* \tag{2.80}$$

At these the correlation length can only be 0 or ∞ since Eq. (2.79) needs to be satisfied. Performing a stability analysis for the linearized RG transformation close to a fixed point $\boldsymbol{K}^*$, i.e. for the matrix

$$M_{nm} = \left.\frac{\partial K'_n}{\partial K_m}\right|_{K=K^*} \tag{2.81}$$

yields *relevant*, *irrelevant* and *marginal* directions in the form of eigenvectors in coupling space. Relevant here means that the respective eigenvalue $\Lambda_k \sim \ell^{y_k}$ has an absolute value larger than one, irrelevant means smaller than one, and marginal equal to one. Or equivalently, that the exponent y_k is larger, smaller, or equal to zero.

The irrelevant couplings span the *critical manifold* and the number of relevant couplings is the codimension of the critical manifold. When starting with a set of couplings $\boldsymbol{K}$ near

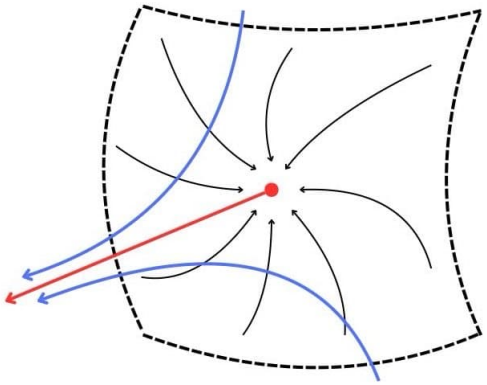

Figure 2.3.: The critical manifold of a fixed point is spanned by the irrelevant directions which flow into it. One relevant direction emerges from it. Flows in the neighborhood are governed by these directions. See also [22].

$\boldsymbol{K}^*$ but not on the critical manifold, the flow is still governed by the fixed points of the RG transformation. The irrelevant couplings are quickly suppressed and the (literally) relevant directions of the fixed points direct the flow. The situation is visualized in Fig. 2.3.

Fixed points can be classified according to their codimension c (the number of relevant directions) and correlation length ξ. A fixed point with $c = 0$ and $\xi = 0$ is a sink and corresponds to a stable phase of matter. A fixed point with $c = 1$ and $\xi = 0$ can either correspond to a first order phase transition or an unstable phase of matter, depending on if the order parameter changes discontinuously or not when crossing the fixed point along the relevant direction. Note however that there are pitfalls for defining an RG map close to a first order phase transition [23]. A fixed point with $c = 2$ and $\xi = \infty$ corresponds to a critical point and second order phase transition. The two relevant directions correspond to the two independent critical exponents, from which all other critical exponents can be derived.

The notion of relevant, irrelevant and marginal are tied to the fixed point under consideration. At a different fixed point the same directions can have a different nature.

Exponent	ϵ-expansion to $O(\epsilon)$	Mean-field theory	Conformal bootstrap
α	0.167	0 (disc.)	0.11008708(35)
β	0.333	0.5	0.32641871(75)
γ	1.167	1	1.23707551(26)
δ	4	3	4.78984254(27)
ν	0.583	0.5	0.62997097(12)
η	0	0	0.036297612(48)

Table 2.1.: Critical exponents from the three-dimensional Ising model. The values of the ϵ-expansion and mean-field theory are taken from [20]. They are compared to the ones obtained via the state of the art conformal bootstrap method in [24].

The Wilson-Fisher fixed point and ϵ-expansion

One method that has proven fruitful to find nontrivial fixed points is the ϵ-expansion in $d = 4 - \epsilon$ dimensions. For the Ising model described via the Hamiltonian

$$\mathcal{H}(\phi) = \int d^d x \, \left[\frac{1}{2} (\nabla \phi)^2 + \frac{1}{2} r_0 \phi^2 + \frac{1}{4} u_0 \phi^4 \right] \tag{2.82}$$

with a momentum cutoff Λ, two fixed points are obtained in one-loop order in a tedious calculation. The Gaussian fixed point

$$r^* = 0, \qquad u^* = 0 \tag{2.83}$$

and the Wilson-Fisher fixed point (to order $O(\epsilon)$)

$$r^* = -\frac{\epsilon \Lambda^2}{6}, \qquad u^* = \frac{8\pi^2}{9} \epsilon. \tag{2.84}$$

In $d = 4$ they coincide. Now even though ϵ was assumed to be small, setting $\epsilon = 1$, i.e. $d = 3$ surprisingly still yields results for the critical exponents which are closer to the true values than the ones obtained via mean-field theory (see Table 2.1). The fixed point situation and the flows in their neighborhood is shown in Fig. 2.4.

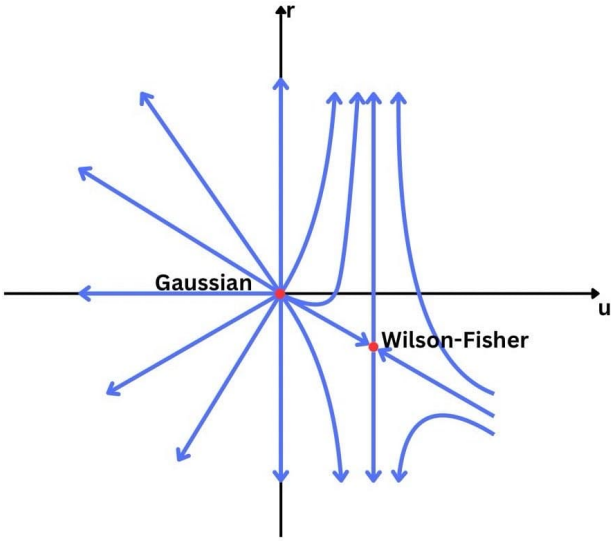

Figure 2.4.: The Gaussian and the Wilson-Fisher fixed point of the three dimensional Ising model. See also [22].

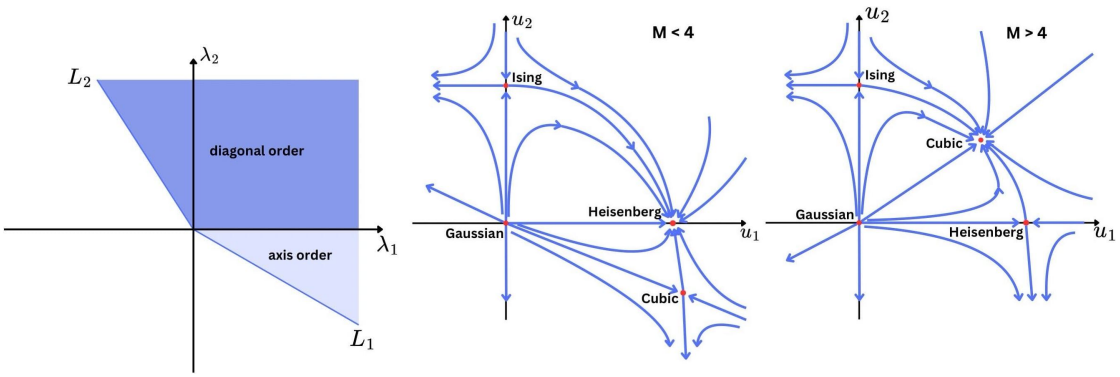

(a) Stability wedge of the classic theory

(b) Flow diagram for $M < 4$ and $M > 4$ obtained in the ϵ-expansion to order $O(\epsilon)$

Figure 2.5.: Classic and RG description of the $O(M)$ model with cubic anisotropy.

Fluctuation induced first order transitions

In some cases mean-field theory predicts a second order transition which does not survive in the RG picture and becomes a first order transition once fluctuations are taken into account (or the other way around). Notably, the Coleman-Weinberg model in four dimensions, where the phenomenon was first described, has a fluctuation induced first order transition. A pedagogical explanation is given in Part II Chapter 4 of [25].

There a $O(M)$ model with a cubic anisotropy (which is typical for crystalline structures) is studied. The interaction Lagrangian density of the model reads

$$\mathcal{L}_{\text{int}} = \frac{1}{4!}\left[\lambda_1\left(\sum_{i=1}^{M}\phi_i^2\right)^2 + \lambda_2\sum_{i=1}^{M}\phi_i^4\right] \tag{2.85}$$

Landau theory predicts a region of second order transitions within a stability wedge (see Fig. 2.5a). However, with the ϵ-expansion four fixed points are obtained (see Fig. 2.5b) and for example for $M > 4$, $\lambda_1 > 0$, $\lambda_2 < 0$ and $|\lambda_2| \ll \lambda_1$ the system will be on a runaway trajectory with λ_2 becoming more and more negative, indicating an instability and first order phase transition. The free energy is calculated to one-loop order and it indeed develops a second minimum away from the origin that becomes the global minimum when the runaway coupling crosses a boundary.

By this a fluctuation induced first order phase transition is described, which was not present in mean-field theory.

2.3.2. The chiral phase transition in QCD

In analogy to the symmetry breaking mechanism responsible for superconductivity, Nambu and Jona-Lasinio put forward the idea of *chiral symmetry breaking* in elementary particle physics in [26, 27]. They based their analysis on a model with massless fermions and a four-fermion interaction which is now called the *NJL model*. This model can now be understood as an effective model for QCD with the four-fermion interaction being effectively generated by the gluons.

Chiral symmetry breaking successfully explains, among other things, the appearance of pions and other mesons as Goldstone bosons as a result of the breaking $SU_L(N_f) \times SU_R(N_f) \to SU_V(N_f)$. The order parameter of this transition is the quark condensate. It assumes a nonzero value $\langle \bar{q}q \rangle = \langle \bar{q}_L q_R + \bar{q}_R q_L \rangle \neq 0$ below a certain temperature T_c, and is restored above it $\langle \bar{q}q \rangle = 0$. The identification of e.g. the pions as pseudo Goldstone bosons even at physical quark masses works reasonably well because the physical quark masses are small compared to typical scales of QCD.

A central question is the order of this transition. For three massless flavors the $U_A(1)$ breaking term Eq. (2.74) is hexalinear in the quark fields, i.e. cubic in the order parameter. A presence of a term of this form directly implies a first order phase transition, see Fig. 2.2. For two massless flavors, if the $U_A(1)$ remains strongly broken at T_{ch}, the η' also remains massive and the transition is governed by the other degrees of freedom and of second order in the $O(4)$ universality class. However, if the anomalous breaking of the $U_A(1)$ becomes sufficiently weak at T_{ch}, a first order transition is possible. Pisarski and Wilczek outlined this in [1].

Their argument is based the analysis of a three-dimensional theory with a complex $N_f \times N_f$ matrix Φ representing the quark bilinears $\Phi_{ij} \sim \langle \bar{q}_i (1+\gamma_5) q_j \rangle$. The Lagrangian reads

$$\mathcal{L}_\Phi = \frac{1}{2} \operatorname{tr}\left(\partial_\mu \Phi^\dagger\right)\left(\partial_\mu \Phi\right) - \frac{1}{2} m_\Phi^2 \operatorname{tr} \Phi^\dagger \Phi - \frac{\pi^2}{3} g_1 \left(\operatorname{tr} \Phi^\dagger \Phi\right)^2 - \frac{\pi^2}{3} g_2 \operatorname{tr}\left(\Phi^\dagger \Phi\right)^2 \tag{2.86}$$

This is invariant under the full $G_f = SU_L(N_f) \times SU_R(N_f) \times U_A(1)$ symmetry. The $U_V(1)$ can be ignored as Φ itself is invariant under it [28]. Adding a term

$$\mathcal{L}'_\Phi = c(T)\left(\det \Phi + \det \Phi^\dagger\right) \tag{2.87}$$

breaks the $U_A(1)$, where the prefactor depends on the instanton density $c(T) \sim d_I(T)$. For increasing temperature Debye screening weakens the instanton effects with an inevitable restoration of $U_A(1)$ for $T \to \infty$.

The theory given by Eq. (2.86) (or rather a more general one that includes it) was studied to one-loop order in the ϵ-expansion in [29]. The beta functions

$$\beta_1 = -\epsilon g_1 + \frac{N_f^2+4}{3} g_1^2 + \frac{4N_f}{3} g_1 g_2 + g_2^2 \tag{2.88}$$

$$\beta_2 = -\epsilon g_2 + 2 g_1 g_2 + \frac{2N_f}{3} g_2^2 \tag{2.89}$$

were obtained, from which the fixed points

$$g_\alpha^* = (0,0) \tag{2.90}$$

$$g_\beta^* = \left(\frac{3\epsilon}{N_f^2+4}, 0 \right) \tag{2.91}$$

$$g_{\delta^+}^* = \left(\frac{\epsilon}{2}\left[1 - \frac{2N_f}{3} A_+\right], \epsilon A_+ \right) \tag{2.92}$$

$$g_{\delta^-}^* = \left(\frac{\epsilon}{2}\left[1 - \frac{2N_f}{3} A_-\right], \epsilon A_- \right) \tag{2.93}$$

with

$$A_\pm = \frac{6N_f\left(N_f^2-5\right) \pm 9\sqrt{8}\sqrt{3-N_f^2}}{4N_f^2\left(N_f^2-8\right)+108} \tag{2.94}$$

were deduced. The stability matrix reads

$$\omega_{ij} = \begin{pmatrix} \frac{2N_f^2+8}{3} g_1 + \frac{4N_f}{3} g_2 - \epsilon & \frac{4N_f}{3} g_1 + 2g_2 \\ 2g_2 & 2g_1 + \frac{4N_f}{3} g_2 - \epsilon \end{pmatrix}. \tag{2.95}$$

For $g_{\delta^\pm}^*$ to be real the condition $N_f \leq \sqrt{3}$ needs to be fulfilled. So these fixed points do not exist in the case with two or more flavors. The stability matrix evaluated at the other two fixed points has eigenvalues

$$y_\alpha = (-\epsilon, -\epsilon) \tag{2.96}$$

$$y_\beta = \left(\epsilon, \epsilon\left[\frac{6}{N_f^2+4} - 1\right] \right). \tag{2.97}$$

So the Gaussian fixed point g_α^* is always unstable for $\epsilon > 0$, and the vector fixed point g_β^* becomes unstable when $N_f > \sqrt{2}$ (in the case of two or more flavors). Since there is no

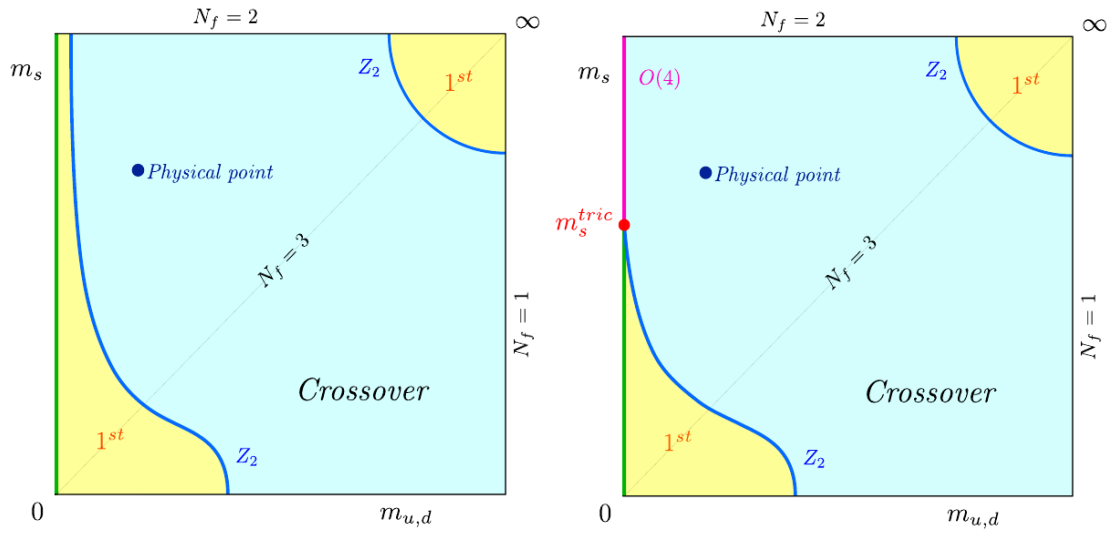

(a) First order scenario (b) Second order scenario

Figure 2.6.: Columbia plots of two possible scenarios for the chiral phase transition. Taken from [31].

stable fixed point a fluctuation induced first order transition is suggested (as described at the end of the previous subsection).

Since the original study by [1] there have also been studies of the model via other methods than the ϵ-expansion. For example in Chapter 5 of [30] a study within the FRG is presented which indeed yields a potential that develops a minimum away from the origin causing a discontinuous change of the order parameter.

This behavior is expected to play a role even away from the chiral limit. While a second order phase transition would immediately turn into a crossover with current quark masses being switched on, a first order transition is more stable against this variation. Lattice and FRG studies indicate that it doesn't persist until the physical point though.

The situation can be visualized with *Columbia plots*. Two possible scenarios are shown in Fig. 2.6. There the up and down quarks are degenerate in mass and the strange quark assumes a different value. The top right corner (the masses of all three quarks are set to infinity and they decouple) represents pure Yang-Mills theory which is known to feature a first order phase transition. The line on the right represents the one flavor case, the line on the top the two flavor case and the diagonal the three flavor case with equal masses.

At the heart of determining the order of the phase transition with two massless flavors

lies the question to what extent the axial anomaly plays a role.

If an effective restoration happens above T_{ch} one can safely assume the transition to be of second order in the $O(4)$ universality class. If, however, the effective $U_A(1)$ restoration coincides with T_{ch} the situation remains undecided and the transition could lie in $O(2) \times O(4)$ and be of fluctuation induced first order. In fact, there is experimental evidence about a drop of the η' mass above the transition which indicates a $U_A(1)$ restoration [32, 33].

2.4. Low Energy Effective Models

2.4.1. Why we need them

Due to its non-perturbative nature at low energies, quantities taking into account fluctuations from QCD at all scales are usually hard to calculate. *lattice QCD* does a direct calculation of the discretized path integral, but is very limited in scope due to the high computational cost. Only comparatively small lattices can be resolved and one has to deal with problems originating from the discretization as well as the finite volume.

Another way to proceed is to choose an appropriate effective model for the situation we wish to describe. This will not include all of the fundamental degrees of freedom, but only the ones most relevant for our scenario. Outside of its region of validity, it usually gives nonsensical results. Any effective model comes with parameters that will have to be fixed by experiment or some more fundamental theory to be able to make predictions.

One has, for example, simple NJL-type models which can qualitatively reproduce important aspects of QCD and give e.g. a consistent picture of the meson masses. See [34, 35] for reviews.

Another example is the more involved chiral effective field theory which successfully describes two- and many-body nuclear forces. It is constructed to respect all symmetries from low-energy QCD, particularly the (approximate) chiral symmetry. The ratio Q/Λ_χ of the pion mass or some small external momentum over the chiral symmetry breaking scale, typically taken to be $\Lambda_\chi \approx 1$ GeV, serves as the small parameter for a starting point of perturbation theory. See [36] for a review.

2.4.2. Chiral Quark-Meson Model

One model which was introduced to specifically investigate the chiral phase transition with FRG methods is the chiral quark-meson model [37, 38]. As the name suggests, it features quarks and mesons interacting via a Yukawa coupling h. The meson fields φ are motivated by bosonizing a four-quark interaction which is generated dynamically by the

gluons. They transform in the $(\bar{\mathbf{N}}, \mathbf{N})$ representation of the $SU_L(N_f) \times SU_R(N_f)$ group. For the transition itself, the gluons are suspected to play a minor role, hence they are neglected in the model. The microscopic action of the chiral quark-meson model reads

$$S = \int d^4x \left\{ \partial_\mu \varphi^*_{ab} \partial^\mu \varphi^{ab} + \bar{q}^a \partial\!\!\!/ q_a + h\bar{q}^a \left[\frac{1+\gamma_5}{2} \varphi_a{}^b - \frac{1-\gamma_5}{2} (\varphi^\dagger)_a{}^b \right] q_b + U(\varphi, \varphi^\dagger) \right\} \tag{2.98}$$

The potential $U(\varphi, \varphi^\dagger)$ is a function of the invariants ξ, ρ and $\tilde{\tau}_i$ with

$$\xi = \det \varphi + \det \varphi^\dagger, \qquad \rho = \operatorname{tr}\left(\varphi^\dagger \varphi\right), \qquad \phi = \varphi^\dagger \varphi - \frac{1}{N_f}\rho, \qquad \tilde{\tau}_i = \operatorname{tr} \phi^i \tag{2.99}$$

It gives qualitatively good results for the pion decay constant f_π, the chiral condensate $\langle \bar{q} q \rangle$, the constituent quark mass M_q, the pion mass m_π, the sigma mass m_σ. These observables are defined by the IR values, i.e $k = 0$, of the following scale-dependent quantities (concepts that will become clearer in the next sections):

$$f_{\pi,k} = 2\sigma_{0,k} \tag{2.100}$$

$$\langle \bar{q} q \rangle_k = -2\overline{m}^2_{k_\Phi} \left[Z^{-1/2}_{\varphi,k} \sigma_{0,k} - \hat{m} \right] \tag{2.101}$$

$$M_{q,k} = Z^{-1/2}_{\varphi,k} Z^{-1}_{q,k} \overline{h}_k \sigma_{0,k} \tag{2.102}$$

$$m^2_{\pi,k} = Z^{-1/2}_{\varphi,k} \frac{\overline{m}^2_{k_\Phi} \hat{m}}{\sigma_{0,k}} \tag{2.103}$$

$$m^2_{\sigma,k} = Z^{-1/2}_{\varphi,k} \frac{\overline{m}^2_{k_\Phi} \hat{m}}{\sigma_{0,k}} + 4\sigma^2_{0,k} Z^{-2}_{\varphi,k} \frac{\partial^2 U_k}{\partial \rho^2} \left(\rho = 2\overline{\sigma}^2_{0,k} \right) \tag{2.104}$$

Here $Z_{\varphi,k}$ and $Z_{q,k}$ are the wave function renormalizations of the meson and the quark fields, $\sigma_{0,k} = Z^{1/2}_{\varphi,k} \overline{\sigma}_{0,k}$ is the renormalized expectation value of the potential, $\hat{m}$ is the light current quark mass, and $\overline{m}^2_{k_\Phi}$ is the coefficient of the quadratic term of the potential at the composition scale $k = k_\Phi$ where the flow is initialized.

Assuming a strong anomaly and an $O(4)$ symmetry, it successfully describes a second order phase transition as done in [38]. There are various extensions of it, for example, one can introduce a nonzero chemical potential. This was done in e.g. [39] to derive a phase diagram.

3. Functional Methods

The flow equation, presented in this chapter, is a method to calculate the path integral and was first put forward by Wetterich in [40]. Its benefits over e.g. lattice QCD are that it allows one to gain more insights into underlying mechanism of the theory that is being studied, and it requires much less computational resources. It is capable to deal with the strong interaction and gravity. One of its successes were that it was able to predict the mass of the Higgs boson up to a few MeV [41]. Parts of this chapter are taken from the author's Master thesis [5]. A pedagogical introduction can be found in [42].

3.1. Flow Equation

From the generating functional $Z[J]$, the so-called quantum effective action $\Gamma[\phi]$ can be derived

$$\Gamma[\phi] = \sup_J \left(J \cdot \phi - \ln Z[J]\right) \tag{3.1}$$

It is a functional of classical fields ϕ and its main advantage over the microscopic action S is that its functional derivatives give the full quantum theory at tree level. It also serves as a starting point to formulate the flow equation, which provides a method to solve non-perturbative problems. The flow equation describes how the scale-dependent *effective average action* Γ_k, also a functional of classical fields, smoothly interpolates between the microscopic action S, valid at a cutoff scale $k = \Lambda$, and the effective action Γ, valid at the macroscopic scale $k = 0$. Its definition can be found in Eq. (A.12), however in practice one can often resort to an ansatz i.e. a truncation of Γ_k that captures all relevant physics.

The interpolation between S and Γ via Γ_k is facilitated via a successive integration of momentum shells in the path integral. This is formally done by inserting a regulator $R_k(q)$ into it, that suppresses all unwanted contributions. Introducing a superfield ϕ containing all bosons and fermions, the flow equation reads

$$\partial_t \Gamma_k[\phi] = \frac{1}{2}\mathrm{STr}\left[\partial_t R_k \left(\Gamma_k^{(2)}[\phi] + R_k\right)^{-1}\right]. \tag{3.2}$$

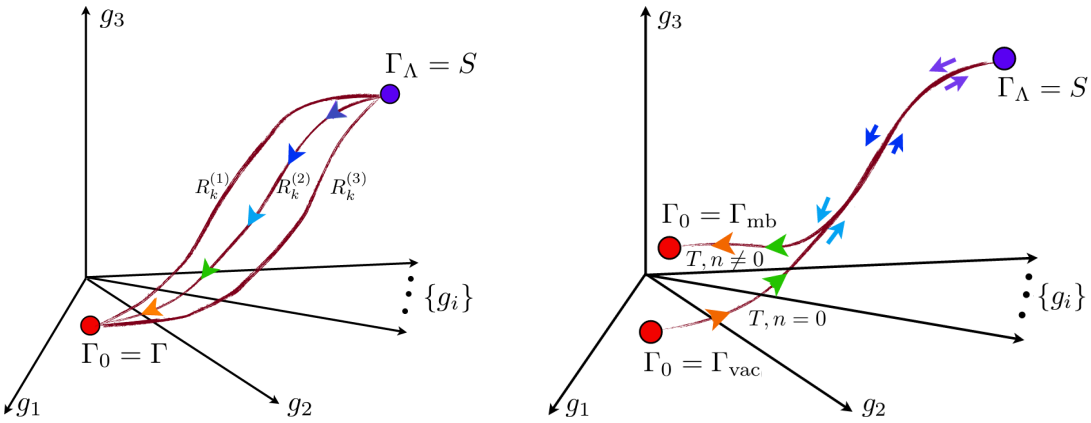

(a) Vacuum flow. Different regulators yield different paths for the flow, but all arrive at the same full quantum effective action.

(b) Flow with temperature. When k reaches the scale of the temperature the flow diverts from the vacuum flow.

Figure 3.1.: Illustrations of FRG flow. Taken from [43].

where $\partial_t = k\partial_k$ and STr denotes the supertrace running over all internal indices and introducing minus signs in the fermionic subspace due to their anti-commuting nature. A derivation is presented in Appendix A.

The flow equation can be diagrammatically represented as

$$\partial_t \Gamma_k[\phi] = \frac{1}{2} \tag{3.3}$$

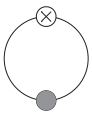

where the crossed vertex and filled circle denote regulator insertion and the fully dressed propagator, i.e.

$$\partial_t R_k = \tag{3.4}$$

$$\left(\Gamma_k^{(2)}[\phi] + R_k\right)^{-1} = \tag{3.5}$$

see also Eq. (A.18).

Notably, the equation has a simple one loop structure even though it is non-perturbative. Another important property is that the flow at scale k only depends on dressed quantities at scale k. No bare quantities are involved once the flow has started to drive the system away from the UV scale.

The final effective action has to be independent of the regulator we chose. Each choice of R_k represents a different way to connect S and Γ in theory space. This is depicted in Fig. 3.1a. If one includes temperature (or chemical potential) effects, they will start to show up when the scale k reaches values of order T. The flowing action then diverts from the vacuum path and arrives at a different Γ at $k = 0$. See Fig. 3.1b.

Unless broken by the regulator, the flow preserves symmetries. To study anomalously broken symmetries, i.e. $U_A(1)$ in QCD, one therefore has to introduce the respective breaking at scale Λ.

3.2. Regulators

For the effective average action to serve as an interpolation between the microscopic action S and the macroscopic effective action Γ, the (bosonic) regulator has to satisfy certain requirements:

1. As an IR regularization it should fulfill
$$\lim_{q^2/k^2 \to 0} R_k(q) > 0 \tag{3.6}$$

2. To recover the full effective action at the macroscopic scale, i.e. $\lim_{k\to 0} \Gamma_k = \Gamma$, we should have
$$\lim_{k^2/q^2 \to 0} R_k(q) = 0 \tag{3.7}$$

3. And finally, to connect the effective average action to the classical action in the UV, i.e. $\lim_{k\to\infty} \Gamma_k = S$, we have the condition
$$\lim_{k \to \infty} R_k(q) = \infty \tag{3.8}$$

For fermionic regulators similar statements hold. Popular regulators include the Litim regulator [44]
$$R_k(q) = Z_k \left(k^2 - q^2\right) \Theta \left(k^2 - q^2\right) \tag{3.9}$$
which, among other things, causes algebraic simplicity of the resulting flow equations, and the exponential regulator
$$R_k(q) = \frac{Z_k q^2}{e^{q^2/k^2} - 1} \tag{3.10}$$
which is sometimes better suited when performing numerical simulations.

3.3. Truncations and technicalities

Exact solutions to the flow equation are rare and one usually has to resort to approximations of the effective average action. Power expansions in the fields as well as their derivatives are mainly used in practice. The flow of each expansion parameter is then obtained by projecting onto the relevant part via performing (functional) derivatives on both sides of the flow equation. Since the right-hand side of the flow equation already contains the second derivative of Γ_k, an infinite tower of coupled differential equations is formed. For that, a suitable truncation, which is able to capture all physics of the specific phenomena one wants to study, has to be chosen.

One way to extract the flow of each parameter in Γ_k is to rewrite Eq. (3.2) into

$$\partial_t \Gamma_k[\phi] = \frac{1}{2}\text{STr}\, \tilde{\partial}_t \ln\left[\Gamma_k^{(2)}[\phi] + R_k\right] \tag{3.11}$$

where the $\tilde{\partial}_t$ only acts on the regulator. Splitting $\Gamma_k^{(2)}[\phi] + R_k = \mathcal{P}_k + \mathcal{F}_k$ into a field-independent part $\mathcal{P}_k$ and a field-dependent part $\mathcal{F}_k$, one gets

$$\partial_t \Gamma_k = \frac{1}{2}\text{STr}\, \tilde{\partial}_t \ln\left(\mathcal{P}_k\right) + \frac{1}{2}\text{STr}\, \tilde{\partial}_t \left(\frac{1}{\mathcal{P}_k}\mathcal{F}_k\right) - \frac{1}{4}\text{STr}\, \tilde{\partial}_t \left(\frac{1}{\mathcal{P}_k}\mathcal{F}_k\right)^2 + \frac{1}{6}\text{STr}\, \tilde{\partial}_t \left(\frac{1}{\mathcal{P}_k}\mathcal{F}_k\right)^3 + \ldots \tag{3.12}$$

Then derivations have to performed on both sides.

3.4. The ϕ^4 theory as an example

In this section we want to showcase the aforementioned technique on a simple example, the ϕ^4 theory. We have the microscopic action

$$S[\phi] = \int d^4x \left[\frac{1}{2}\left(\partial_\mu \phi\right)^2 + \frac{m^2}{2}\phi^2 + \frac{\lambda}{4!}\phi^4\right] \tag{3.13}$$

We assume to be in the symmetric regime, with $m^2 > 0$. As an ansatz for the effective average action we choose the following truncation

$$\Gamma_k[\phi] = \int d^4x \left[\frac{1}{2}\left(\partial_\mu \phi\right)^2 + \frac{m_k^2}{2}\phi^2 + \frac{\lambda_k}{4!}\phi^4\right] \tag{3.14}$$

with scale-dependent coefficients m_k and λ_k. We could of course also include terms of higher order in the truncation but we want to keep it simple. Our goal is to derive the

differential equations which describe the flow of m_k and λ_k with the scale k. For this we first switch to Fourier space

$$\begin{aligned}\Gamma_k[\phi] = \int \frac{d^4p}{(2\pi)^4}\left[\left(\frac{1}{2}p^2+\frac{1}{2}m_k^2\right)\phi(-p)\phi(p)\right] \\ + \int \frac{d^4p}{(2\pi)^4}\frac{d^4k}{(2\pi)^4}\frac{d^4l}{(2\pi)^4}\left[\frac{\lambda_k}{4!}\phi(p)\phi(k)\phi(l)\phi(-p-k-l)\right]\end{aligned} \tag{3.15}$$

Then we take the second functional derivative. Since we are only dealing with a single scalar we do not need to worry about performing them from the left or right and get

$$\frac{\delta^2\Gamma_k[\phi]}{\delta\phi(-q_2)\delta\phi(q_1)} = \left(q_1^2+m_k^2\right)(2\pi)^4\delta^4(-q_1+q_2)+\frac{\lambda_k}{2}\int\frac{d^4p}{(2\pi)^4}\left[\phi(p)\phi(q_2-q_1-p)\right] \tag{3.16}$$

So with a regulator that is also diagonal in momentum space we get for the field-independent part $\mathcal{P}_k$ and field-dependent part $\mathcal{F}_k$ of $\Gamma_k^{(2)}[\phi]+R_k$

$$\mathcal{P}_k[\phi](q_1,q_2) = \left(q_1+m_k^2+R_k(q_1)\right)(2\pi)^4\delta^4(q_2-q_1) \tag{3.17}$$

$$\mathcal{F}_k[\phi](q_1,q_2) = \frac{\lambda_k}{2}\int\frac{d^4p}{(2\pi)^4}\phi(p)\phi(q_2-q_1-p) \tag{3.18}$$

Now, to extract the flow for both coefficients via Eq. (3.12) we evaluate both sides with the constant field configuration

$$\phi(p) = \hat{\phi}(p) \equiv \hat{\phi}(2\pi)^4\delta^4(p) \tag{3.19}$$

With this the field-dependent part also becomes diagonal in momentum space

$$\mathcal{F}_k[\phi]|_{\phi=\hat{\phi}}(q_1,q_2) = \frac{\lambda_k}{2}\hat{\phi}^2(2\pi)^4\delta^4(q_2-q_1) \tag{3.20}$$

and we have

$$\left(\mathcal{P}_k^{-1}\mathcal{F}_k\right)[\phi]|_{\phi=\hat{\phi}}(q_1,q_2) = \frac{\lambda_k}{2}\frac{1}{q_1^2+m_k^2+R_k(q_1)}\hat{\phi}^2(2\pi)^4\delta^4(q_2-q_1) \tag{3.21}$$

$$\left(\mathcal{P}_k^{-1}\mathcal{F}_k\mathcal{P}_k^{-1}\mathcal{F}_k\right)[\phi]|_{\phi=\hat{\phi}}(q_1,q_2) = \left(\frac{\lambda_k}{2}\right)^2\frac{1}{\left(q_1^2+m_k^2+R_k(q_1)\right)^2}\hat{\phi}^4(2\pi)^4\delta^4(q_2-q_1) \tag{3.22}$$

For the effective average action, we get

$$\Gamma_k[\phi]|_{\phi=\hat{\phi}} = \left[\frac{m_k^2}{2}\hat{\phi}^2+\frac{\lambda_k}{4!}\hat{\phi}^4\right](2\pi)^4\delta^4(0) \tag{3.23}$$

Now, matching the right orders of $\hat{\phi}$ on both sides of Eq. (3.12) yields

$$\partial_t \left(\frac{m_k^2}{2}\right) \hat{\phi}^2 (2\pi)^4 \delta^4(0) = \frac{1}{2} \text{Tr}\, \tilde{\partial}_t \left(\mathcal{P}_k^{-1} \mathcal{F}_k\right) \tag{3.24}$$

$$= \frac{1}{2} \tilde{\partial}_t \int \frac{d^4p}{(2\pi)^4} \frac{\lambda_k}{2} \frac{1}{p^2 + m_k^2 + R_k(p)} \hat{\phi}^2 (2\pi)^4 \delta^4(0) \tag{3.25}$$

$$\partial_t \left(\frac{\lambda_k}{4!}\right) \hat{\phi}^4 (2\pi)^4 \delta^4(0) = -\frac{1}{4} \text{Tr}\, \tilde{\partial}_t \left(\mathcal{P}_k^{-1} \mathcal{F}_k\right)^2 \tag{3.26}$$

$$= -\frac{1}{4} \tilde{\partial}_t \int \frac{d^4p}{(2\pi)^4} \left(\frac{\lambda_k}{2}\right)^2 \frac{1}{\left(p^2 + m_k^2 + R_k(p)\right)^2} \hat{\phi}^4 (2\pi)^4 \delta^4(0) \tag{3.27}$$

And after simplifying

$$\partial_t m_k^2 = -\frac{\lambda_k}{2} \int \frac{d^4p}{(2\pi)^4} \frac{\partial_t R_k(p)}{\left(p^2 + m_k^2 + R_k(p)\right)^2} \tag{3.28}$$

$$\partial_t \lambda_k = 3\lambda_k^2 \int \frac{d^4p}{(2\pi)^4} \frac{\partial_t R_k(p)}{\left(p^2 + m_k^2 + R_k(p)\right)^3} \tag{3.29}$$

This is now a set of coupled differential equations for m_k^2 and λ_k. The regulator can still be chosen. Since the effective average action is fixed in the UV $k = \Lambda$ to be $\Gamma_{k=\Lambda} = S$, we have $m^2_{k=\Lambda} = m^2$ and $\lambda_{k=\Lambda} = \lambda$ as initial conditions. What we usually want to find out is the value of the coefficients at $k = 0$ in the IR by integrating this set of differential equations, which in most cases will have to be done numerically.

If we had a free theory, i.e. $\lambda = 0$ in the microscopic action, also no interaction term would be generated by the flow, since $\partial_t \lambda_k \sim \lambda_k^2$ and the mass term would stay constant, since $\partial_t m_k^2 \sim \lambda_k$. However, if the interaction is turned on in the UV also any other interaction term that we include in the truncation and that is consistent with the symmetries, such as $\alpha\phi^6$, would be generated by the flow.

If the flow drives the mass term to a negative value we would enter a regime of spontaneously broken symmetry and would need another set of flow equations that properly account for the minimum of the potential then being at a non-zero value.

Here we just looked at a scalar field. A more involved example of deriving flow equations with this scheme, including a gauge field, a complex scalar and one fermion species, can be found in [45].

3.5. Dynamical bosonization

Before applying the FRG formalism to the chiral transition in the next chapter we need to introduce one more concept: *Dynamical bosonization*. It is based on the Hubbard-Stratonovich transformation

$$\exp\left[\int d^4x\ \lambda\left(\bar{\psi}\psi\right)^2\right] = \mathcal{N}\int \mathcal{D}\sigma \exp\left[\int d^4x\ \left(\frac{\sigma^2}{4\lambda} + \bar{\psi}\psi\sigma\right)\right] \tag{3.30}$$

by which a four-fermion interaction can be transformed away, giving rise to a new bosonic field and a Yukawa interaction term in the path integral.

As mentioned previously, potentially all interaction terms compatible with the symmetries of the microscopic action are generated during the RG evolution. With dynamical bosonization all four-fermion interactions that pop up are immediately transformed away at every RG step. This makes higher order interaction terms of the fermions computationally more accessible as they now correspond to powers of the composite bosonic field. This formulation also has the benefit that the composite degrees of freedom, which are the ones observed at low energies, naturally show up during the RG evolution. This idea was put forward in [45] and illustrated with the gauged NJL model. We reproduce the main steps here.

3.5.1. Flow equations for the gauged NJL model without dynamical bosonization

The microscopic action of the gauged NJL model reads

$$S = \int d^4x\ \left[\bar{\psi}i\gamma^\mu\left(\partial_\mu + ieA_\mu\right)\psi + 2\lambda_{\text{NJL}}\left(\bar{\psi}_R\psi_L\right)\left(\bar{\psi}_L\psi_R\right) + \frac{1}{4}F_{\mu\nu}F_{\mu\nu} + \frac{1}{2\alpha}\left(\partial_\mu A_\mu\right)^2\right] \tag{3.31}$$

and describes one fermion flavor coupled to a gauge field (with constant e) and a four-fermion interaction. For the truncation

$$\begin{aligned}\Gamma_k = \int d^4x \Big\{ & \bar{\psi}i\gamma^\mu\left(\partial_\mu + ieA_\mu\right)\psi + \frac{1}{4}F_{\mu\nu}F_{\mu\nu} + 2\bar{\lambda}_{\sigma,k}\bar{\psi}_R\psi_L\bar{\psi}_L\psi_R \\ & + Z_{\phi,k}\partial_\mu\phi^*\partial_\mu\phi + \bar{m}_k^2\phi^*\phi + \bar{h}_k\left(\bar{\psi}_R\psi_L\phi - \bar{\psi_L}\psi_R\phi^*\right) + \frac{1}{2\alpha}\left(\partial_\mu A_\mu\right)^2\Big\}\end{aligned} \tag{3.32}$$

is chosen. The flow starts at scale Λ where the interaction λ_{NJL} is fully bosonized giving rise to the complex scalar appearing in the truncation. As initial conditions we have

$\lambda_{\text{NJL}} = \bar{h}_\Lambda^2/(2\bar{m}_\Lambda^2)$, $\bar{\lambda}_{\sigma,\Lambda} = 0$ and $Z_{\phi,\Lambda} = 0$. The gauge-fixing constant is set to $\alpha = 1$. By the method described in the previous sections flow equations of the couplings are derived:

$$\partial_t \bar{m}_k^2 \equiv \beta_m = 8k^2 v_4 l_1^{(F)\,4}(0)\, \bar{h}_k^2, \tag{3.33}$$

$$\partial_t \bar{h}_k \equiv \beta_h = -16k^2 v_4 l_1^{(F)\,4}(0)\, \bar{\lambda}_{\sigma,k} \bar{h}_k - 16 v_4 l_{1,1}^{(FB)\,4}(0,0)\, e^2 \bar{h}_k, \tag{3.34}$$

$$\begin{aligned} \partial_t \bar{\lambda}_{\sigma,k} \equiv \beta_{\lambda_\sigma} = {} & -24k^{-2} v_4 l_{1,2}^{(FB)\,4}(0,0)\, e^4 - 32 v_4 l_{1,1}^{(FB)\,4}(0,0)\, e^2 \bar{\lambda}_{\sigma,k} - 8k^2 v_4 l_1^{(F)\,4}(0)\, \bar{\lambda}_{\sigma,k}^2 \\ & + 8 v_4 \frac{1}{Z_{\phi,k}} l_{1,1}^{(FB)\,4}\left(0, \frac{\bar{m}_k^2}{Z_{\phi,k} k^2}\right) \bar{h}_k^2 \bar{\lambda}_{\sigma,k} + \frac{2 v_4}{Z_{\phi,k}^2 k^2} l_{1,2}^{(FB)4}\left(0, \frac{\bar{m}_k^2}{Z_{\phi,k} k^2}\right) \bar{h}_k^4 \end{aligned} \tag{3.35}$$

Here $v_4 = 1/(32\pi^2)$ and the threshold functions for the Litim regulator (which was used in [45]) read

$$l_n^{(F)d}(\omega) = (\delta_{n,0} + n) \frac{2}{d} \frac{1}{(1+\omega)^{n+1}} \tag{3.36}$$

$$l_{n_1,n_2}^{(FB)d}(\omega_1, \omega_2) = \frac{2}{d} \frac{1}{(1+\omega_1)^{n_1} (1+\omega_2)^{n_2}} \left[\frac{n_1}{1+\omega_1} + \frac{n_2}{1+\omega_2} \right] \tag{3.37}$$

see also Appendix D. The flow of $Z_{\phi,k}$ is not considered.

Notably, varying Eq. (3.32) w.r.t. ϕ and ϕ^* yields for the stationary point

$$\phi(q) = \frac{\bar{h}_k \left(\bar{\psi}_L \psi_R\right)(q)}{\bar{m}_k^2 + Z_{\phi,k} q^2}, \quad \phi^*(q) = -\frac{\bar{h}_k \left(\bar{\psi}_R \psi_L\right)(-q)}{\bar{m}_k^2 + Z_{\phi,k} q^2}. \tag{3.38}$$

which, when plugged back into Eq. (3.32), gives for the effective four-fermion interaction

$$\int d^4 q \left(2\bar{\lambda}_{\sigma,k} + \frac{\bar{h}_k^2}{\bar{m}_k^2 + Z_{\phi,k} q^2} \right) \left(\bar{\psi}_R \psi_L\right)(-q) \left(\bar{\psi}_L \psi_R\right)(q). \tag{3.39}$$

So there is a redundancy in our description and $\bar{\lambda}_{\sigma,k}$, $\bar{h}_k$ and $\bar{m}_k$ can be changed while keeping the effective four-fermion interaction fixed.

3.5.2. Dynamical bosonization via scale dependent fields

This redundancy can be exploited to keep $\bar{\lambda}_{\sigma,k} = 0$ at all scales. For this scale dependent fields ϕ_k, ϕ_k^* are introduced which get contributions from fermion bilinears during the flow:

$$\partial_t \phi_k(q) = -\left(\bar{\psi}_L \psi_R\right)(q) \partial_t \alpha_k(q) \tag{3.40}$$

$$\partial_t \phi_k^*(q) = \left(\bar{\psi}_R \psi_L\right)(-q) \partial_t \alpha_k(q). \tag{3.41}$$

with an arbitrary $\alpha_k(q)$. The modified flow equation in terms of these fields reads

$$\partial_t \Gamma_k[\phi_k, \phi_k^*] = \partial_t \Gamma_k[\phi_k, \phi_k^*]\big|_{\phi_k, \phi_k^*} + \int_q \left(\frac{\delta \Gamma_k}{\delta \phi_k(q)} \, \partial_t \phi_k(q) + \frac{\delta \Gamma_k}{\delta \phi_k^*(q)} \, \partial_t \phi_k^*(q) \right) \tag{3.42}$$

where the fields are held constant for the first term. The modified flows of the couplings are

$$\partial_t \bar{m}_k^2 = \partial_t \bar{m}_k^2\big|_{\phi_k, \phi_k^*} \tag{3.43}$$

$$\partial_t \bar{h}_k = \partial_t \bar{h}_k\big|_{\phi_k, \phi_k^*} + (\bar{m}_k^2 + Z_{\phi,k} q^2) \partial_t \alpha_k(q) \tag{3.44}$$

$$\partial_t \bar{\lambda}_{\sigma,k} = \partial_t \bar{\lambda}_{\sigma,k}\big|_{\phi_k, \phi_k^*} - \bar{h}_k \, \partial_t \alpha_k(q). \tag{3.45}$$

We only look at the point like limit $q = 0$ and choose $\partial_t \alpha_k(0) = \beta_{\lambda_\sigma} / \bar{h}_k$. So as desired, we have $\partial_t \bar{\lambda}_{\sigma,k} = 0$ and in turn we get an additional contribution to the Yukawa coupling

$$\partial_t \bar{h}_k = \partial_t \bar{h}_k\big|_{\phi_k, \phi_k^*} + \frac{\bar{m}_k^2}{\bar{h}_k} \beta_{\lambda_\sigma}. \tag{3.46}$$

This method is applied to a more complicated model in the next chapter.

4. Chiral Transition

Armed with the theoretical foundations from the previous chapters, we can now turn our attention to the main subject of this thesis, the chiral transition.

With a Taylor expansion of the potential of the order parameter around the minimum (as done in this chapter), a finite pion mass stabilizes the flow equations which otherwise become numerically unstable [46, 47]. So we cannot perform the calculation directly in the chiral limit. Instead our goal is to compute susceptibilities and pseudo-critical temperatures for decreasing pion masses, so that we can extrapolate to the chiral limit. We do our calculations with an ab-initio approach within the FRG framework, that can then be compared to results from other approaches.

We employ the simulation code written in Fortran that has already served as the basis for the results in [48], and which is called *easy QCD* or shorter *eQCD* within the collaboration.

4.1. Inner workings of the eQCD code

The eQCD code was developed by the authors of [48] to study the QCD phase structure at finite density and temperature. Here the same code is reused with the chemical potential being set to zero. In this section we give an overview about the truncation and approximation schemes used and the resulting differential equations describing the flow of the parameters of the theory.

Given specific initial conditions in the UV, these flow equations are then solved numerically with a Cash-Karp Runge-Kutta solver with adaptive step size control by the code. As results we get the parameters of the truncation in the IR with all quantum fluctuations integrated out.

4.1.1. Truncation

As discussed in the previous chapter, the flow equation cannot be solved exactly. We therefore have to use a sensible approximation that encapsulates all important physical

mechanisms. In our case the following truncation is employed:

$$\begin{aligned}\Gamma_k = \int_x \Big\{ & \frac{1}{4} F^a_{\mu\nu} F^a_{\mu\nu} + Z_{c,k} \left(\partial_\mu \bar{c}^a\right) D^{ab}_\mu c^b + \frac{1}{2\xi} (\partial_\mu A^a_\mu)^2 \\ & + \frac{1}{2} \int_p A^a_\mu(-p) \left(\Gamma^{(2)\,ab}_{AA\,\mu\nu}(p) - Z_{A,k} \Pi^{\perp}_{\mu\nu} \delta^{ab} p^2 \right) A^b_\nu(p) \\ & + \bar{q} \left[Z_{q,k} \gamma_\mu D_\mu + m_s(\sigma_s) \right] q - \lambda_{q,k} \left[(\bar{q}\, \tau^0 q)^2 + (\bar{q}\, \boldsymbol{\tau} q)^2 \right] + h_k\, \bar{q} \left(\tau^0 \sigma + \boldsymbol{\tau} \cdot \boldsymbol{\pi} \right) q \\ & + \frac{1}{2} Z_{\phi,k} \left(\partial_\mu \phi\right)^2 + V_k(\rho, A_0) - c_\sigma\, \sigma - \frac{1}{\sqrt{2}}\, c_{\sigma_s}\, \sigma_s \Big\} \end{aligned} \tag{4.1}$$

It includes the field strength tensor, ghost and gauge-fixing terms, a non-trivial momentum dependence for the gluon propagation, kinetic terms for quarks and mesons, a Yukawa interaction between them, a four-quark interaction, a potential of $\rho = \phi^2/2$ with $\phi = (\sigma, \boldsymbol{\pi})$ for the mesons, and the Polyakov loop potential for the gluons (this is approximated to be only dependent on the temporal mode A^0). Lastly, explicit symmetry breaking terms are included for the σ and σ_s fields. The meson fields in the FRG framework arise naturally by dynamical hadronization (see Section 3.5), of the four-quark interaction. Only the $\sigma - \pi$ channel is considered here, as it is expected to give the most dominant contribution.

This truncation is $O(4)$ symmetric, so in this chapter we leave no room for $U_A(1)$ restoration. That is more closely looked at in the next chapter via a truncation with a Fierz complete set of four-quark couplings, where effective $U_A(1)$ restoration is defined as the magnitude of the $U_A(1)$ violating parts of the couplings going below a certain threshold.

4.1.2. Flow equations

In this subsection the flow equations and involved approximations for the parameters in Eq. (4.1) are summarized. By nature the presentation is heavily based on the original paper [48].

Gluon potential

The effective potential is separated into a purely gluonic and a matter part

$$V_k\left(\rho, L, \bar{L}\right) = V_{\text{glue},k}\left(L, \bar{L}\right) + V_{\text{mat},k}\left(\rho, L, \bar{L}\right) \tag{4.2}$$

where subleading ρ-dependencies are ignored in the gluonic part (see Section III C in [48]). Here L and $\bar{L}$ are the traced Polyakov loops

$$L(\boldsymbol{x}) = \frac{1}{N_c} \left\langle \operatorname{tr} \mathcal{P}(\boldsymbol{x}) \right\rangle, \qquad \bar{L}(\boldsymbol{x}) = \frac{1}{N_c} \left\langle \operatorname{tr} \mathcal{P}^\dagger(\boldsymbol{x}) \right\rangle \tag{4.3}$$

	1	2	3	4	5
a_i	-44.14	151.4	-90.0677	2.77173	3.56403
b_i	-0.32665	-82.9823	3.0	5.85559	
c_i	-50.7961	114.038	-89.4596	3.08718	6.72812
d_i	27.0885	-56.0859	71.2225	2.9715	6.61433

Table 4.1.: Constants in Eq. (4.8) and Eq. (4.9). Taken from [48].

with

$$\mathcal{P}(\boldsymbol{x}) = \mathcal{P}\exp\left(ig\int_0^\beta d\tau\ \hat{A}_0(\boldsymbol{x},\tau)\right) \tag{4.4}$$

where the $\mathcal{P}$ without an argument stands for the path ordering operator. With the expectation value $A_0 = \langle\hat{A}_0\rangle$ the following approximation is made

$$L\left[A_0\right] \approx \frac{1}{N_c}\operatorname{tr}\mathcal{P}\left[A_0\right]. \tag{4.5}$$

Errors of the approximation can largely be attributed to a temperature dependent rescaling (see Section III F in [48]).

This approximation justifies the usage of lattice results for $V_{\text{glue},k}\left(L,\bar{L}\right)$, i.e. the flow of the gluonic potential is not evolved. Instead, for it the following parametrization is taken:

$$V_{\text{glue}}\left(L,\bar{L}\right) = -\frac{a(T)}{2}\bar{L}L + b(T)\ln M_H\left(L,\bar{L}\right) + \frac{c(T)}{2}\left(L^3+\bar{L}^3\right) + d(T)\left(\bar{L}L\right)^2 \tag{4.6}$$

where M_H is the Haar measure

$$M_H\left(L,\bar{L}\right) = 1 - 6\bar{L}L + 4\left(L^3+\bar{L}^3\right) - 3\left(\bar{L}L\right)^2 \tag{4.7}$$

The temperature dependent functions a, b, c and d are defined by

$$x(T) = \frac{x_1 + x_2/(t_{\text{YM}}+1) + x_3/(t_{\text{YM}}+1)^2}{1 + x_4/(t_{\text{YM}}+1) + x_5/(t_{\text{YM}}+1)^2} \tag{4.8}$$

for $x \in \{a, c, d\}$, and

$$b(T) = b_1(t_{\text{YM}}+1)^{-b_4}\left(1 - e^{b_2/(t_{\text{YM}}+1)^{b_3}}\right) \tag{4.9}$$

with the coefficients shown in Table 4.1. Unquenching effects are accounted for, by setting $t_{\text{YM}} = \alpha\, t_{\text{glue}}$ with $t_{\text{glue}} = (T - T_c^{\text{glue}})/T_c^{\text{glue}}$, $\alpha = 0.57$ and $T_c^{\text{glue}} = 250$ MeV for $N_f = 2$ and $T_c^{\text{glue}} = 225$ MeV for $N_f = 2+1$ (see Appendix G of [48]).

The presence of a non-trivial Polyakov loop expectation value affects the flow of the other parameters that are being evolved by modifying the quark distribution function (see Appendix N of [48]):

$$n_F(m^2;T,L,\bar{L}) = \frac{1+2\bar{L}e^{x/T}+Le^{2x/T}}{1+3\bar{L}e^{x/T}+3Le^{2x/T}+e^{3x/T}} \tag{4.10}$$

with $x = k(1+m^2)^{1/2}$ (assuming a vanishing chemical potential). This reduces to the ordinary quark distribution function in the trivial case $L = \bar{L} = 1$. For brevity the dependence of n_F on the Polyakov loop expectation value is not written out explicitly after this.

Matter potential

The flow equation presented in the previous chapter gives us the following expression for the evolution of the potential, a function of $\rho = (\sigma^2 + \vec{\pi}^2)/2$,

$$\begin{aligned}\partial_t V_{\mathrm{mat},k}(\rho) = \frac{k^4}{4\pi^2}\Big[&(N_f^2-1)l_0^{(B,4)}(\tilde{m}^2_{\pi,k},\eta_{\phi,k};T) + l_0^{(B,4)}(\tilde{m}^2_{\sigma,k},\eta_{\phi,k};T) \\ &- 4N_cN_f l_0^{(F,4)}(\tilde{m}^2_{q,k},\eta_{q,k};T)\Big]\end{aligned} \tag{4.11}$$

where all regulator dependence has been absorbed into the threshold functions $l_0^{(B/F,4)}$ defined in Appendix D. They depend on the dimensionless quark and meson masses

$$\tilde{m}^2_{q,k} = \frac{h_k^2\rho}{2k^2Z^2_{q,k}}, \qquad \tilde{m}^2_{\pi,k} = \frac{V_k'(\rho)}{k^2\bar{Z}_{\phi,k}}, \qquad \tilde{m}^2_{\sigma,k} = \frac{V_k'(\rho)+2\rho V_k''(\rho)}{k^2\bar{Z}_{\phi,k}} \tag{4.12}$$

with the anomalous dimensions $\eta_{q,k} = -\partial_t Z_{q,k}/Z_{q,k}$, $\eta_{\phi,k} = -\partial_t Z_{\phi,k}/Z_{\phi,k}$ and $\bar{Z}_{\phi,k}$ to be defined in the next subsubsection.

For the functional form of the potential a Taylor expansion is chosen

$$V_{\mathrm{mat},k}(\rho) = \sum_{n=0}^{N_v}\frac{\lambda_{n,k}}{n!}(\rho-\kappa_k)^n \tag{4.13}$$

with $N_v = 5$. For convenience a switch to RG-invariant variables $\bar{\rho} = \bar{Z}_{\phi,k}\rho$, $\bar{\kappa}_k = \bar{Z}_{\phi,k}\kappa_k$, and $\bar{\lambda}_{n,k} = \lambda_{n,k}/\bar{Z}^n_{\phi,k}$ is performed, such that

$$V_{\mathrm{mat},k}(\rho) = \bar{V}_{\mathrm{mat},k}(\bar{\rho}) = \sum_{n=0}^{N_v}\frac{\bar{\lambda}_{n,k}}{n!}(\bar{\rho}-\bar{\kappa}_k)^n. \tag{4.14}$$

For the expansion point $\bar{\kappa}_k$ the minimum of the potential is chosen.

By performing derivatives w.r.t $\bar{\rho}$ and evaluating at the expansion point, the flow of the individual Taylor coefficients is obtained:

$$\partial_t \bar{\lambda}_{n,k} = \partial_{\bar{\rho}}^n \big(\partial_t\big|_\rho \bar{V}_k(\bar{\rho})\big)\Big|_{\bar{\rho}=\bar{\kappa}_k} + n\eta_{\phi,k}\bar{\lambda}_{n,k} + \big(\partial_t\bar{\kappa}_k + \eta_{\phi,k}\bar{\kappa}_k\big)\bar{\lambda}_{n+1,k}$$

The flow of the minimum itself can be found via the condition

$$\frac{\partial}{\partial\bar{\rho}}\Big(\bar{V}_k(\bar{\rho}) - \bar{c}_k\bar{\sigma}\Big)\Big|_{\bar{\rho}=\bar{\kappa}_k} = 0 \tag{4.15}$$

resulting in

$$\partial_t\bar{\kappa}_k = -\frac{\bar{c}_k^2}{\bar{\lambda}_{1,k}^3 + \bar{c}_k^2\bar{\lambda}_{2,k}}\left[\eta_{\phi,k}\Big(\frac{\bar{\lambda}_{1,k}}{2} + \bar{\kappa}_k\bar{\lambda}_{2,k}\Big) + \partial_{\bar{\rho}}\partial_t\big|_\rho\bar{V}_k(\bar{\rho})\big)\Big|_{\bar{\rho}=\bar{\kappa}_k}\right]. \tag{4.16}$$

See Appendix F of [48].

To incorporate the strange sector a simple approximation

$$V_k(\rho,\rho_s) \approx V_k(\rho) + \frac{1}{2}V_k(2\rho_s) \tag{4.17}$$

is chosen. So the expectation value for σ_s is specified by the potential $V_k(\rho)$ as well, but with a different coefficient for the explicit symmetry breaking (see Appendix A of [48]).

The light and strange quark masses are given by the expectation values such that

$$\bar{m}_l = \frac{1}{2}\bar{h}\bar{\sigma} \qquad \text{and} \qquad \bar{m}_s = \frac{1}{\sqrt{2}}\bar{h}\bar{\sigma}_s, \tag{4.18}$$

see Section III C of [48].

Meson wave function renormalization

The meson two-point functions for a given $\phi_0 = (\sigma_0, \boldsymbol{\pi} = 0)$ read

$$\Gamma^{(2)}_{\sigma\sigma}(p) = Z_{\sigma,k}(p)\,p^2 + m_\sigma^2 \tag{4.19}$$

$$\Gamma^{(2)}_{\pi_i\pi_i}(p) = Z_{\pi,k}(p)\,p^2 + m_\pi^2. \tag{4.20}$$

with the masses and wave function renormalizations

$$m_\pi^2 = \partial_\rho V_k \qquad m_\sigma^2 = m_\pi^2 + 2\rho\,\partial_\rho^2 V_k \tag{4.21}$$

$$Z_\pi(p) = Z_\phi(p) \qquad Z_\sigma(p) = Z_\phi(p) + \rho\partial_\rho Z_\phi(p). \tag{4.22}$$

The mesonic wave function renormalization is approximated to not depend on the mesonic field since those contributions are suppressed at low energies which is the only regime where they could come into play. So the mesonic wave function renormalization is fully specified by the pion two-point function, i.e.

$$Z_\phi(p) = \frac{1}{3}\delta_{ij}\frac{1}{p^2}\left[\Gamma^{(2)}_{\pi_i\pi_j}(p) - \Gamma^{(2)}_{\pi_i\pi_j}(0)\right]. \tag{4.23}$$

Also any thermal splitting is ignored and only the part transversal to the heat bath is used. Instead of the full momentum spectrum, only two specific momentum values of the wave function renormalization are evolved, $Z_\phi(0)$ and $Z_\phi(k)$. The reasoning is the following:

First, by definition we have for the two-point function with the physical pion pole mass

$$0 = \Gamma^{(2)}_{\pi_i\pi_i}(p_0 = im_{\pi,\text{pol}},\, \boldsymbol{p}^2 = 0) \overset{(4.20)}{=} Z_{\pi,k}(im_{\pi,\text{pol}}, 0)\left(im_{\pi,\text{pol}}\right)^2 + m_\pi^2. \tag{4.24}$$

Since we are restricted to $p_0^2 \geq 0$, we approximate $Z_\pi(im_{\pi,\text{pol}}, 0) \approx Z_\pi(0,0) = Z_\phi(0)$ and have

$$m^2_{\pi,\text{pol}} = \frac{1}{Z_\phi(0)} m_\pi^2. \tag{4.25}$$

So $Z_\phi(0)$ is necessary to obtain the physical pion mass from the curvature of the potential once the flow equations are integrated out. It is obtained from Eq. (4.23) by first setting $p_0 = 0$ and then taking $\boldsymbol{p}^2 \to 0$ yielding

$$Z_\phi(0) = \frac{1}{3}\delta_{ij}\left[\frac{\partial\Gamma^{(2)}_{\pi_i\pi_j}}{\partial\boldsymbol{p}^2}\right](p=0) \tag{4.26}$$

and for the anomalous dimension

$$\eta_\phi(0) = -\partial_t Z_\phi(0)/Z_\phi(0) = -\frac{1}{3Z_\phi(0)}\delta_{ij}\left[\frac{\partial}{\partial\boldsymbol{p}^2}\partial_t\Gamma^{(2)}_{\pi_i\pi_j}\right](p=0). \tag{4.27}$$

Secondly, within the loop of the flow equation the momentum integration is peaked around k for vanishing external momentum. This justifies the usage of

$$\bar{Z}_{\phi,k} \equiv Z_\phi(k) \overset{(4.23)}{=} \frac{1}{3}\delta_{ij}\frac{1}{k^2}\left[\Gamma^{(2)}_{\pi_i\pi_j}(0,k) - \Gamma^{(2)}_{\pi_i\pi_j}(0,0)\right] \tag{4.28}$$

in the flow equation when meson propagators are part of the loop. Here $(0,k)$ stands for $(p_0 = 0, \boldsymbol{p}^2 = k^2)$. For the corresponding anomalous dimension we have

$$\eta_\phi(0,k) = -\partial_t\bar{Z}_{\phi,k}/\bar{Z}_{\phi,k} = -\frac{\delta_{ij}}{3\bar{Z}_{\phi,k}}\frac{\partial_t\Gamma^{(2)}_{\pi_i\pi_j}(0,k) - \partial_t\Gamma^{(2)}_{\pi_i\pi_j}(0,k)}{k^2}. \tag{4.29}$$

see Section IV A 1. of [48].

By carrying out the derivations specified on the right sides of Eq. (4.27) and Eq. (4.29), the expressions

$$\eta_\phi(0) = \frac{\bar{Z}_\phi}{Z_\phi(0)} \frac{1}{6\pi^2} \Bigg\{ \frac{4}{k^2} \bar{\kappa}_k (\bar{V}_k''(\bar{\kappa}_k))^2 \mathcal{BB}_{(2,2)}(\tilde{m}^2_{\pi,k}, \tilde{m}^2_{\sigma,k}; T) + N_c \bar{h}_k^2 \Big[(2\eta_{q,k} - 3) \mathcal{F}_{(2)}(\tilde{m}^2_{q,k}; T, \mu_q) - 4(\eta_{q,k} - 2) \mathcal{F}_{(3)}(\tilde{m}^2_{q,k}; T, \mu_q) \Big] \Bigg\} \tag{4.30}$$

and

$$\begin{aligned} \eta_\phi(0,k) =& \frac{2}{3\pi^2} \frac{1}{k^2} \bar{\kappa}_k (\bar{V}_k''(\bar{\kappa}_k))^2 \mathcal{BB}_{(2,2)}(\tilde{m}^2_{\pi,k}, \tilde{m}^2_{\sigma,k}; T) - \frac{N_c}{\pi^2} \bar{h}_k^2 \int_0^1 dx \Big[(1 - \eta_{q,k}) \sqrt{x} + \eta_{q,k} x \Big] \\ & \times \int_{-1}^1 d\cos\theta \Bigg\{ \Big[\Big(\mathcal{FF}_{(1,1)}(\tilde{m}^2_{q,k}, \tilde{m}^2_{q,k}) - \mathcal{F}_{(2)}(\tilde{m}^2_{q,k}) \Big) - \Big(\mathcal{FF}_{(2,1)}(\tilde{m}^2_{q,k}, \tilde{m}^2_{q,k}) - \mathcal{F}_{(3)}(\tilde{m}^2_{q,k}) \Big) \Big] \\ & + \Big[\Big(\sqrt{x} - \cos\theta \Big) \Big(1 + r_F(x') \Big) \mathcal{FF}_{(2,1)}(\tilde{m}^2_{q,k}, \tilde{m}^2_{q,k}) - \mathcal{F}_{(3)}(\tilde{m}^2_{q,k}) \Big] \\ & - \frac{1}{2} \Big[\Big(\sqrt{x} - \cos\theta \Big) \Big(1 + r_F(x') \Big) \mathcal{FF}_{(1,1)}(\tilde{m}^2_{q,k}, \tilde{m}^2_{q,k}) - \mathcal{F}_{(2)}(\tilde{m}^2_{q,k}) \Big] \Bigg\} \end{aligned} \tag{4.31}$$

are obtained for the anomalous dimensions within the truncation. In Eq. (4.31) $x = \boldsymbol{q}^2/k^2$ and $x' = (\boldsymbol{q} - \boldsymbol{p})^2/k^2$ with loop and external momentum $\boldsymbol{q}$ and $\boldsymbol{p}$, respectively. The angle between them is denoted by θ and for the absolute value of the external momentum $|\mathbf{p}| = k$ is used. See Appendix I of [48].

The threshold functions and regulator shape functions in Eq. (4.30) and Eq. (4.31) are defined in Appendix D

Quark wave function renormalization

The quark two-point function reads

$$\Gamma^{(2)}_{q\bar{q}}(p) = \; Z_q(p) \; \left[i\not{p} + M_q(p) \right]. \tag{4.32}$$

The wave function renormalization can be extracted via

$$Z_{q_i}(p) = \; \frac{1}{4N_c} \frac{1}{p^2} \, \mathrm{tr} \not{p} \, \Gamma^{(2)}_{q_i \bar{q}_i}(p) \tag{4.33}$$

Also here thermal splitting is ignored and only the part transversal to the heat bath is used. Only one momentum value is evolved, a small $p_0 > 0$ and $\boldsymbol{p} = 0$. The anomalous dimension reads

$$\eta_{q_i}(p_0) = -\partial_t Z_{q_i,k}(p_0)/Z_{q_i,k}(p_0) = \frac{1}{4\, Z_{q_i,k}(p_0)} \mathrm{Re}\left[i \frac{\partial}{\partial \boldsymbol{p}^2} \mathrm{tr}\, \boldsymbol{\gamma} \cdot \boldsymbol{p}\, \partial_t \Gamma^{(2)}_{\bar{q}_i q_i, k}(p) \right]_{\boldsymbol{p}=0}, \quad (4.34)$$

see Section IV A 1. in [48].

Plugging this into the flow equation for the given truncation results in

$$\begin{aligned} \eta_{q,k} =& \frac{1}{24\pi^2 N_f}(4 - \eta_{\phi,k})\bar{h}_k^2 \\ & \times \left\{ (N_f^2 - 1)\mathcal{FB}_{(1,2)}(\tilde{m}^2_{q,k}, \tilde{m}^2_{\pi,k}; T, p_{0,\mathrm{ex}}) + \mathcal{FB}_{(1,2)}(\tilde{m}^2_{q,k}, \tilde{m}^2_{\sigma,k}; T, p_{0,\mathrm{ex}}) \right\} \\ & + \frac{1}{24\pi^2} \frac{N_c^2 - 1}{2N_c} g^2_{\bar{q}Aq,k} \times \Big\{ 2(4 - \eta_{A,k})\mathcal{FB}_{(1,2)}(\tilde{m}^2_{q,k}, 0; T, p_{0,\mathrm{ex}}) \\ & + 3(3 - \eta_{q,k}) \Big(\mathcal{FB}_{(1,1)}(\tilde{m}^2_{q,k}, 0; T, p_{0,\mathrm{ex}}) - 2\mathcal{FB}_{(2,1)}(\tilde{m}^2_{q,k}, 0; T, p_{0,\mathrm{ex}}) \Big) \Big\}. \end{aligned} \quad (4.35)$$

The threshold functions here are defined in Appendix D. The fermionic Matsubara modes are $p_0 = (2n+1)\pi T$ with $n \in \mathbb{Z}$, so $p_{0,\mathrm{ex}}$ cannot chosen to be zero. Ideally, the whole momentum spectrum could be resolved, however this is computationally very demanding. Instead, a modification of the lowest Matsubara mode is chosen, $p_{0,\mathrm{ex}} = (\pi T)\exp\{-k/(\pi T)\}$ for the vacuum parts and $p_{0,\mathrm{ex}} = \pi T$ for the thermal parts, see Appendix J of [48].

Gluon anomalous dimension

The gluon anomalous dimension is split into a vacuum term and finite temperature contributions of gluons and quarks:

$$\eta_A = \eta^{\mathrm{QCD}}_{A,\mathrm{vac}} + \Delta\eta^{\mathrm{glue}}_A + \Delta\eta^q_A \quad (4.36)$$

For the first term results from [49] are used. There the full momentum dependence of $Z^{\mathrm{QCD}}_{A,k=0}(p)$ for two-flavor QCD was computed. This is now evaluated at $p = k$ to obtain

$$\eta^{\mathrm{QCD}}_{A,\mathrm{vac}}\Big|_{N_f=2} = -\left.\frac{\partial_t Z^{\mathrm{QCD}}_{A,k=0}(p)}{Z^{\mathrm{QCD}}_{A,k=0}(p)}\right|_{p=k}. \quad (4.37)$$

The contribution of the strange quark is added separately:

$$\eta^{\text{QCD}}_{A,\text{vac}} = \eta^{\text{QCD}}_{A,\text{vac}}\Big|_{N_f=2} + \eta^{s}_{A,\text{vac}} \tag{4.38}$$

The vacuum QCD gluon anomalous dimension is a sum of the pure Yang-Mills part and a separate matter term

$$\eta^{\text{QCD}}_{A,\text{vac},k} = \eta^{\text{glue}}_{A,\text{vac}}\left(\alpha_k, \bar{m}^2_{A,k}\right) + \eta^{\text{quark}}_{A,\text{vac},k} \tag{4.39}$$

where $\eta^{\text{glue}}_{A,\text{vac}}$ depends on the coupling ,α_k and renormalized transversal gluon mass $\bar{m}^2_{A,k}$ (see Section III B of [48]). Back coupling of the quarks to the first term is taken into account by their contributions to α_k and $\bar{m}^2_{A,k}$. For the thermal contributions no back coupling is taken into account. See Section IV A 2 of [48].

As an explicit expression for the third term in Eq. (4.36) one has

$$\Delta\eta^q_A = \eta^q_A - \eta^q_A\big|_{T=0} \tag{4.40}$$

with

$$\begin{aligned}\eta^q_A = &-\frac{N_f}{\pi^2} g^2_{\bar{q}Aq,k} \int_0^1 dx \left[(1-\eta_{q,k})\sqrt{x} + \eta_{q,k}x\right] \\ &\times \int_{-1}^{1} d\cos\theta \left[\left(\mathcal{FF}_{(1,1)}(\tilde{m}^2_{q,k}, \tilde{m}^2_{q,k}) - \mathcal{FF}_{(2,1)}(\tilde{m}^2_{q,k}, \tilde{m}^2_{q,k})\right) + \left(\sqrt{x}\cos^2\theta - \cos\theta\right)\right. \\ &\left.\times \left(1 + r_F(x')\right)\left(\mathcal{FF}_{(2,1)}(\tilde{m}^2_{q,k}, \tilde{m}^2_{q,k}) - \frac{1}{2}\mathcal{FF}_{(1,1)}(\tilde{m}^2_{q,k}, \tilde{m}^2_{q,k})\right)\right]\end{aligned} \tag{4.41}$$

Here $x = \boldsymbol{q}^2/k^2$ and $x' = (\boldsymbol{q}-\boldsymbol{p})^2/k^2$ with loop and external momentum $\boldsymbol{q}$ and $\boldsymbol{p}$, respectively. The angle between them is denoted by θ and for the absolute value of the external momentum $|\mathbf{p}| = k$ is used.

The second term of Eq. (4.36) is accounted for by the introduction of a thermal screening mass for the gluon by setting

$$\bar{Z}_{A,k}k^2 = Z_{A,k}k^2 + \Delta m^2_{\text{scr}}(k,T). \tag{4.42}$$

Applying ∂_t to this equality leads to

$$\bar{\eta}_A = \eta_A + \frac{\Delta m^2_{\text{scr}}(k,T)}{\bar{Z}_A k^2}(2-\eta_A) - \frac{1}{\bar{Z}_A k^2}\partial_t\left(\Delta m^2_{\text{scr}}(k,T)\right).$$

with $\bar{\eta}_A = -\partial_t \bar{Z}_A / \bar{Z}_A$ being the anomalous dimension that includes the effect of the screening mass. For the screening mass the term

$$\Delta m_{\text{scr}}^2(k,T) = 4T^2 \exp\left[-\left(\frac{k}{\pi T}\right)^2\right] \tag{4.43}$$

is chosen. See Appendix H of [48].

Yukawa and four-quark coupling

The dynamical bosonization method presented in the previous chapter is applied to the truncation. It is crucial as it keeps the resonant interaction channels under control (see Section III A of [48]).

For the scale dependent meson field

$$\langle \partial_t \hat{\phi}_k \rangle = \dot{A}_k \, \bar{q} \tau q \tag{4.44}$$

is chosen. As illustrated in Section 3.5 this now leads to

$$\partial_t \bar{\lambda}_q - 2\,(1+\eta_q)\,\bar{\lambda}_q - \bar{h}\,\dot{\bar{A}} = \overline{\text{Flow}}^{(4)}_{(\bar{q}\tau q)(\bar{q}\tau q)} \tag{4.45}$$

with the renormalized quantities $\bar{\lambda}_q = \lambda_q \, k^2 / Z_q^2$, $\bar{h} = h/(Z_\phi^{1/2} Z_q)$ and $\dot{\bar{A}} = Z_\phi^{1/2} \dot{A} \, k^2 / Z_q$. The r.h.s. consists of contributions from two gluon exchange processes, two meson exchange processes and a mixed term with one gluon and one meson being exchanged. The two gluon exchange dominates the large and intermediate scales, the two meson exchange dominates the low scales. Therefore the mixed contributions are neglected. To fully hadronize the four-quark interaction

$$\dot{\bar{A}} = -\frac{1}{\bar{h}} \, \overline{\text{Flow}}^{(4)}_{(\bar{q}\tau q)(\bar{q}\tau q)} \tag{4.46}$$

is chosen. This keeps the four-quark interaction constantly zero (if it is initially set to zero when the RG evolution starts). See Section III E of [48].

For the Yukawa coupling any dependence on ρ is considered subleading and is neglected. Since the pions are massless and we have three of them (instead of one sigma), the vertex involving the pion is used to define a single Yukawa coupling for the truncation. For the flow of it the result is

$$\partial_t \bar{h} = \left(\frac{1}{2}\eta_\phi + \eta_q\right) \bar{h} - \bar{m}_\pi^2 \, \dot{\bar{A}} + \overline{\text{Flow}}^{(3)}_{(\bar{q}\boldsymbol{\tau} q)\boldsymbol{\pi}}. \tag{4.47}$$

However, there is a simpler expression utilizing the quark two-point function:

$$\partial_t \bar{h} = \left(\frac{1}{2}\eta_\phi + \eta_q\right)\bar{h} - \bar{m}_\pi^2\,\dot{\bar{A}} + \frac{1}{\bar{\sigma}}\mathrm{Re}\,\overline{\mathrm{Flow}}^{(2)}_{\bar{q}\tau^0 q} \tag{4.48}$$

See Section IV C of [48].

The explicit expressions for the flows are

$$\begin{aligned}\mathrm{Re}\big(\overline{\mathrm{Flow}}^{(2)}_{(\bar{q}\tau^0 q)}\big)/\bar{\sigma} = \frac{1}{4\pi^2 N_f}\bar{h}_k^3\Big[&-(N_f^2-1)L^{(4)}_{(1,1)}\left(\tilde{m}^2_{q,k},\tilde{m}^2_{\pi,k},\eta_{q,k},\eta_{\phi,k};T,p_{0,\mathrm{ex}}\right)\\ &+ L^{(4)}_{(1,1)}\left(\tilde{m}^2_{q,k},\tilde{m}^2_{\sigma,k},\eta_{q,k},\eta_{\phi,k};T,p_{0,\mathrm{ex}}\right)\Big] - \frac{3}{2\pi^2}\frac{N_c^2-1}{2N_c}g^2_{\bar{q}Aq,k}\bar{h}_k L^{(4)}_{(1,1)}\left(\tilde{m}^2_{q,k},0,\eta_{q,k},\eta_{A,k};T,p_{0,\mathrm{ex}}\right)\end{aligned} \tag{4.49}$$

with $p_{0,\mathrm{ex}}$ as for the quark anomalous dimension, see Appendix K of [48]. And for the two gluon and two meson exchange contributions to the four-quark coupling (or rather the hadronization function Eq. (4.46))

$$\begin{aligned}\overline{\mathrm{Flow}}^{(4),A}_{(\bar{q}q)(\bar{q}q)} = &-\frac{3}{2\pi^2}\frac{N_c^2-1}{2N_c}\Big(\frac{3}{4}-\frac{1}{N_c^2}\Big)g^4_{\bar{q}Aq,k}\\ &\times\Big\{\frac{2}{15}(5-\eta_{A,k})\Big[\mathcal{FB}_{(1,3)}(\tilde{m}^2_{q,k},0)-\bar{m}^2_{q,k}\mathcal{FB}_{(2,3)}(\tilde{m}^2_{q,k},0)\Big]\\ &+\frac{1}{12}(4-\eta_{q,k})\Big[\mathcal{FB}_{(2,2)}(\tilde{m}^2_{q,k},0)-2\bar{m}^2_{q,k}\mathcal{FB}_{(3,2)}(\tilde{m}^2_{q,k},0)\Big]\Big\}\end{aligned} \tag{4.50}$$

and

$$\begin{aligned}\overline{\mathrm{Flow}}^{(4),\phi}_{(\bar{q}q)(\bar{q}q)} = &\frac{1}{32\pi^2}\frac{N_f^2-2}{N_f N_c}\bar{h}_k^4\Big\{\frac{2}{15}(5-\eta_{\phi,k})\\ &\times\Big[\Big(\mathcal{FBB}_{(1,1,2)}(\tilde{m}^2_{q,k},\tilde{m}^2_{\pi,k},\tilde{m}^2_{\sigma,k})+\mathcal{FBB}_{(1,1,2)}(\tilde{m}^2_{q,k},\tilde{m}^2_{\sigma,k},\tilde{m}^2_{\pi,k})\\ &-2\mathcal{FB}_{(1,3)}(\tilde{m}^2_{q,k},\tilde{m}^2_{\pi,k})\Big)-\tilde{m}^2_{q,k}\Big(\mathcal{FBB}_{(2,1,2)}(\tilde{m}^2_{q,k},\tilde{m}^2_{\pi,k},\tilde{m}^2_{\sigma,k})\\ &+\mathcal{FBB}_{(2,2,1)}(\tilde{m}^2_{q,k},\tilde{m}^2_{\pi,k},\tilde{m}^2_{\sigma,k})-2\mathcal{FB}_{(2,3)}(\tilde{m}^2_{q,k},\tilde{m}^2_{\pi,k})\Big)\Big]\\ &+\frac{1}{6}(4-\eta_{q,k})\times\Big[\Big(\mathcal{FBB}_{(2,1,1)}(\tilde{m}^2_{q,k},\tilde{m}^2_{\pi,k},\tilde{m}^2_{\sigma,k})-\mathcal{FB}_{(2,2)}(\tilde{m}^2_{q,k},\tilde{m}^2_{\pi,k})\Big)\\ &-2\tilde{m}^2_{q,k}\Big(\mathcal{FBB}_{(3,1,1)}(\tilde{m}^2_{q,k},\tilde{m}^2_{\pi,k},\tilde{m}^2_{\sigma,k})-\mathcal{FB}_{(3,2)}(\tilde{m}^2_{q,k},\tilde{m}^2_{\pi,k})\Big)\Big]\Big\}\end{aligned} \tag{4.51}$$

are obtained. See Appendix L of [48]. With this all contributions to the Yukawa coupling are specified.

Strong couplings

Two different strong couplings are considered in the truncation, $g_{\bar{q}Aq}$ and g_{A^3}. They appear in the covariant derivative and gluonic field strength tensor of the truncation:

$$D_\mu = \partial_\mu - iZ_A^{1/2} g_{\bar{q}Aq} A_\mu^a t^a \,, \tag{4.52}$$

$$F_{\mu\nu}^a = Z_A^{1/2} \left(\partial_\mu A_\nu^a - \partial_\nu A_\mu^a + Z_A^{1/2} g_{A^3} f^{abc} A_\mu^b A_\nu^c \right) \tag{4.53}$$

For the quark-gluon coupling $g_{\bar{q}Aq}$ only the classical tensor structure is considered in the flow. This leads to an underestimation of the true strength in the IR. To properly account for that an IR enhancement of the flow at lower scales is done. See Section IV B 1 of [48].

The flow of $g_{\bar{q}Aq}$ receives contributions from meson and gluon exchanges. For the light quarks the following expressions are obtained:

$$\partial_t g_{\bar{l}Al} = \left(\frac{1}{2}\eta_A + \eta_q \right) g_{\bar{l}Al} + \left(N_f \, \overline{\text{Flow}}_{(\bar{l}Al)}^{(3),A} + \overline{\text{Flow}}_{(\bar{l}Al)}^{(3),\phi} \right) \Big|_{N_f=2} \tag{4.54}$$

with the gluonic contribution

$$\begin{aligned}
\overline{\text{Flow}}_{(\bar{q}Aq)}^{(3),A} = {} & \frac{3}{8\pi^2 N_c} g_{\bar{q}Aq}^3 \tilde{m}_{q,k}^2 \left\{ \frac{2}{15}(5-\eta_{A,k}) \mathcal{FB}_{(2,2)}(\tilde{m}_{q,k}^2, 0) + \frac{1}{3}(4-\eta_{q,k}) \mathcal{FB}_{(3,1)}(\tilde{m}_{q,k}^2, 0) \right\} \\
& + \frac{3N_c}{8\pi^2} g_{\bar{q}Aq}^2 g_{A^3} \left\{ \frac{1}{20}(5-\eta_{q,k}) \mathcal{FB}_{(1,2)}(\tilde{m}_{q,k}^2, 0) - \frac{1}{6}(4-\eta_{q,k}) \mathcal{FB}_{(2,1)}(\tilde{m}_{q,k}^2, 0) \right. \\
& + \frac{1}{30}(5-2\eta_{q,k}) \mathcal{FB}_{(2,2)}(\tilde{m}_{q,k}^2, 0) - \frac{4}{15}(5-\eta_{A,k}) \mathcal{FB}_{(1,2)}(\tilde{m}_{q,k}^2, 0) \\
& \left. + \frac{1}{30}(10-3\eta_{A,k}) \mathcal{FB}_{(1,3)}(\tilde{m}_{q,k}^2, 0) \right\}
\end{aligned} \tag{4.55}$$

and the mesonic contribution

$$\begin{aligned}\overline{\text{Flow}}^{(3),\phi}_{(\bar{q}Aq)} = &-\frac{1}{8\pi^2 N_f} g_{\bar{q}Aq}\bar{h}_k^2 \Bigg\{ \frac{1}{6}(4-\eta_{q,k})\Big[\mathcal{FB}_{(2,1)}(\tilde{m}_{q,k}^2,\tilde{m}_{\sigma,k}^2) + 2\tilde{m}_{q,k}^2 \mathcal{FB}_{(3,1)}(\tilde{m}_{q,k}^2,\tilde{m}_{\sigma,k}^2)\Big] \\ &+ \frac{2}{15}(5-\eta_{\phi,k})\Big[\mathcal{FB}_{(1,2)}(\tilde{m}_{q,k}^2,\tilde{m}_{\sigma,k}^2) + \tilde{m}_{q,k}^2 \mathcal{FB}_{(2,2)}(\tilde{m}_{q,k}^2,\tilde{m}_{\sigma,k}^2)\Big]\Bigg\} \\ &- \frac{N_f^2-1}{8\pi^2 N_f} g_{\bar{q}Aq}\bar{h}_k^2 \Bigg\{ \frac{1}{6}(4-\eta_{q,k})\Big[\mathcal{FB}_{(2,1)}(\tilde{m}_{q,k}^2,\tilde{m}_{\pi,k}^2) + 2\tilde{m}_{q,k}^2 \mathcal{FB}_{(3,1)}(\tilde{m}_{q,k}^2,\tilde{m}_{\pi,k}^2)\Big] \\ &+ \frac{2}{15}(5-\eta_{\phi,k})\Big[\mathcal{FB}_{(1,2)}(\tilde{m}_{q,k}^2,\tilde{m}_{\pi,k}^2) + \tilde{m}_{q,k}^2 \mathcal{FB}_{(2,2)}(\tilde{m}_{q,k}^2,\tilde{m}_{\pi,k}^2)\Big]\Bigg\}. \end{aligned} \tag{4.56}$$

See Appendix M of [48].

For the strange quark coupling only the gluon exchange is considered:

$$\partial_t g_{\bar{s}As} = \left(\frac{1}{2}\eta_A + \eta_q\right) g_{\bar{s}As} + \overline{\text{Flow}}^{(3),A}_{(\bar{s}As)} \tag{4.57}$$

See Appendix C of [48].

The previously mentioned phenomenological infrared enhancement is implemented by the modification

$$\partial_t \bar{g}_{\bar{q}Aq} \to \bar{g}_{\bar{q}Aq}\, \partial_t \varsigma_{a,b}(k) + \varsigma_{a,b}(k) \partial_t \bar{g}_{\bar{q}Aq} \tag{4.58}$$

with the function

$$\varsigma_{a,b}(k) = 1 + a\frac{(k/b)^\delta}{\exp[(k/b)^\delta]-1}\,. \tag{4.59}$$

and parameters $b = 2$ GeV, $\delta = 2$ and $a = 0.034$ (for $N_f = 2+1$) which were determined by fitting the physical constituent quark masses. This leads to an enhancement factor of 1.034 in the IR. See Appendix E 2 of [48].

For the gluon coupling g_{A^3} the vacuum part $g_{A^3,\text{vac}}$ computed in [50] has been reused. This takes into account more tensor structures than just the classical ones and accordingly no IR enhancement procedure is performed for it. The temperature dependent part $\partial_t \Delta g_{A^3} = \partial_t g_{A^3} - \partial_t g_{A^3,\text{vac}}$ is taken to be equal to the one of the quark-gluon couplings, i.e. $\partial_t \Delta g_{A^3} = \partial_t \Delta g_{\bar{q}Aq}$. This is due to "RG-consistency", see Section IV B 2 of [48].

4.1.3. Initial conditions

The flow is started at the UV scale $\Lambda = 20$ GeV. At a pion mass of 140 MeV the strange to light quark mass ratio is fixed at 27 to enable comparisons with lattice studies.

The strong coupling is set to $g^2_{\bar{q}Aq,\Lambda}/(4\pi) = g^2_{A^3,\Lambda}/(4\pi) = 0.233$ to fix the peak position of the susceptibility at $T_{\text{peak}} = 156.5$ MeV at the pion mass of 140 MeV.

Then multiple runs of the eQCD code are executed with varying explicit symmetry breaking c in the UV, approaching the chiral limit.

4.2. Susceptibilities

In order to study the chiral transition, which is not easily directly numerically accessible, we instead look at the behavior of chiral susceptibilities when approaching the chiral limit. We can then extrapolate e.g. pseudo-critical temperatures (the peak position of the susceptibility for a given pion mass) to infer a transition temperature at the chiral limit.

Susceptibilities are defined as partial derivatives of condensates with respect to the "external field" which in our case is the light-quark current mass m_l^0:

$$\chi_M^{(i)}(T) = -\frac{\partial}{\partial m_l^0}\left(\frac{\Delta_i(T)}{m_l^0}\right) \tag{4.60}$$

For us, mostly the susceptibilities for the light-quark condensate, as well as the reduced condensate, are relevant. The first one comes more naturally in the FRG framework, while the second one is commonly used in lattice studies.

The individual quark condensates are defined as follows:

$$\begin{aligned}\Delta_{q_i} &= m_{q_i}^0 \frac{\partial \Omega(m_{q_i}); T}{\partial m_{q_i}^0} \\ &= m_{q_i}^0 \frac{T}{V}\int_0^{\frac{1}{T}} d\tau \int_V d^3x \, \langle \bar{q}_i(\tau,\vec{x}) q_i(\tau,\vec{x})\rangle\end{aligned} \tag{4.61}$$

where Ω is the grand potential and the chemical potentials have been set to zero in our case. We assume identical light-quark masses, such that

$$m_u^0 = m_d^0 = m_l^0 \qquad \text{and} \qquad \Delta_u = \Delta_d = \Delta_l \tag{4.62}$$

The previously mentioned reduced condensate is defined as

$$\Delta_{(l,s)} = \frac{1}{\mathcal{N}_{(l,s)}}\left[\Delta_l(T) - \left(\frac{m_l^0}{m_s^0}\right)^2 \Delta_s(T)\right] \tag{4.63}$$

We also have the renormalized condensate

$$\Delta_{(l,R)} = \frac{1}{\mathcal{N}_R}\left[\Delta_l(T) - \Delta_l(0)\right] \tag{4.64}$$

but since we are concerned about the temperature behavior of the susceptibilities, concentrating on $\Delta_l(T)$ is sufficient for us. $\mathcal{N}_{(l,s)}$ and $\mathcal{N}_R$ are m_l^0 independent normalization constants in the equations above. Both expressions remove the renormalization scheme dependence via the finite difference.

4.3. Data generation and analysis

This section describes how the author of the thesis obtained the results presented in the next section. Multiple runs of the eQCD code were performed with different explicit symmetry breaking terms c in the UV as initial condition. For each run the corresponding value for c was set in the Fortran source code, which was then compiled and executed. A Python orchestrator script was used to perform these steps in parallel for multiple values of $c \propto m_l^0$. In this way the chiral limit $c \to 0$ was approached. As output the eQCD code produced one `<quantity_name>.dat` file for each run for every quantity of interest in the `buffer` subfolder. This file contained a column vector with the IR values of the respective quantity for different temperatures in 1 MeV steps.

Once all runs were completed the data was collected from the subfolders, analyzed with a Mathematica notebook and the plots were created by Python scripts. The susceptibilities, as derivatives of $\Delta_{l,s}$ (the reduced condensate) or $\Delta_{l,R}$ (the renormalized condensate) with respect to m_l^0, were obtained via 1-dimensional Chebyshev interpolations for any fixed value of T, according to Section 5.9 of [51], to avoid numerical difficulties when performing the derivatives.

The eQCD code puts the renormalized σ-expectation value, $\langle\sigma_R\rangle$, into the file `fpi.dat`, so to get to the expectation value of the quark condensate one needs to divide by $\sqrt{Z_\sigma}$, see e.g. [37, 38], which can be read from `Zphi.dat`. So with $\langle\sigma\rangle$ denoting the bare expectation values, we have $-\Delta_{l,R}(T)/m_l^0 \propto [\langle\sigma\rangle(T) - \langle\sigma\rangle(T=0)]$, up to c-independent constants.

The file `Delta_ls.dat` actually contains the values for $\langle\sigma\rangle\left(1 - \frac{V'(\rho)}{V'(2\rho_s)}\right)$. After some manipulations (see also Appendix A in [48]) one sees that

$$\begin{aligned}\langle\sigma\rangle\left(1-\frac{V'(\rho)}{V'(2\rho_s)}\right) &= \left(\langle\sigma\rangle - \sqrt{2}\langle\sigma_s\rangle\frac{c_\sigma}{c_{\sigma_s}}\right) = -2\left(\frac{\Delta_l}{c_\sigma} - \frac{\Delta_s}{c_{\sigma_s}}\frac{c_\sigma}{c_{\sigma_s}}\right) \\ &= -\frac{2}{c_{\sigma_s}}\left(\frac{m_s}{m_l}\Delta_l - \frac{m_l}{m_s}\Delta_s\right) \propto -\Delta_{l,s}/m_l^0,\end{aligned} \tag{4.65}$$

where the proportionality is c-independent. So to calculate the reduced susceptibility, we can directly work with the output of the code. The normalizations and c-independent

factors do not affect our results, since we normalize everything by the peak height of the respective susceptibility at a pion mass of 140 MeV. Note that our definition of the reduced susceptibility is equivalent (up to c-independent factors) to the one of the lattice study in [52].

Apart from the numerical derivative in the c-direction, the renormalized susceptibility can also be directly calculated via the correlation length i.e. the inverse sigma mass [20], obtained via `mSigma.dat`. We have

$$\chi_M^{(l)} \propto \frac{1}{Z_\sigma m_\sigma^2} \tag{4.66}$$

This alternative method to obtain $\chi_M^{(l)}$ serves as an error estimate / consistency check for our results. The pion mass for each run is read from `mpion_phy.dat`.

Internally the code works with a Taylor expansion of the potential in ρ to order 5. Unfortunately other cases than order 5 don't seem to perform well in the c-direction, even though at fixed c the T-direction may look fine. For this reason a convergence analysis could not be performed.

The final results were produced with revision eQCDv43d7 of the code. Earlier versions contained some flaws leading to nonsensical results when approaching the chiral limit, which were discovered while tying to compute the susceptibilities as described in this section. These bugs were fixed by the maintainers of the code.

4.4. Results

In this section, we will look at the results of our simulations for the light-quark and the reduced susceptibility. Since we are ultimately interested in the behavior of the pseudo-critical temperature when the pion mass approaches zero, we can skip an investigation of the renormalized susceptibility, as previously explained.

Within the scaling regime of the theory, we can approximate

$$T_{pc}^{(i)} \approx T_c + c_i m_\pi^p \tag{4.67}$$

with $(i) = (l), (l,s)$ where T_c is the transition temperature in the chiral limit, $p = 2/(\beta\delta)$ for the universal critical exponents β and δ, and $c_{(i)}$ is a constant.

Eq. (4.67) can be found from Widom's scaling relation [53] via appropriate derivatives. Employing critical exponents of the 3d $O(4)$ universality class, we would have $p \approx 1.08$ [54–56]. However, based on previous FRG studies [57–60], we expect it to be slightly smaller.

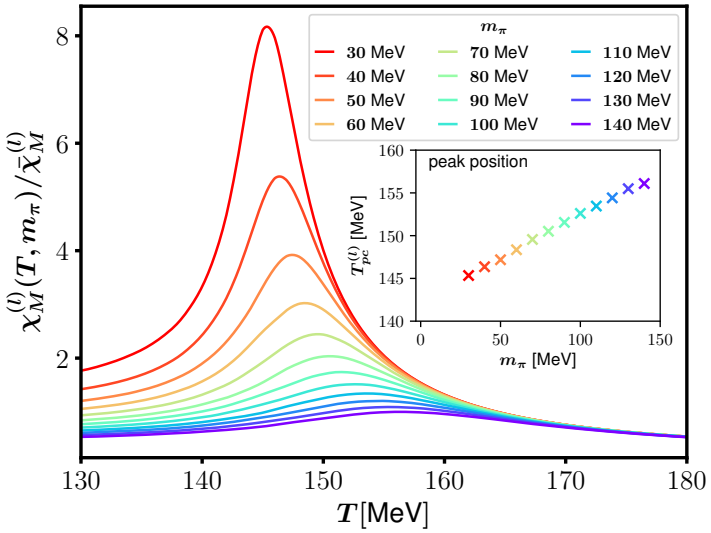

Figure 4.1.: Light-quark susceptibility $\chi_M^{(l)}$ as a function of temperature. The inset shows the respective peak positions. Taken from [61].

For the light-quark susceptibility, we obtain the results shown in Fig. 4.1

They are normalized with the value of the maximum of the susceptibility for $m_\pi = 140$ MeV, i.e.

$$\bar{\chi}_M^{(i)} = \max_T \chi_M^{(i)}(T)\Big|_{m_\pi = 140 \text{ MeV}} \tag{4.68}$$

As expected the susceptibilities approach a divergence for decreasing pion masses.

Performing a fit of the Eq. (4.67) for our data of the peak positions of the susceptibilities, we obtain

$$\begin{aligned} T_c &\approx 141.4^{+0.5}_{-0.5} \text{ MeV} \\ c_{(l)} &\approx 0.19^{+0.05}_{-0.05} \text{ MeV}^{1-p} \\ p &\approx 0.88^{+0.05}_{-0.05} \end{aligned} \tag{4.69}$$

The clear deviation of p from the 3d $O(4)$ value suggests that we are still far away from the scaling regime. Our results are in line with [62] that also found approximately linear behavior for the peak positions for pion masses $m_\pi > 75$ MeV and that the onset of actual scaling behavior is only below a pion mass of 1 MeV.

Since the behavior that we found is approximately linear, and we also expect the behavior in the true scaling regime to be approximately linear, we consider a linear fit of the results

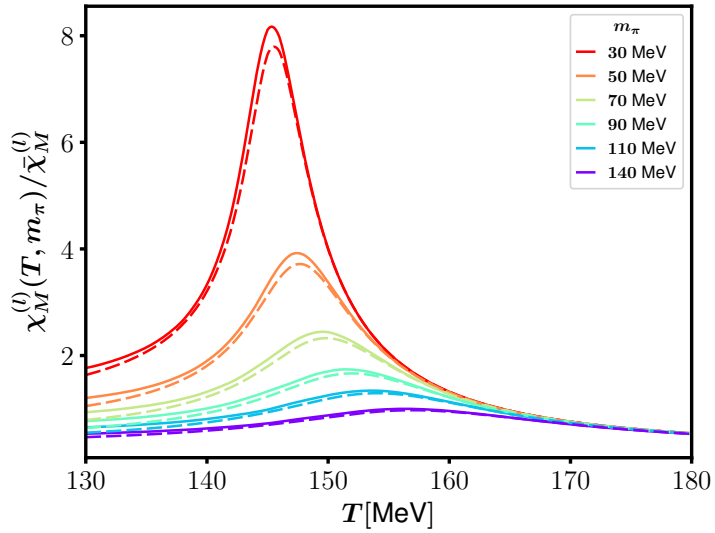

Figure 4.2.: Comparison of both methods by which $\chi_M^{(l)}$ was obtained. The solid lines correspond to the numerical derivative, the dashed lines to inverse sigma mass relation. Taken from [61].

for the pseudo-critical temperatures reasonable for a prediction of the chiral transition temperature, and obtain

$$T_c \approx 142.4^{+0.1}_{-0.1}\ \text{MeV} \tag{4.70}$$

Calculation of $\chi_M^{(l)}$ via Eq. (4.66) and comparing it with the previous results obtained via the numerical derivative allows us to check for self-consistency. The comparison is shown in Fig. 4.2. Both methods yield similar curves.

We also compare the quantity

$$D_{(l)}(m_\pi) = \frac{T_{pc}^{(l)(m_\pi)} - T_c}{T_c} \tag{4.71}$$

to previous studies. In [63] the quark-meson model was employed and a value of

$$D_{(l)}^{QM}(m_\pi = 140\ \text{MeV}) \approx 0.28 \tag{4.72}$$

was obtained. In our present study we instead find

$$D_{(l)}^{QCD}(m_\pi = 140\ \text{MeV}) \approx 0.10 \tag{4.73}$$

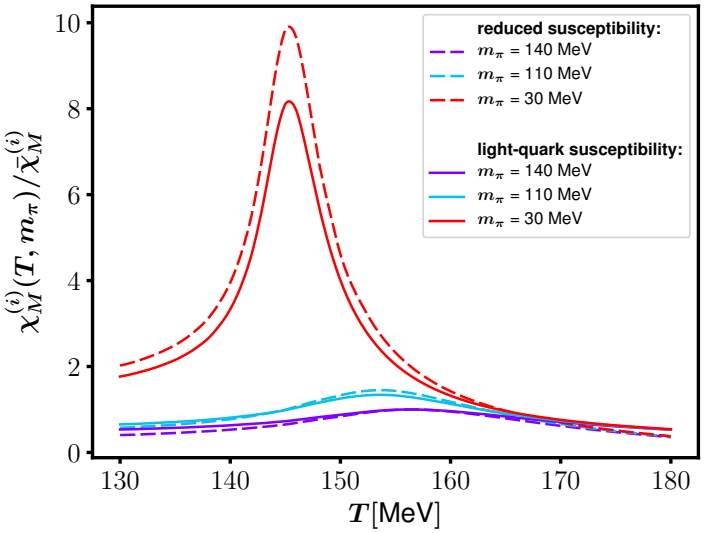

Figure 4.3.: Light-quark susceptibility $\chi_M^{(l)}$ compared to the reduced susceptibility $\chi_M^{(l,s)}$. Taken from [61].

We now turn to our results for the reduced susceptibility. In Fig. 4.3 a comparison to our previous results for the light-quark susceptibility is shown.

As expected, it also diverges when approaching the chiral limit. By fitting the peak positions to the scaling relation, we obtain

$$\begin{aligned} T_c &\approx 141.6^{+0.3}_{-0.3}\ \text{MeV} \\ c_{(l,s)} &\approx 0.17^{+0.03}_{-0.03}\ \text{MeV}^{1-p} \\ p &\approx 0.91^{+0.03}_{-0.03} \end{aligned} \tag{4.74}$$

which is consistent within errors with our previous results. We conclude that we are not in the scaling regime for pion masses $m_\pi > 30$ MeV that we considered.

The value for $D^{QCD}_{(l,s)}(m_\pi = 140\ \text{MeV})$ almost coincides with the previously obtained one.

As mentioned earlier, the reduced susceptibility is also computable via lattice QCD simulations. A comparison of our results with the ones from the HotQCD collaboration [52] is shown in Fig. 4.4 We have excellent agreement for pion masses $m_\pi > 100$ MeV. For smaller masses there are some deviations which may be caused to some degree by finite size effects for the lattice simulations.

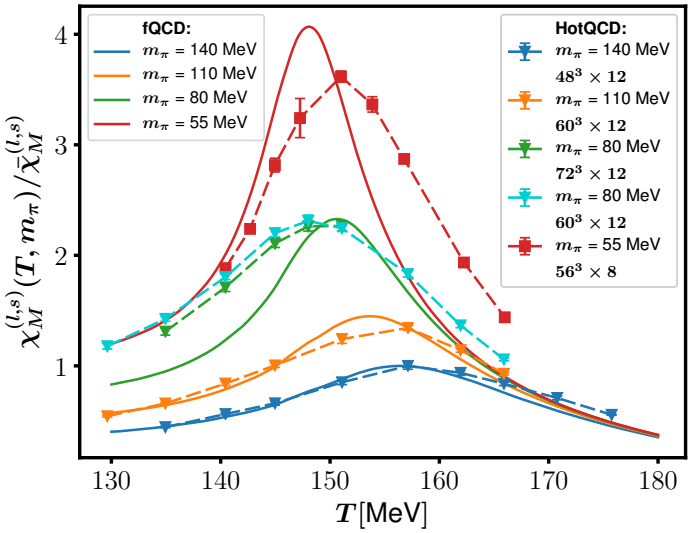

Figure 4.4.: Comparison of our results for the reduced susceptibility $\chi_M^{(l,s)}$ with the data from [52]. Taken from [61].

A linear fit of the peak positions for the lattice data gives

$$\begin{aligned} T_c &\approx 144.6^{+0.5}_{-0.5} \text{ MeV} \quad \text{for} \quad N_\tau = 8 \\ T_c &\approx 138.0^{+2.3}_{-2.3} \text{ MeV} \quad \text{for} \quad N_\tau = 12 \end{aligned} \tag{4.75}$$

which is consistent with our results.

The chiral extrapolation of lattice data is complicated and the following implicit definition for another pseudo-critical temperature T_{60} has been introduced in [52]

$$\chi_M^{(l,s)}(T_{60}^{(l,s)}, m_\pi) = 0.6 \max_T \chi_M^{(l,s)}(T, m_\pi) \tag{4.76}$$

If the pion mass approaches 0, also T_{60} converges to T_c.

In the results from the HotQCD collaboration a value of

$$T_c^{\text{lattice}} = 132^{+3}_{-6} \text{ MeV} \tag{4.77}$$

was obtained by this method.

For our reduced susceptibility data we obtain

$$T_{60}^{(l,s)} \approx 142.4 \text{ MeV} \tag{4.78}$$

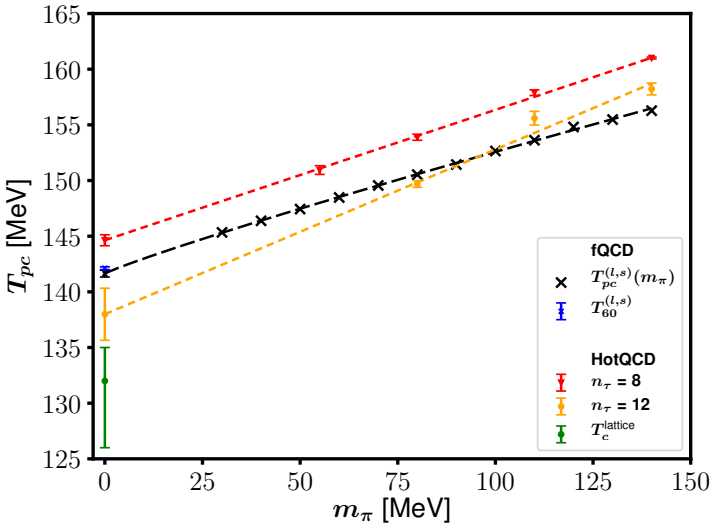

Figure 4.5.: Comparison of our results to the ones of of the HotQCD collaboration [52]. Taken from [61].

In both cases it was observed that $T_{60}(m_\pi)$ almost stays constant.

In Fig. 4.5 the results from us and the lattice QCD study for critical and pseudo-critical temperatures are summarized. We conclude that

$$T_c \approx 142 \text{ MeV} \tag{4.79}$$

The disagreement with the lattice results at smaller pion masses may partially be attributed to finite size effects on the lattice. Otherwise there are also various uncertainties in our numerical setup, for example the Taylor expansion of the potential did not converge yet for $N_v < 5$ and was numerically unstable for $N_v > 5$. That might be improved in the future by different parametrizations and numerical solvers for the potential. Otherwise approximations such as Eq. (4.58) implemented in the eQCD code could lead to some quantitative errors. However, the consistency check shown in Fig. 4.2 of the two different methods by which $\chi_M^{(l)}$ was obtained, gives some confidence in the results.

The results of this study have been published in [61]. The author of this thesis contributed to the discussions, performed the simulations with the eQCD code, computed the susceptibilities and created the plots.

5. Four-Fermion Couplings

In the previous chapter we assumed the $U_A(1)$ symmetry to be broken. In fact the employed approximation left no room for a restoration of the $U_A(1)$ symmetry which will inevitably happen for increasing temperatures.

Following that, in this chapter we want to study how this $U_A(1)$ restoration temperature depends on the strength of the anomaly in a simplified NJL model. Models of this kind have been proven useful in the past as low-energy descriptions to study the phase structure of the strong interaction [34]. If the $U_A(1)$ restoration temperature T_{res} and the chiral symmetry breaking temperature T_{cr} for our two-flavor model are clearly separated in temperature, a fluctuation-induced first order transition is ruled out and the transition should be in the $O(4)$ universality class.

The current chapter presents the results published in and is largely based on [64]. The results were obtained by numerical simulations within an existing Mathematica code, which was developed within the thesis [65].

5.1. Inner workings of the simulation code

5.1.1. Truncation

The following Fierz-complete truncation from [66] for $N_f = 2$ is employed:

$$\Gamma_k = \int \mathrm{d}^4x \left[\frac{1}{4} F^a_{\mu\nu} F^a_{\mu\nu} + \bar{q} \left(\mathrm{i}\partial\!\!\!/ + g_k A\!\!\!/ \right) q + S_{\text{gf}} + S_{\text{gh}} \right] + \Delta\Gamma_{\text{4-quark},k} \tag{5.1}$$

with a Fierz complete set of local four-quark interactions $\Delta\Gamma_{\text{4-quark},k} = \sum_i \int \mathrm{d}^4x \bar{\lambda}_{i,k} \mathcal{L}_i$. It also includes a kinetic term for the quarks, which are coupled to a gluon field. The running of the wave-function renormalization of the quarks is neglected as it was found to be negligible in e.g. [48, 67].

Within this truncation, only the evolution of the four-fermion interactions $\bar{\lambda}_{i,k}$ is computed, i.e. we are not concerned with the terms $\frac{1}{4} F^a_{\mu\nu} F^a_{\mu\nu} + S_{\text{gf}} + S_{\text{gh}}$ which are only given for completeness. For the strong coupling the results from [68] are used, where its

flow was calculated with a truncation more involved than Eq. (5.1). A summary of the procedure is given in Section 5.1.2. No back-coupling of the four-quark interactions into the flow of the strong coupling was considered.

In the following the k-dependence of the strong coupling constant and the four-quark interactions is dropped and implicit.

5.1.2. Flow equations

Four-quark couplings

The term $\Delta\Gamma_{\text{4-quark},k}$ contains the following $SU\left(N_{\mathrm{c}}\right) \otimes SU_L\left(N_{\mathrm{f}}\right) \otimes SU_R\left(N_{\mathrm{f}}\right) \otimes U_V\left(1\right) \otimes U_A\left(1\right)$ symmetric four-quark interactions at finite temperature:

$$\mathcal{L}_{(V+A)_{\parallel}} = \left(\bar{q}\gamma_0 q\right)^2 + \left(\bar{q}\mathrm{i}\gamma_0\gamma_5 q\right)^2 \tag{5.2a}$$

$$\mathcal{L}_{(V+A)_{\perp}} = \left(\bar{q}\gamma_i q\right)^2 + \left(\bar{q}\mathrm{i}\gamma_i\gamma_5 q\right)^2 \tag{5.2b}$$

$$\mathcal{L}_{(V-A)_{\parallel}} = \left(\bar{q}\gamma_0 q\right)^2 - \left(\bar{q}\mathrm{i}\gamma_0\gamma_5 q\right)^2 \tag{5.2c}$$

$$\mathcal{L}_{(V-A)_{\perp}} = \left(\bar{q}\gamma_i q\right)^2 - \left(\bar{q}\mathrm{i}\gamma_i\gamma_5 q\right)^2 \tag{5.2d}$$

$$\mathcal{L}_{(V+A)_{\parallel}^{\text{adj}}} = \left(\bar{q}\gamma_0 T^a q\right)^2 + \left(\bar{q}\mathrm{i}\gamma_0\gamma_5 T^a q\right)^2 \tag{5.2e}$$

$$\mathcal{L}_{(V-A)_{\perp}^{\text{adj}}} = \left(\bar{q}\gamma_i T^a q\right)^2 - \left(\bar{q}\mathrm{i}\gamma_i\gamma_5 T^a q\right)^2 \tag{5.2f}$$

As well as the explicitly $U_A\left(1\right)$ breaking interactions:

$$\mathcal{L}_{(\sigma\text{-}\pi)} = \left(\bar{q}q\right)^2 - \left(\bar{q}\gamma_5\tau_i q\right)^2 \tag{5.3a}$$

$$\mathcal{L}_{\text{top}} = \det{}_{ij}\left[\bar{q}_i P_{\mathrm{L}} q_j\right] + \det{}_{ij}\left[\bar{q}_i P_{\mathrm{R}} q_j\right] \tag{5.3b}$$

$$\mathcal{L}_{\text{csc}} = 4\left(\mathrm{i}\bar{q}\gamma_5\tau_2 T^A q^C\right)\left(\mathrm{i}\bar{q}^C\gamma_5\tau_2 T^A q\right) \tag{5.3c}$$

$$\mathcal{L}_{(S+P)_{-}^{\text{adj}}} = \left(\bar{q}T^a q\right)^2 - \left(\bar{q}\gamma_5\tau_i T^a q\right)^2 + \left(\bar{q}\gamma_5 T^a q\right)^2 - \left(\bar{q}\tau_i T^a q\right)^2 \tag{5.3d}$$

The second set of interactions is mostly phenomenologically motivated by the scalar-pseudoscalar four-quark channel Eq. (5.3a), the "topological channel" Eq. (5.3b) which is a result of the integration performed in Section 2.2.6 and the conventional two-flavor diquark channel Eq. (5.3c). For $\mathcal{L}_{\text{top}}$ the flavor-space determinant only gives a four-quark interaction here because we have set $N_f = 2$.

The $U_A(1)$ invariance of the first set of equations can be seen by executing infinitesimal shifts of the form $q \to (1 + ia\gamma_5)q$ and observing invariance of the expression, see also Section 2.2.4. Any other four-quark interaction compatible with the symmetries can be decomposed into our set via Fierz identities [69], hence the term "Fierz-complete". A

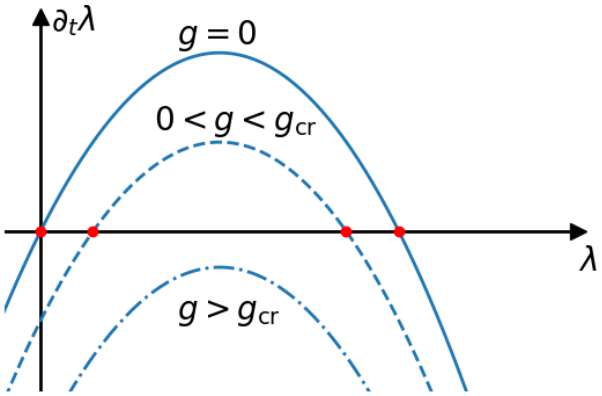

Figure 5.1.: Four-quark coupling fixed points governed by the strong coupling

Fierz-complete set of $(2+1)$-flavor four-quark interactions, derived by the author of the thesis, is given in Appendix B.

The flow of each coupling was derived as described in Chapter 3 with the help of the Mathematica packages *DoFun* [70, 71] and *FormTracer* [72] and Feynman gauge was used. The result is of the following form

$$\partial_t \lambda_i = 2\lambda_i - \sum_{jl} \lambda_j A^{(i)}_{jl} \lambda_l - \sum_j B^{(i)}_j \lambda_j g^2 - C^{(i)} g^4. \tag{5.4}$$

where dimensionless couplings $\lambda_i = \bar{\lambda}_i k^2$ have been introduced.

Although the author of this thesis was not directly involved in the derivation of these flow equations, he discovered a critical bug in DoFun amounting to a sign error in some of the "triangle diagrams" (the second sum in Eq. (5.4)). This was fixed by the maintainer of the code.

The full set of the flow equations of the four-quark couplings is too large to be printed here (it would span over an estimated few hundred pages). However, in Appendix C the set with vanishing g, taken from [73], is given.

The four-fermion flows as a function of the self-interactions take the shape of parabolas intersecting the axis, see Fig. 5.1. For vanishing strong coupling there is an IR attractive Gaussian fixed point. This becomes slightly shifted for non-zero strong coupling. As soon as the strong coupling surpasses a critical value g_{cr} the fixed points vanish, and the four-quark couplings grow rapidly and diverge. This signals the onset of chiral symmetry breaking since the inverse of the four-quark coupling corresponds to the mass of the corresponding bosons, see Eq. (3.30), i.e. the potential becomes flat in the origin and is about to develop

a non-zero expectation value. See also [74]. Unfortunately our truncation is not capable of entering the region of broken chiral symmetry.

Strong coupling

The flow of the strong coupling that is used by the simulation code enters via tabulated data from the calculation detailed in [74]. There, a finite temperature computation of the flow of the strong coupling was performed with the background field method in a propertime formalism via a Borel resummation of the anomalous dimension. It includes an infinite set of gauge-field operators

$$\Gamma_k^{YM}[A] = \int d^4x\, \mathcal{W}_k(\Theta) \qquad \text{with} \qquad \mathcal{W}_k(\Theta) = W_{1,k}\Theta + \frac{1}{2}W_{2,k}\Theta^2 + \frac{1}{3!}W_{3,k}\Theta^3 + \dots \tag{5.5}$$

and $\Theta = \frac{1}{4}F^a_{\mu\nu}F^a_{\mu\nu}$. Note that this is only a subset of all possible gauge-invariant operators of the gauge field, chosen to make the problem tractable. This truncation is one source of systematic errors introduced into the procedure.

The computation also takes into account the contribution of the fermion loops to the anomalous dimension, i.e. their screening nature (so it is not the same as the quenched approximation), but neglects the contribution of the back-coupling of the four-quark interaction. The justification follows from the following argument: From a regulator-dependent Ward-Takahashi identity, the following constraint can be derived:

$$\partial_t g^2 = \eta g^2 - 4v_4 l_1^{(F)} \frac{g^2}{1 - 2v_4 l_1^{(F)} \sum c_i \lambda_i} \partial_t \sum c_i \lambda_i \tag{5.6}$$

Now, in the chirally symmetric phase the λ_i stay close to the shifted Gaussian fixed point and therefore the flow $\partial_t \lambda_i$ stays small [75]. Only when g surpasses the critical value g_{cr} the four-quark couplings start to grow rapidly which indicates chiral symmetry breaking. But as long as this does not happen and we stay in the chirally symmetric phase, the approximation is valid and the contribution of the λ_i to the flow of g^2 can be neglected.

5.2. Sumrules and effective $U_A(1)$ restoration

Since the $U_A(1)$ symmetric subspace of the above total set of 10 interactions is actually 8-dimensional, there are two $U_A(1)$ invariant combinations among the four-quark

interactions in the second set. This leads to the following two sumrules

$$S_1 = \mathcal{N}_1 \left(\lambda_{\text{csc}} + \lambda_{(S+P)^{\text{adj}}_{-}} \right) , \tag{5.7a}$$

$$S_2 = \mathcal{N}_2 \left(\lambda_{\text{top}} - \frac{N_\text{c}-1}{2N_\text{c}} \lambda_{\text{csc}} + \frac{1}{2} \lambda_{(\sigma\text{-}\pi)} \right) , \tag{5.7b}$$

where we have chosen the normalization factors

$$\mathcal{N}_1 = \frac{1}{2} \lambda^{-1}_{(\sigma\text{-}\pi)} \quad \text{and} \quad \mathcal{N}_2 = \frac{2N_\text{c}}{4N_\text{c}-1} \lambda^{-1}_{(\sigma\text{-}\pi)} . \tag{5.7c}$$

In a $U_A\,(1)$ symmetric scenario both evaluate to zero. Otherwise they take finite values. They therefore serve as a measure of the strength of $U_A\,(1)$ breaking. These sumrules were already presented with a different normalization factor in [73]. We based the normalization factors here on $\lambda_{(\sigma\text{-}\pi)}$ since that turns out to be the most dominant four-quark interaction, see Section 5.5.1.

As a criterion when effective $U_A(1)$ symmetry restoration is happening, we define a threshold of 0.5% for the average of the absolute value of both sums

$$S_\Sigma = \frac{1}{2} \left(|S_1| + |S_2| \right) < S_{\text{cr}} = 0.005 \tag{5.8}$$

so that T_{res} is implicitly defined as

$$S_\Sigma(T_{\text{res}}) = S_{\text{cr}} \tag{5.9}$$

The $U_A(1)$ restoration is bound to happen in some point for growing temperatures since the instanton density will be thermally suppressed. T_{cr} is defined as the temperature at which the four-quark couplings diverge [73].

5.3. Initial conditions

Since the flow equation conserves symmetries, we need to already specify a $U_A(1)$ violation in the UV starting conditions, to observe one in the IR. As soon as the flow starts, all couplings change their values. If we would choose $U_A(1)$ symmetric starting conditions, also $U_A(1)$ violating couplings given in Eq. (5.3) would be generated, but the overall $U_A(1)$ violation of all involved couplings would exactly cancel at all times.

We want to study the $U_A(1)$ restoration, so we need to allow for a $U_A(1)$ violation. To obtain our results we set all couplings to zero at the UV scale $\Lambda = 10$ GeV, except λ_{top}.

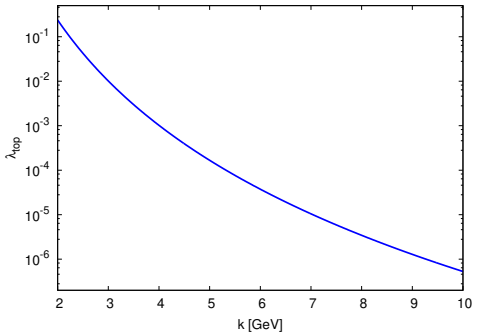

Figure 5.2.: Scale dependence of λ_{top} induced by instantons. It is governed by a prefactor $\sim e^{-8\pi^2/g^2}$ and therefore grows towards small k [76]. Taken from [64].

The window in which the values of λ_{top} should be tuned is obtained from [76]. There the scale dependence of λ_{top} was estimated to be as shown in Fig. 5.2 via a dilute gas approximation. From this we take $\lambda_{\text{top}}(\Lambda) \in [10^{-7}, 10^{-1}]$.

Another input that is required for our flows is the strong coupling g at the UV scale. To find this we set all four-quark couplings to zero (i.e. no $U_A(1)$ violation) and fix g such that T_{cr}, i.e. the temperature at which the flow of the four-quark couplings show a divergence, is equal to $T_0 = 132$ MeV, an estimate taken from [52]. For growing λ_{top} then T_{cr} changes of course.

5.4. Data generation and analysis

The author of this thesis was provided with the simulation code that was developed within the thesis [65]. It comes in the form of Mathematica WorkBench files that export a function `SymmetryBreaking`. The user of the code has to specify the initial conditions, the temperature and the chemical potential (in our case zero) when calling this function. In the code the flow equations for the four-quark couplings as described in Section 5.1.2 are implemented. For the flow of the strong coupling the user has the choice between using the results from [74] (which we do), or alternatively a one-loop approximation. The code then solves this set of coupled differential equations. As return values the user gets the full set of fermion flows and a statement if a divergence occurred (i.e. we are in the chirally broken phase) or not. In case a divergence occurred the scale k_{SB} at which this happened is also returned.

The author of the thesis used this code to obtain the four-quark flows for varying initial

conditions of λ_{top} and temperatures. The sumrules presented in the previous section were calculated and the boundaries for which set of initial conditions chiral symmetry breaking and the $U_A(1)$ restoration happens was sampled partly manually and partly with Mathematica methods.

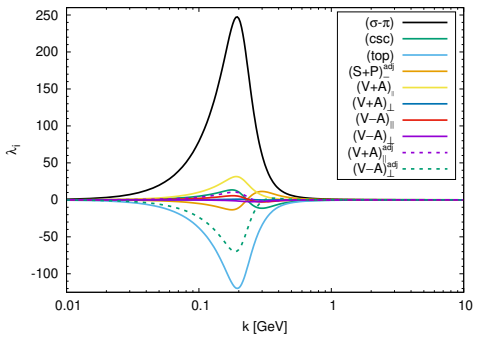

Figure 5.3.: Exemplary flow of four-quark couplings above the chiral transition in the $U\left(1\right)_{\mathrm{A}}$ symmetric case. Taken from [64].

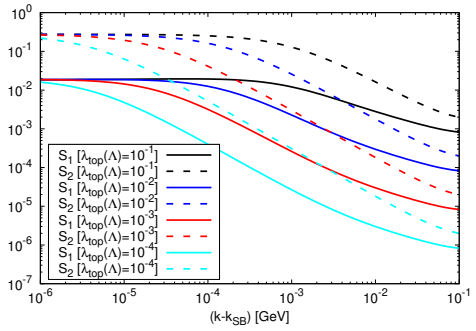

Figure 5.4.: Scale dependence of the sumrules for zero temperature for varying initial values of the t' Hooft coupling. Taken from [64].

5.5. Results

5.5.1. Four-Fermion flows

Before discussing the results on the sumrules, we present an exemplary result on the flow of the four-quark couplings right above the chiral transition. This is shown in Fig. 5.3. All couplings are set to zero at the initial scale Λ in this case, and the flow therefore stays $U_A\left(1\right)$ symmetric.

The flow of the four-quark couplings is governed by fixed points induced by the strong coupling, see also Section 5.1.2. Since we are in the chirally symmetric regime no divergence of the four-fermion couplings occurs. One clearly sees the dominating nature of the $\lambda_{(\sigma\text{-}\pi)}$ coupling.

5.5.2. Sumrules and effective $U_A(1)$ restoration

First we show the sumrules in the zero temperature case for varying values of $\lambda_{\mathrm{top}}(\Lambda)$ in Fig. 5.4. That is in the chirally broken regime with $k_{\mathrm{SB}} \approx 0.346$ GeV. We observe that S_1 and S_2 become almost independent of the initial values and converge towards $S_1 \approx 0.019$ and $S_2 \approx 0.25$ when k approaches k_{SB} over a large range of initial values for $\lambda_{\mathrm{top}}(\Lambda)$.

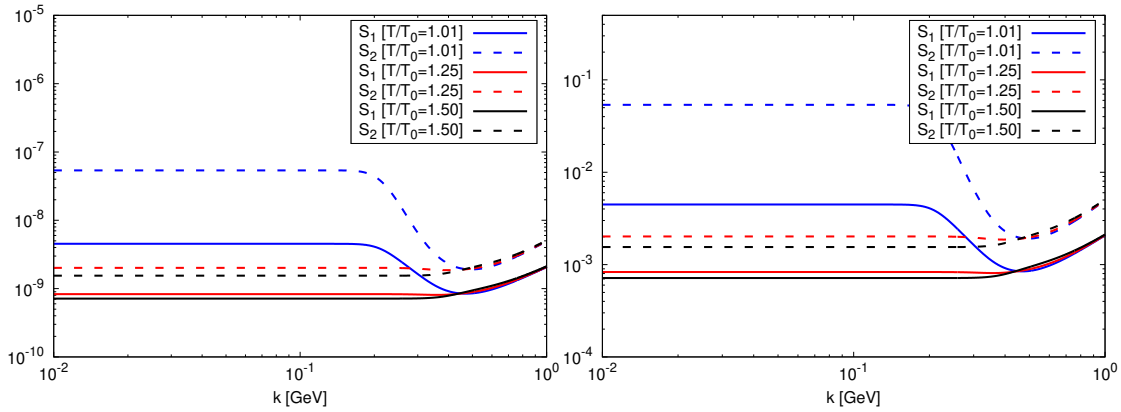

Figure 5.5.: Sumrule flows in the chirally symmetric regime for various temperatures. In the left panel we have set $\lambda_{\text{top}}(\Lambda) = 10^{-7}$ and in the right $\lambda_{\text{top}}(\Lambda) = 10^{-1}$. Taken from [64].

In Fig. 5.5 we show the flows of the sumrules for the smallest and largest value in our sampling interval $\lambda_{\text{top}}(\Lambda) \in [10^{-7}, 10^{-1}]$ specified in Section 5.3. One can see that in both cases increasing temperatures lead to decreasing IR values for the sumrules, i.e. $U_A(1)$ gets restored at higher temperatures. As mentioned in Section 2.3.2 this is explained by the suppression of the quark fluctuations by the thermal mass. On the other hand when the temperatures approach T_0 the IR values of S_1 and S_2 grow. This is expected since chiral symmetry breaking (which happens at T_0) also implies breaking of the $U_A(1)$ symmetry.

Now, according to our condition Eq. (5.8) for $\lambda_{\text{top}}(\Lambda) = 10^{-7}$ we clearly are in the regime of restored $U_A(1)$ symmetry even for $T = 1.01\ T_0$. For $\lambda_{\text{top}}(\Lambda) = 10^{-1}$ this is not the case anymore, there at $T = 1.01\ T_0$ our sumrules clearly lie above our threshold and we consider $U_A(1)$ to be broken. Only at higher temperatures it is restored again.

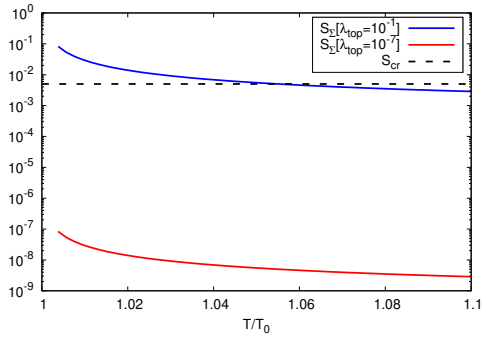

Figure 5.6.: The IR value of S_Σ for varying temperature for $\lambda_{\text{top}}(\Lambda) = 10^{-7}$ and $\lambda_{\text{top}}(\Lambda) = 10^{-1}$. The dashed line marks our threshold where we consider $U_A(1)$ to be restored. Taken from [64].

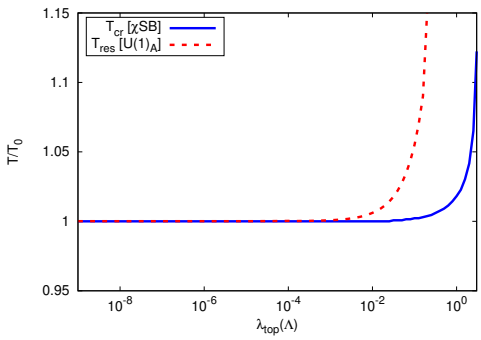

Figure 5.7.: The chiral symmetry breaking temperatures $T_{\text{cr}}[\chi SB]$ and restoration temperatures $T_{\text{res}}[U_A(1)]$ over a large range of initial values for λ_{top}. Taken from [64].

In Fig. 5.6 we show the temperature dependence for the IR values of S_Σ for $\lambda_{\text{top}}(\Lambda) = 10^{-7}$ and $\lambda_{\text{top}}(\Lambda) = 10^{-1}$. As previously noted it decreases monotonically. While $S_\Sigma\left(\lambda_{\text{top}}(\Lambda) = 10^{-7}\right)$ stays below the threshold for all temperatures that we sampled, $S_\Sigma\left(\lambda_{\text{top}}(\Lambda) = 10^{-1}\right)$ crosses it at a restoration temperature of roughly $T_{\text{res}} \approx 1.05\, T_0$.

The full set of restoration temperatures T_{res} over the whole range of $\lambda_{\text{top}}(\Lambda) \in [10^{-7}, 10^{-1}]$ is shown in Fig. 5.7. It is compared with the results for the chiral transition temperatures (where divergence occurs in the flow of the couplings). The fact that they almost coincide over a large range of UV values for $\lambda_{\text{top}}(\Lambda)$ is the central result of this study.

In [1] it has been shown that a $U_A(1)$ restoration right at the chiral transition temperature affects the order and the universality class of the phase transition. A second order phase transition in the $O(4)$ universality class is only likely if there is a clear separation in temperature. In our case that happens for $\lambda_{\text{top}}(\Lambda) \gtrsim 10^{-1}$.

We believe that we actually are in this regime of separated temperatures, since the topological contributions to the flow calculated in [76] and shown in Fig. 5.2, which we neglected, would lead to a significant increase of λ_{top}. We therefore conclude that the $O(4)$ scenario for the chiral phase transition is more likely.

The results of this study have been published in [64]. The author of this thesis contributed to the discussions, obtained the results for the sumrules with the simulation code and created some of the plots. He also derived the Fierz basis given in Appendix B.

6. Conclusion

In this work we used two different existing simulation frameworks to study the chiral phase transition.

First we looked at susceptibilities for decreasing pion masses, approaching the chiral limit. With this we were able to extrapolate pseudo-critical temperature results to the chiral limit and make a prediction for the chiral transition temperature. Our results are consistent with the results from the lattice QCD study [52]. By construction we did not allow for a $U_A(1)$ restoration. Here we could only reach a pion mass of 30 MeV, due to limitations of the numerical implementation.

Secondly, we did a simulation directly in the chiral limit, varied the degree of the $U_A(1)$ violation in the UV and studied how it manifested in the IR. We measured the $U_A(1)$ violation by the strength of the violation of sumrules, and inspected at what temperature the symmetry was approximately restored. We found that this restoration temperature coincides with the chiral transition temperature for small $U_A(1)$ violations in the UV. We believe however, that the topological contributions will lead to a larger effective $U_A(1)$ breaking in the UV, therefore T_{cr} and T_{res} are different, and we have an $O(4)$ transition.

In the future, more elaborate studies are in order to deal with the complications that arise from the involved differential equations. To fully understand the nature of the chiral phase transition, we need to specify a model that allows a possible $U_A(1)$ restoration and have a numerical implementation that can resolve discontinuities associated with a first order phase transition. Steps into this direction have been undertaken in [77–79].

A. Derivation of the Flow Equation

The derivation shown here is based on the presentation in [42]. It was derived by Wetterich and presented in e.g. [40].

In Euclidean space

$$Z[J] = e^{W[J]} = \int \mathcal{D}\varphi \; e^{-S[\varphi]+J\cdot\varphi}. \tag{A.1}$$

From this we construct the effective action, a functional of classical fields

$$\Gamma[\phi] = \sup_J \Big(J \cdot \phi - W[J] \Big). \tag{A.2}$$

With this

$$\phi = \langle \varphi \rangle_{J=J_{\text{sup}}} = \left. \frac{\delta W[J]}{\delta J} \right|_{J=J_{\text{sup}}}. \tag{A.3}$$

Similar to the classical case, the field expectation value ϕ follows an equation of motion

$$\frac{\delta \Gamma[\phi]}{\delta \phi(x)} = J(x). \tag{A.4}$$

From this an equation for the effective action can be derived

$$e^{-\Gamma[\phi]} = \int \mathcal{D}\varphi \; \exp\left(S[\phi+\varphi] + \frac{\delta \Gamma[\phi]}{\delta \phi} \cdot \varphi \right). \tag{A.5}$$

Solving this for Γ corresponds to solving the full theory. Only a few exact solutions are known. One method to find approximate solutions is Wilson's idea of integrating out momentum modes successively from high to low. This results in a scale-dependent effective action $\Gamma_k[\phi]$ interpolating between the microscopic action S at $k = \Lambda$ and the full quantum effective action Γ at $k = 0$.

The goal is then to find an expression for $\partial_k \Gamma_k$ to be able to find Γ for a given S.

The procedure of successive momentum integration is done with the help of a regulator $R_k(q)$ exhibiting the limits

$$\lim_{q^2/k^2\to 0} R_k(q) > 0 \tag{A.6}$$

$$\lim_{k\to 0} R_k(q) = 0 \tag{A.7}$$

$$\lim_{k\to\Lambda\to\infty} R_k(q) \to \infty \tag{A.8}$$

A term

$$\Delta S_k[\varphi] = \frac{1}{2}\int \frac{d^D q}{(2\pi)^D}\varphi(-q)R_k(q)\varphi(q) \tag{A.9}$$

is added to the action and W_k is constructed analogously as before

$$e^{W_k[J]} = Z_k[J] = \int \mathcal{D}\varphi\, e^{-S[\varphi]-\Delta S_k[\varphi]+J\cdot\varphi} \tag{A.10}$$

The first limit of R_k serves as an IR regularization. The second and third ensure the correct behavior of Γ_k in the following way:

For $k = 0$, $W_k[J]$ just becomes $W[J]$ from before. For $k \to \infty$, we have by the saddle point approximation

$$W_\Lambda[J] \to -S[\varphi_J] - \Delta S_k[\varphi_J] + J\cdot\varphi_J \quad \text{with} \quad \left.\frac{\delta(S[\varphi]+\Delta S_k[\varphi])}{\delta\varphi}\right|_{\varphi=\varphi_J} = J \tag{A.11}$$

i.e. W_Λ is the Legendre transform of $S[\varphi]+\Delta S_\Lambda[\varphi]$. Defining Γ_k as the modified Legendre transform

$$\Gamma_k[\phi] = \sup_J (J\cdot\phi - W_k[J]) - \Delta S_k[\phi] \tag{A.12}$$

we have

$$\Gamma_{k=\Lambda} = S \quad \text{and} \quad \Gamma_{k=0} = \Gamma \tag{A.13}$$

i.e. Γ_k exhibits the correct limits.

Now to find an expression for $\partial_k\Gamma_k$ we will first need to see how the expressions (A.3) and (A.4) change. As before, we have

$$\phi(x) = \langle\varphi(x)\rangle_J = \left.\frac{\delta W_k[J]}{\delta J}\right|_{J=J_{\sup}} \tag{A.14}$$

with a k-dependent $J_{\sup}$ from Eq. (A.12). The equation of motion for Γ_k follows by derivating Eq. (A.12) with respect to ϕ

$$J(x) = \frac{\delta\Gamma_k[\phi]}{\delta\phi(x)} + (R_k\phi)(x). \tag{A.15}$$

Therefore

$$\frac{\delta J(x)}{\delta\phi(x)} = \frac{\delta^2\Gamma_k[\phi]}{\delta\phi(x)\delta\phi(y)} + R_k(x,y). \tag{A.16}$$

From Eq. (A.15) we have for the k-dependent connected propagator

$$G_k(y,x') = \frac{\delta^2 W_k[J]}{\delta J(x')\delta J(y)} = \frac{\delta\phi(y)}{\delta J(x')}. \tag{A.17}$$

Combining Eq. (A.16) and Eq. (A.17) yields

$$\mathbb{I} = (\Gamma_k^{(2)} + R_k)G_k \quad \text{or} \quad G_k = (\Gamma_k^{(2)} + R_k)^{-1} \tag{A.18}$$

On the other hand

$$G_k(x,y) = \frac{\delta^2 W_k[J]}{\delta J(y)\delta J(x)} = \frac{\delta^2 \ln Z_k[J]}{\delta J(y)\delta J(x)} = \langle\varphi(x)\varphi(y)\rangle - \langle\varphi(x)\rangle\langle\varphi(y)\rangle \tag{A.19}$$

with this we get for $\partial_k W_k[J]$ (holding J fixed)

$$\partial_k W_k[J] = -\frac{1}{2}\int \mathcal{D}\varphi \int \frac{d^Dq}{(2\pi)^D}\varphi(-q)R_k(q)\varphi(q)e^{-S[\varphi]-\Delta S_k[\varphi]+J\cdot\varphi} \tag{A.20}$$

$$= -\frac{1}{2}\int \frac{d^Dq}{(2\pi)^D}\partial_k R_k(q)G_k(q) - \partial_k\Delta S_k[\phi]. \tag{A.21}$$

Now, we are in position to derive an expression for $\partial_k\Gamma_k$:

$$\partial_k\Gamma_k[\phi] = -\partial_k\left(W_k[J]\right) + \partial_k J\cdot\phi - \partial_k\Delta S_k[\phi] \tag{A.22}$$

$$= -\left(\partial_k W_k\right)[J] - \underbrace{\frac{\delta W_k[J]}{\delta J}}_{=\phi}\partial_k J + \partial_k J\cdot\phi - \partial_k\Delta S_k[\phi] \tag{A.23}$$

$$\overset{(A.21)}{=} \frac{1}{2}\int \frac{d^Dq}{(2\pi)^D}\partial_k R_k(q)G_k(q) \tag{A.24}$$

$$\overset{(A.18)}{=} \frac{1}{2}\mathrm{Tr}\left[\partial_k R_k\left(\Gamma_k^{(2)}[\phi] + R_k\right)^{-1}\right] \tag{A.25}$$

This is the *flow equation*. It is an exact one loop equation for the evolution of Γ_k. Among other things it has proven fruitful for performing non-perturbative calculations.

B. Fierz-complete four-quark basis for $(2+1)$-flavor QCD

Here, we present a Fierz-complete basis of four-quark interaction channels for QCD with two massless and one heavy quark flavor. The $U_A(1)$-symmetric limit of this system is spanned by a minimal set of 26 four-quark interaction channels which may be divided into interactions in the subspace of the two massless quark flavors,

$$\mathcal{L}_{(V+A)_{\parallel,l}} = \left(\bar{q}\gamma_0 1^l q\right)^2 + \left(\bar{q}\gamma_0\gamma_5 1^l q\right)^2 \tag{B.1a}$$

$$\mathcal{L}_{(V+A)_{\perp,l}} = \left(\bar{q}\gamma_i 1^l q\right)^2 + \left(\bar{q}\gamma_i\gamma_5 1^l q\right)^2 \tag{B.1b}$$

$$\mathcal{L}_{(V-A)_{\parallel,l}} = \left(\bar{q}\gamma_0 1^l q\right)^2 - \left(\bar{q}\gamma_0\gamma_5 1^l q\right)^2 \tag{B.1c}$$

$$\mathcal{L}_{(V-A)_{\perp,l}} = \left(\bar{q}\gamma_i 1^l q\right)^2 - \left(\bar{q}\gamma_i\gamma_5 1^l q\right)^2 \tag{B.1d}$$

$$\mathcal{L}_{(V+A)^{\text{adj}}_{\parallel,l}} = \left(\bar{q}\gamma_0 T^a 1^l q\right)^2 + \left(\bar{q}\gamma_0\gamma_5 T^a 1^l q\right)^2 \tag{B.1e}$$

$$\mathcal{L}_{(V+A)^{\text{adj}}_{\perp,l}} = \left(\bar{q}\gamma_i T^a 1^l q\right)^2 + \left(\bar{q}\gamma_i\gamma_5 T^a 1^l q\right)^2 \tag{B.1f}$$

$$\mathcal{L}_{(V-A)^{\text{adj}}_{\parallel,l}} = \left(\bar{q}\gamma_0 T^a 1^l q\right)^2 - \left(\bar{q}\gamma_0\gamma_5 T^a 1^l q\right)^2 \tag{B.1g}$$

$$\mathcal{L}_{(V-A)^{\text{adj}}_{\perp,l}} = \left(\bar{q}\gamma_i T^a 1^l q\right)^2 - \left(\bar{q}\gamma_i\gamma_5 T^a 1^l q\right)^2 \tag{B.1h}$$

and interactions in the strange-quark subspace,

$$\mathcal{L}_{(V+A)_{\parallel,s}} = \left(\bar{q}\gamma_0 1^s q\right)^2 + \left(\bar{q}\gamma_0\gamma_5 1^s q\right)^2 \tag{B.2a}$$

$$\mathcal{L}_{(V-A)_{\parallel,s}} = \left(\bar{q}\gamma_0 1^s q\right)^2 - \left(\bar{q}\gamma_0\gamma_5 1^s q\right)^2 \tag{B.2b}$$

$$\mathcal{L}_{(V+A)^{\text{adj}}_{\perp,s}} = \left(\bar{q}\gamma_i T^a 1^s q\right)^2 + \left(\bar{q}\gamma_i\gamma_5 T^a 1^s q\right)^2 \tag{B.2c}$$

$$\mathcal{L}_{(V-A)^{\text{adj}}_{\perp,s}} = (\bar{q}\gamma_i T^a 1^s q)^2 - (\bar{q}\gamma_i\gamma_5 T^a 1^s q)^2 \tag{B.2d}$$

$$\mathcal{L}_{(S-P)_s} = (\bar{q}1^s q)^2 - (\bar{q}\gamma_5 1^s q)^2 \tag{B.2e}$$

$$\mathcal{L}_{(S-P)^{\text{adj}}_s} = (\bar{q}T^a 1^s q)^2 - (\bar{q}\gamma_5 T^a 1^s q)^2 \tag{B.2f}$$

and interactions “living" in the whole three-flavor space,

$$\mathcal{L}_{(V+A)_\parallel} = (\bar{q}\gamma_0 q)^2 + (\bar{q}\gamma_0\gamma_5 q)^2 \tag{B.3a}$$

$$\mathcal{L}_{(V+A)_\perp} = (\bar{q}\gamma_i q)^2 + (\bar{q}\gamma_i\gamma_5 q)^2 \tag{B.3b}$$

$$\mathcal{L}_{(V-A)_\parallel} = (\bar{q}\gamma_0 q)^2 - (\bar{q}\gamma_0\gamma_5 q)^2 \tag{B.3c}$$

$$\mathcal{L}_{(V-A)_\perp} = (\bar{q}\gamma_i q)^2 - (\bar{q}\gamma_i\gamma_5 q)^2 \tag{B.3d}$$

$$\mathcal{L}_{(V+A)^{\text{adj}}_\parallel} = (\bar{q}\gamma_0 T^a q)^2 + (\bar{q}\gamma_0\gamma_5 T^a q)^2 \tag{B.3e}$$

$$\mathcal{L}_{(V+A)^{\text{adj}}_\perp} = (\bar{q}\gamma_i T^a q)^2 + (\bar{q}\gamma_i\gamma_5 T^a q)^2 \tag{B.3f}$$

$$\mathcal{L}_{(V-A)^{\text{adj}}_\parallel} = (\bar{q}\gamma_0 T^a q)^2 - (\bar{q}\gamma_0\gamma_5 T^a q)^2 \tag{B.3g}$$

$$\mathcal{L}_{(V-A)^{\text{adj}}_\perp} = (\bar{q}\gamma_i T^a q)^2 - (\bar{q}\gamma_i\gamma_5 T^a q)^2 \tag{B.3h}$$

$$\mathcal{L}_{(S-P)_{1+\text{ISO}}} = (\bar{q}q)^2 - (\bar{q}\gamma_5 q)^2 + \sum_{k=1}^{3}\left[(\bar{q}\tau_k q)^2 - (\bar{q}\gamma_5\tau_k q)^2\right] \tag{B.3i}$$

$$\mathcal{L}_{(S-P)^{\text{adj}}_{1+\text{ISO}}} = (\bar{q}T^a q)^2 - (\bar{q}\gamma_5 T^a q)^2 + \sum_{k=1}^{3}\left[(\bar{q}\tau_k T^a q)^2 - (\bar{q}\gamma_5\tau_k T^a q)^2\right] \tag{B.3j}$$

$$\mathcal{L}_{T_{\perp-\parallel,1+\text{ISO}}} = (\bar{q}\sigma_{ij} q)^2 - 2\,(\bar{q}\sigma_{0i} q)^2 + \sum_{k=1}^{3}\left[(\bar{q}\sigma_{ij}\tau_k q)^2 - 2\,(\bar{q}\sigma_{0i}\tau_k q)^2\right] \tag{B.3k}$$

$$\mathcal{L}_{T^{\text{adj}}_{\perp-\parallel,1+\text{ISO}}} = \sum_{k=1}^{3}\left[(\bar{q}\sigma_{ij}\tau_k T^a q)^2 - 2\,(\bar{q}\sigma_{0i}\tau_k T^a q)^2\right] + (\bar{q}\sigma_{ij} T^a q)^2 - 2\,(\bar{q}\sigma_{0i} T^a q)^2 \tag{B.3l}$$

Here, $\sigma_{\mu\nu} = (i/4)[\gamma_\mu, \gamma_\nu]$, the T^a's are the generators of $SU(N_c)$, and the τ_k's are related to the generators of the $SU(3)$ flavor space in the same way as the Pauli matrices are related to the generators of $SU(2)$. The indices l and s in these expressions refer to the subspace of the two light quark flavors and the strange quark, respectively. Moreover,

$$1^l \otimes 1^l = \frac{4}{9}\left(1 \otimes 1 + \frac{\sqrt{3}}{2}[1 \otimes \tau_8 + \tau_8 \otimes 1] + \frac{3}{4}\tau_8 \otimes \tau_8\right) \tag{B.4}$$

and

$$1^s \otimes 1^s = \frac{1}{3} 1 \otimes 1 - \frac{1}{2} 1^l \otimes 1^l + \frac{2}{3}\, \tau_8 \otimes \tau_8 \,. \tag{B.5}$$

In the case of broken $U_A(1)$ symmetry, we have 6 additional channels,

$$\mathcal{L}_{(S+P)_{1^l-\text{ISO}}} = \left(\bar{q} 1^l q\right)^2 + \left(\bar{q}\gamma_5 1^l q\right)^2 - \sum_{k=1}^{3} \left[\left(\bar{q}\gamma_5 \tau_k q\right)^2 + \left(\bar{q}\tau_k q\right)^2 \right] \tag{B.6a}$$

$$\mathcal{L}_{(S+P)^{\text{adj}}_{1^l-\text{ISO}}} = \left(\bar{q} 1^l T^a q\right)^2 + \left(\bar{q}\gamma_5 1^l T^a q\right)^2 - \sum_{k=1}^{3} \left[\left(\bar{q}\gamma_5 \tau_k T^a q\right)^2 + \left(\bar{q}\tau_k T^a q\right)^2 \right] \tag{B.6b}$$

$$\mathcal{L}_{(S+P)_s} = \left(\bar{q} 1^s q\right)^2 + \left(\bar{q}\gamma_5 1^s q\right)^2 \tag{B.6c}$$

$$\mathcal{L}_{(S+P)^{\text{adj}}_s} = \left(\bar{q} T^a 1^s q\right)^2 + \left(\bar{q}\gamma_5 T^a 1^s q\right)^2 \tag{B.6d}$$

$$\mathcal{L}_{T_{\perp+\parallel,1-\text{ISO}}} = \left(\bar{q}\sigma_{ij} q\right)^2 + 2\left(\bar{q}\sigma_{0i} q\right)^2 - \sum_{k=1}^{3} \left[\left(\bar{q}\sigma_{ij}\tau_k q\right)^2 + 2\left(\bar{q}\sigma_{0i}\tau_k q\right)^2 \right] \tag{B.6e}$$

$$\mathcal{L}_{T^{\text{adj}}_{\perp+\parallel,1-\text{ISO}}} = -\sum_{k=1}^{3} \left[\left(\bar{q}\sigma_{ij}\tau_k T^a q\right)^2 + 2\left(\bar{q}\sigma_{0i}\tau_k T^a q\right)^2 \right] + \left(\bar{q}\sigma_{ij} T^a q\right)^2 + 2\left(\bar{q}\sigma_{0i} T^a q\right)^2 \tag{B.6f}$$

Thus, in total, we end up with 32 four-quark interaction channels in case of QCD with two massless and one heavy quark flavor. Finally, we add that we can relate this basis to the basis underlying our studies of two-flavor QCD. For example, the associated scalar-pseudoscalar and diquark channel are given by

$$\mathcal{L}_{(\sigma^l-\pi)} = -\mathcal{L}_{(V+A)^{\text{adj}}_{\parallel,l}} - \mathcal{L}_{(V+A)^{\text{adj}}_{\perp,l}} - \frac{1}{2N_c}\mathcal{L}_{(V+A)_{\parallel,l}} - \frac{1}{2N_c}\mathcal{L}_{(V+A)_{\perp,l}} + \frac{1}{2}\mathcal{L}_{(S+P)_{1^l-\text{ISO}}} \tag{B.7}$$

and

$$\mathcal{L}_{\text{csc}} = \mathcal{L}_{(S+P)^{\text{adj}}_{1^l-\text{ISO}}} + \mathcal{L}_{(V-A)^{\text{adj}}_{\parallel,l}} + \mathcal{L}_{(V-A)^{\text{adj}}_{\perp,l}} - \frac{N_c-1}{2N_c}\left(\mathcal{L}_{(S+P)_{1^l-\text{ISO}}} + \mathcal{L}_{(V-A)_{\parallel,l}} + \mathcal{L}_{(V-A)_{\perp,l}} \right) \tag{B.8}$$

respectively. The use of these channels may be more convenient in phenomenological applications.

C. Coupling flows of Fierz-complete $N_f = 2$ NJL model

Flows of the whole set of Fierz-complete four-quark interactions at finite temperature and zero chemical potential with strong coupling turned off. The k-dependence of the couplings are implicit, the dimensionless temperature is denoted by $\tau = T/k$ and the constant $v_4 = 1/(32\pi^2)$ was introduced. The threshold functions are defined in Appendix D. Taken from [73].

$$
\begin{aligned}
\partial_t \lambda_{(\sigma\text{-}\pi)} \;=\; & 2\lambda_{(\sigma\text{-}\pi)} + 64 v_4 \Big(-\lambda_{(\sigma\text{-}\pi)}^2 - 4\lambda_{(\sigma\text{-}\pi)}\lambda_{(S+P)_-} - 4\lambda_{(S+P)_-}^2 + \lambda_{(\sigma\text{-}\pi)}\lambda_{(V+A)_\parallel} \\
& + \lambda_{(\sigma\text{-}\pi)}\lambda_{(V-A)_\parallel} + 3\lambda_{(\sigma\text{-}\pi)}\lambda_{(V+A)_\perp} - \lambda_{(V+A)_\parallel^{\text{adj}}}\lambda_{(V+A)_\perp} + \lambda_{(\sigma\text{-}\pi)}\lambda_{(V-A)_\perp} \\
& + 2\lambda_{(\sigma\text{-}\pi)}\lambda_{(V-A)_\perp^{\text{adj}}} - \frac{1}{N_c^2}\lambda_{(S+P)_-^{\text{adj}}}^2 + \frac{2}{N_c}\lambda_{(\sigma\text{-}\pi)}\lambda_{(S+P)_-^{\text{adj}}} + \frac{4}{N_c}\lambda_{(S+P)_-}\lambda_{(S+P)_-^{\text{adj}}} \\
& + \frac{1}{N_c}\lambda_{(S+P)_-^{\text{adj}}}^2 - \frac{1}{2N_c}\lambda_{(\sigma\text{-}\pi)}\lambda_{(V+A)_\parallel^{\text{adj}}} - \frac{1}{2N_c}\lambda_{(\sigma\text{-}\pi)}\lambda_{(V-A)_\perp^{\text{adj}}} - 2N_c\lambda_{(\sigma\text{-}\pi)}^2 \\
& - 4N_c\lambda_{(\sigma\text{-}\pi)}\lambda_{(S+P)_-} - 4N_c\lambda_{(S+P)_-}^2 - N_c\lambda_{(\sigma\text{-}\pi)}\lambda_{(S+P)_-^{\text{adj}}} - 2N_c\lambda_{(S+P)_-}\lambda_{(S+P)_-^{\text{adj}}} \\
& + \frac{N_c}{2}\lambda_{(\sigma\text{-}\pi)}\lambda_{(V+A)_\parallel^{\text{adj}}} + \lambda_{(\sigma\text{-}\pi)}\lambda_{\text{csc}} - \lambda_{(S+P)_-^{\text{adj}}}\lambda_{\text{csc}} + N_c\lambda_{(\sigma\text{-}\pi)}\lambda_{\text{csc}} \\
& + 2N_c\lambda_{(S+P)_-}\lambda_{\text{csc}} + N_c\lambda_{(S+P)_-^{\text{adj}}}\lambda_{\text{csc}} \Big) l_\parallel^{(\text{F})}(\tau,0,0) \\
& + 64 v_4 \Big(-\lambda_{(\sigma\text{-}\pi)}\lambda_{(V+A)_\parallel} + \lambda_{(\sigma\text{-}\pi)}\lambda_{(V+A)_\perp} + \lambda_{(V+A)_\parallel^{\text{adj}}}\lambda_{(V+A)_\perp} \\
& + \frac{1}{2N_c}\lambda_{(\sigma\text{-}\pi)}\lambda_{(V+A)_\parallel^{\text{adj}}} \Big) l_\parallel^{(\text{F})}(\tau,0,0) \\
& + 64 v_4 \Big(-\lambda_{(\sigma\text{-}\pi)}^2 - 4\lambda_{(\sigma\text{-}\pi)}\lambda_{(S+P)_-} - 4\lambda_{(S+P)_-}^2 - \frac{2}{3}\lambda_{(\sigma\text{-}\pi)}\lambda_{(S+P)_-^{\text{adj}}} \\
& - \frac{4}{3}\lambda_{(S+P)_-}\lambda_{(S+P)_-^{\text{adj}}} + \lambda_{(\sigma\text{-}\pi)}\lambda_{(V+A)_\parallel} + \frac{1}{3}\lambda_{(\sigma\text{-}\pi)}\lambda_{(V-A)_\parallel} - \frac{1}{3}\lambda_{(V+A)_\parallel}\lambda_{(V+A)_\parallel^{\text{adj}}} \\
& + 3\lambda_{(\sigma\text{-}\pi)}\lambda_{(V+A)_\perp} - \frac{2}{3}\lambda_{(V+A)_\parallel^{\text{adj}}}\lambda_{(V+A)_\perp} + \frac{1}{3}\lambda_{(\sigma\text{-}\pi)}\lambda_{(V-A)_\perp} + \frac{2}{3}\lambda_{(\sigma\text{-}\pi)}\lambda_{(V-A)_\perp^{\text{adj}}}
\end{aligned}
$$

$$
\begin{aligned}
&-\frac{1}{N_c^2}\lambda^2_{(S+P)^{\text{adj}}_-}+\frac{2}{N_c}\lambda_{(\sigma\text{-}\pi)}\lambda_{(S+P)^{\text{adj}}_-}+\frac{4}{N_c}\lambda_{(S+P)_-}\lambda_{(S+P)^{\text{adj}}_-}+\frac{5}{3N_c}\lambda^2_{(S+P)^{\text{adj}}_-}\\
&-\frac{1}{2N_c}\lambda_{(\sigma\text{-}\pi)}\lambda_{(V+A)^{\text{adj}}_\parallel}+\frac{1}{6N_c}\lambda^2_{(V+A)^{\text{adj}}_\parallel}-\frac{1}{6N_c}\lambda_{(\sigma\text{-}\pi)}\lambda_{(V-A)^{\text{adj}}_\perp}-2N_c\lambda^2_{(\sigma\text{-}\pi)}\\
&-4N_c\lambda_{(\sigma\text{-}\pi)}\lambda_{(S+P)_-}-4N_c\lambda^2_{(S+P)_-}-N_c\lambda_{(\sigma\text{-}\pi)}\lambda_{(S+P)^{\text{adj}}_-}-2N_c\lambda_{(S+P)_-}\lambda_{(S+P)^{\text{adj}}_-}\\
&-\frac{N_c}{3}\lambda^2_{(S+P)^{\text{adj}}_-}+\frac{N_c}{2}\lambda_{(\sigma\text{-}\pi)}\lambda_{(V+A)^{\text{adj}}_\parallel}-\frac{N_c}{12}\lambda^2_{(V+A)^{\text{adj}}_\parallel}-\frac{1}{3}\lambda_{(\sigma\text{-}\pi)}\lambda_{\text{csc}}-\frac{4}{3}\lambda_{(S+P)_-}\lambda_{\text{csc}}\\
&-\frac{1}{3}\lambda_{(S+P)^{\text{adj}}_-}\lambda_{\text{csc}}+\frac{2}{3N_c}\lambda_{(S+P)^{\text{adj}}_-}\lambda_{\text{csc}}+N_c\lambda_{(\sigma\text{-}\pi)}\lambda_{\text{csc}}+2N_c\lambda_{(S+P)_-}\lambda_{\text{csc}}\\
&+\frac{N_c}{3}\lambda_{(S+P)^{\text{adj}}_-}\lambda_{\text{csc}}+\frac{2}{3}\lambda^2_{\text{csc}}-\frac{N_c}{3}\lambda^2_{\text{csc}}\Big)l^{(\text{F})}_\perp(\tau,0,0)\\
&+64v_4\Big(\frac{1}{3}\lambda_{(\sigma\text{-}\pi)}\lambda_{(V+A)_\parallel}+\frac{1}{3}\lambda_{(V+A)_\parallel}\lambda_{(V+A)^{\text{adj}}_\parallel}-\frac{5}{3}\lambda_{(\sigma\text{-}\pi)}\lambda_{(V+A)_\perp}\\
&-\frac{2}{3}\lambda_{(V+A)^{\text{adj}}_\parallel}\lambda_{(V+A)_\perp}-\frac{1}{6N_c}\lambda_{(\sigma\text{-}\pi)}\lambda_{(V+A)^{\text{adj}}_\parallel}-\frac{1}{6N_c}\lambda^2_{(V+A)^{\text{adj}}_\parallel}\Big)l^{(\text{F})}_\perp(\tau,0,0)\ ,
\end{aligned}
$$

$$
\begin{aligned}
\partial_t\lambda_{\text{csc}} \;=\;& 2\lambda_{\text{csc}}+64v_4\Big(-\lambda^2_{(\sigma\text{-}\pi)}+2\lambda_{(\sigma\text{-}\pi)}\lambda_{(V+A)^{\text{adj}}_\parallel}-\lambda^2_{(V+A)^{\text{adj}}_\parallel}+3\lambda_{(V-A)_\perp}\lambda_{(V-A)^{\text{adj}}_\perp}\\
&-\frac{3}{2N_c}\lambda^2_{(V-A)^{\text{adj}}_\perp}+\frac{3N_c}{4}\lambda^2_{(V-A)^{\text{adj}}_\perp}+2\lambda_{(V-A)_\parallel}\lambda_{\text{csc}}-\frac{3}{2}\lambda_{(V-A)^{\text{adj}}_\perp}\lambda_{\text{csc}}\\
&+\frac{3N_c}{2}\lambda_{(V-A)^{\text{adj}}_\perp}\lambda_{\text{csc}}-2\lambda^2_{\text{csc}}+N_c\lambda^2_{\text{csc}}\Big)l^{(\text{F})}_\parallel(\tau,0,0)\\
&+64v_4\Big(-\lambda^2_{(\sigma\text{-}\pi)}-4\lambda_{(\sigma\text{-}\pi)}\lambda_{(S+P)_-}-4\lambda^2_{(S+P)_-}-4\lambda_{(\sigma\text{-}\pi)}\lambda_{(S+P)^{\text{adj}}_-}\\
&-8\lambda_{(S+P)_-}\lambda_{(S+P)^{\text{adj}}_-}-\lambda^2_{(S+P)^{\text{adj}}_-}-3\lambda_{(V-A)_\perp}\lambda_{(V-A)^{\text{adj}}_\perp}-\frac{1}{N_c^2}\lambda^2_{(S+P)^{\text{adj}}_-}\\
&+\frac{2}{N_c}\lambda_{(\sigma\text{-}\pi)}\lambda_{(S+P)^{\text{adj}}_-}+\frac{4}{N_c}\lambda_{(S+P)_-}\lambda_{(S+P)^{\text{adj}}_-}+\frac{4}{N_c}\lambda^2_{(S+P)^{\text{adj}}_-}+\frac{3}{2N_c}\lambda^2_{(V-A)^{\text{adj}}_\perp}\\
&-2\lambda_{(\sigma\text{-}\pi)}\lambda_{\text{csc}}-4\lambda_{(S+P)_-}\lambda_{\text{csc}}+2\lambda_{(S+P)^{\text{adj}}_-}\lambda_{\text{csc}}-\lambda_{(V-A)_\parallel}\lambda_{\text{csc}}\\
&-3\lambda_{(V-A)_\perp}\lambda_{\text{csc}}+\frac{3}{2}\lambda_{(V-A)^{\text{adj}}_\perp}\lambda_{\text{csc}}+\frac{2}{N_c}\lambda_{(S+P)^{\text{adj}}_-}\lambda_{\text{csc}}+\frac{3}{2N_c}\lambda_{(V-A)^{\text{adj}}_\perp}\lambda_{\text{csc}}\\
&+4\lambda^2_{\text{csc}}\Big)l^{(\text{F})}_\parallel(\tau,0,0)\\
&+64v_4\Big(\lambda^2_{(\sigma\text{-}\pi)}-2\lambda_{(\sigma\text{-}\pi)}\lambda_{(V+A)^{\text{adj}}_\parallel}+\lambda^2_{(V+A)^{\text{adj}}_\parallel}+\lambda_{(V-A)_\parallel}\lambda_{(V-A)^{\text{adj}}_\perp}\\
&-2\lambda_{(V-A)_\perp}\lambda_{(V-A)^{\text{adj}}_\perp}+\frac{1}{N_c}\lambda^2_{(V-A)^{\text{adj}}_\perp}-\frac{N_c}{2}\lambda^2_{(V-A)^{\text{adj}}_\perp}+2\lambda_{(V-A)_\perp}\lambda_{\text{csc}}
\end{aligned}
$$

$$
\begin{aligned}
&+\frac{1}{2}\lambda_{(V-A)_\perp^{\text{adj}}}\lambda_{\text{csc}}-\frac{1}{N_c}\lambda_{(V-A)_\perp^{\text{adj}}}\lambda_{\text{csc}}-\frac{N_c}{2}\lambda_{(V-A)_\perp^{\text{adj}}}\lambda_{\text{csc}}\Big)l_\perp^{(\text{F})}(\tau,0,0)\\
&+64v_4\Big(\lambda_{(\sigma\text{-}\pi)}^2+4\lambda_{(\sigma\text{-}\pi)}\lambda_{(S+P)_-}+4\lambda_{(S+P)_-}^2+\lambda_{(S+P)_-^{\text{adj}}}^2-\lambda_{(V-A)_\parallel}\lambda_{(V-A)_\perp^{\text{adj}}}\\
&-2\lambda_{(V-A)_\perp}\lambda_{(V-A)_\perp^{\text{adj}}}+\frac{1}{N_c^2}\lambda_{(S+P)_-^{\text{adj}}}^2-\frac{2}{N_c}\lambda_{(\sigma\text{-}\pi)}\lambda_{(S+P)_-^{\text{adj}}}-\frac{4}{N_c}\lambda_{(S+P)_-}\lambda_{(S+P)_-^{\text{adj}}}\\
&+\frac{1}{N_c}\lambda_{(V-A)_\perp^{\text{adj}}}^2-2\lambda_{(\sigma\text{-}\pi)}\lambda_{\text{csc}}-4\lambda_{(S+P)_-}\lambda_{\text{csc}}+2\lambda_{(S+P)_-^{\text{adj}}}\lambda_{\text{csc}}-\lambda_{(V-A)_\parallel}\lambda_{\text{csc}}\\
&-3\lambda_{(V-A)_\perp}\lambda_{\text{csc}}+\frac{3}{2}\lambda_{(V-A)_\perp^{\text{adj}}}\lambda_{\text{csc}}+\frac{2}{N_c}\lambda_{(S+P)_-^{\text{adj}}}\lambda_{\text{csc}}+\frac{3}{2N_c}\lambda_{(V-A)_\perp^{\text{adj}}}\lambda_{\text{csc}}\\
&+4\lambda_{\text{csc}}^2\Big)l_\perp^{(\text{F})}(\tau,0,0)\ ,
\end{aligned}
$$

$$
\begin{aligned}
\partial_t\lambda_{(S+P)_-^{\text{adj}}} \;=\;& 2\lambda_{(S+P)_-^{\text{adj}}}+64v_4\Big(\lambda_{(\sigma\text{-}\pi)}^2+2\lambda_{(S+P)_-^{\text{adj}}}\lambda_{(V+A)_\parallel}-\frac{3}{2}\lambda_{(\sigma\text{-}\pi)}\lambda_{(V+A)_\parallel^{\text{adj}}}\\
&+\lambda_{(S+P)_-}\lambda_{(V+A)_\parallel^{\text{adj}}}+\lambda_{(V+A)_\parallel^{\text{adj}}}^2+2\lambda_{(\sigma\text{-}\pi)}\lambda_{(V+A)_\perp}+4\lambda_{(S+P)_-}\lambda_{(V+A)_\perp}\\
&+2\lambda_{(S+P)_-^{\text{adj}}}\lambda_{(V+A)_\perp}-3\lambda_{(V-A)_\perp}\lambda_{(V-A)_\perp^{\text{adj}}}-\frac{3}{2N_c}\lambda_{(S+P)_-^{\text{adj}}}\lambda_{(V+A)_\parallel^{\text{adj}}}\\
&-\frac{2}{N_c}\lambda_{(S+P)_-^{\text{adj}}}\lambda_{(V+A)_\perp}+\frac{3}{2N_c}\lambda_{(V-A)_\perp^{\text{adj}}}^2+\frac{N_c}{2}\lambda_{(S+P)_-^{\text{adj}}}\lambda_{(V+A)_\parallel^{\text{adj}}}\\
&-\frac{3N_c}{4}\lambda_{(V-A)_\perp^{\text{adj}}}^2+2\lambda_{(V+A)_\parallel}\lambda_{\text{csc}}-2\lambda_{(V-A)_\parallel}\lambda_{\text{csc}}-\frac{1}{2}\lambda_{(V+A)_\parallel^{\text{adj}}}\lambda_{\text{csc}}\\
&+\frac{3}{2}\lambda_{(V-A)_\perp^{\text{adj}}}\lambda_{\text{csc}}-\frac{1}{N_c}\lambda_{(V+A)_\parallel^{\text{adj}}}\lambda_{\text{csc}}+\frac{N_c}{2}\lambda_{(V+A)_\parallel^{\text{adj}}}\lambda_{\text{csc}}-\frac{3N_c}{2}\lambda_{(V-A)_\perp^{\text{adj}}}\lambda_{\text{csc}}\\
&+2\lambda_{\text{csc}}^2-N_c\lambda_{\text{csc}}^2\Big)l_\parallel^{(\text{F})}(\tau,0,0)\\
&+64v_4\Big(\lambda_{(\sigma\text{-}\pi)}^2+4\lambda_{(\sigma\text{-}\pi)}\lambda_{(S+P)_-}+4\lambda_{(S+P)_-}^2+4\lambda_{(\sigma\text{-}\pi)}\lambda_{(S+P)_-^{\text{adj}}}\\
&+8\lambda_{(S+P)_-}\lambda_{(S+P)_-^{\text{adj}}}+\lambda_{(S+P)_-^{\text{adj}}}^2-\lambda_{(S+P)_-^{\text{adj}}}\lambda_{(V-A)_\parallel}+2\lambda_{(\sigma\text{-}\pi)}\lambda_{(V-A)_\perp}\\
&+4\lambda_{(S+P)_-}\lambda_{(V-A)_\perp}-\lambda_{(S+P)_-^{\text{adj}}}\lambda_{(V-A)_\perp}-\frac{1}{2}\lambda_{(\sigma\text{-}\pi)}\lambda_{(V-A)_\perp^{\text{adj}}}-\lambda_{(S+P)_-}\lambda_{(V-A)_\perp^{\text{adj}}}\\
&+\lambda_{(S+P)_-^{\text{adj}}}\lambda_{(V-A)_\perp^{\text{adj}}}+3\lambda_{(V-A)_\perp}\lambda_{(V-A)_\perp^{\text{adj}}}+\frac{1}{N_c^2}\lambda_{(S+P)_-^{\text{adj}}}^2+\frac{1}{N_c^2}\lambda_{(S+P)_-^{\text{adj}}}\lambda_{(V-A)_\perp^{\text{adj}}}\\
&-\frac{2}{N_c}\lambda_{(\sigma\text{-}\pi)}\lambda_{(S+P)_-^{\text{adj}}}-\frac{4}{N_c}\lambda_{(S+P)_-}\lambda_{(S+P)_-^{\text{adj}}}-\frac{4}{N_c}\lambda_{(S+P)_-^{\text{adj}}}^2-\frac{2}{N_c}\lambda_{(S+P)_-^{\text{adj}}}\lambda_{(V-A)_\perp}\\
&-\frac{1}{N_c}\lambda_{(\sigma\text{-}\pi)}\lambda_{(V-A)_\perp^{\text{adj}}}-\frac{2}{N_c}\lambda_{(S+P)_-}\lambda_{(V-A)_\perp^{\text{adj}}}+\frac{1}{N_c}\lambda_{(S+P)_-^{\text{adj}}}\lambda_{(V-A)_\perp^{\text{adj}}}
\end{aligned}
$$

$$
\begin{aligned}
&-\frac{3}{2N_c}\lambda^2_{(V-A)^{\text{adj}}_{\perp}}\Big)l^{(\text{F})}_{\parallel}(\tau,0,0)\\
&+64v_4\Big(-\lambda^2_{(\sigma\text{-}\pi)}+\frac{2}{3}\lambda_{(\sigma\text{-}\pi)}\lambda_{(V+A)_{\parallel}}+\frac{4}{3}\lambda_{(S+P)_-}\lambda_{(V+A)_{\parallel}}+\frac{2}{3}\lambda_{(S+P)^{\text{adj}}_-}\lambda_{(V+A)_{\parallel}}\\
&+\frac{11}{6}\lambda_{(\sigma\text{-}\pi)}\lambda_{(V+A)^{\text{adj}}_{\parallel}}-\frac{1}{3}\lambda_{(S+P)_-}\lambda_{(V+A)^{\text{adj}}_{\parallel}}-\lambda^2_{(V+A)^{\text{adj}}_{\parallel}}+\frac{4}{3}\lambda_{(\sigma\text{-}\pi)}\lambda_{(V+A)_{\perp}}\\
&+\frac{8}{3}\lambda_{(S+P)_-}\lambda_{(V+A)_{\perp}}+\frac{10}{3}\lambda_{(S+P)^{\text{adj}}_-}\lambda_{(V+A)_{\perp}}-\lambda_{(V-A)_{\parallel}}\lambda_{(V-A)^{\text{adj}}_{\perp}}\\
&+2\lambda_{(V-A)_{\perp}}\lambda_{(V-A)^{\text{adj}}_{\perp}}+\frac{1}{3N_c^2}\lambda_{(S+P)^{\text{adj}}_-}\lambda_{(V+A)^{\text{adj}}_{\parallel}}-\frac{2}{3N_c}\lambda_{(S+P)^{\text{adj}}_-}\lambda_{(V+A)_{\parallel}}\\
&-\frac{1}{3N_c}\lambda_{(\sigma\text{-}\pi)}\lambda_{(V+A)^{\text{adj}}_{\parallel}}-\frac{2}{3N_c}\lambda_{(S+P)_-}\lambda_{(V+A)^{\text{adj}}_{\parallel}}-\frac{1}{6N_c}\lambda_{(S+P)^{\text{adj}}_-}\lambda_{(V+A)^{\text{adj}}_{\parallel}}\\
&-\frac{4}{3N_c}\lambda_{(S+P)^{\text{adj}}_-}\lambda_{(V+A)_{\perp}}-\frac{1}{N_c}\lambda^2_{(V-A)^{\text{adj}}_{\perp}}-\frac{N_c}{6}\lambda_{(S+P)^{\text{adj}}_-}\lambda_{(V+A)^{\text{adj}}_{\parallel}}+\frac{N_c}{2}\lambda^2_{(V-A)^{\text{adj}}_{\perp}}\\
&+\frac{1}{6}\lambda_{(V+A)^{\text{adj}}_{\parallel}}\lambda_{\text{csc}}+2\lambda_{(V+A)_{\perp}}\lambda_{\text{csc}}-2\lambda_{(V-A)_{\perp}}\lambda_{\text{csc}}-\frac{1}{2}\lambda_{(V-A)^{\text{adj}}_{\perp}}\lambda_{\text{csc}}\\
&+\frac{1}{N_c}\lambda_{(V-A)^{\text{adj}}_{\perp}}\lambda_{\text{csc}}-\frac{N_c}{6}\lambda_{(V+A)^{\text{adj}}_{\parallel}}\lambda_{\text{csc}}+\frac{N_c}{2}\lambda_{(V-A)^{\text{adj}}_{\perp}}\lambda_{\text{csc}}\Big)l^{(\text{F})}_{\perp}(\tau,0,0)\\
&+64v_4\Big(-\lambda^2_{(\sigma\text{-}\pi)}-4\lambda_{(\sigma\text{-}\pi)}\lambda_{(S+P)_-}-4\lambda^2_{(S+P)_-}-\lambda^2_{(S+P)^{\text{adj}}_-}+\frac{2}{3}\lambda_{(\sigma\text{-}\pi)}\lambda_{(V-A)_{\parallel}}\\
&+\frac{4}{3}\lambda_{(S+P)_-}\lambda_{(V-A)_{\parallel}}-\frac{1}{3}\lambda_{(S+P)^{\text{adj}}_-}\lambda_{(V-A)_{\parallel}}+\frac{4}{3}\lambda_{(\sigma\text{-}\pi)}\lambda_{(V-A)_{\perp}}\\
&+\frac{8}{3}\lambda_{(S+P)_-}\lambda_{(V-A)_{\perp}}-\frac{5}{3}\lambda_{(S+P)^{\text{adj}}_-}\lambda_{(V-A)_{\perp}}-\frac{5}{6}\lambda_{(\sigma\text{-}\pi)}\lambda_{(V-A)^{\text{adj}}_{\perp}}\\
&-\frac{5}{3}\lambda_{(S+P)_-}\lambda_{(V-A)^{\text{adj}}_{\perp}}+\frac{2}{3}\lambda_{(S+P)^{\text{adj}}_-}\lambda_{(V-A)^{\text{adj}}_{\perp}}+\lambda_{(V-A)_{\parallel}}\lambda_{(V-A)^{\text{adj}}_{\perp}}\\
&+2\lambda_{(V-A)_{\perp}}\lambda_{(V-A)^{\text{adj}}_{\perp}}-\frac{1}{N_c^2}\lambda^2_{(S+P)^{\text{adj}}_-}+\frac{2}{3N_c^2}\lambda_{(S+P)^{\text{adj}}_-}\lambda_{(V-A)^{\text{adj}}_{\perp}}\\
&+\frac{2}{N_c}\lambda_{(\sigma\text{-}\pi)}\lambda_{(S+P)^{\text{adj}}_-}+\frac{4}{N_c}\lambda_{(S+P)_-}\lambda_{(S+P)^{\text{adj}}_-}-\frac{2}{3N_c}\lambda_{(S+P)^{\text{adj}}_-}\lambda_{(V-A)_{\parallel}}\\
&-\frac{4}{3N_c}\lambda_{(S+P)^{\text{adj}}_-}\lambda_{(V-A)_{\perp}}-\frac{2}{3N_c}\lambda_{(\sigma\text{-}\pi)}\lambda_{(V-A)^{\text{adj}}_{\perp}}-\frac{4}{3N_c}\lambda_{(S+P)_-}\lambda_{(V-A)^{\text{adj}}_{\perp}}\\
&+\frac{5}{3N_c}\lambda_{(S+P)^{\text{adj}}_-}\lambda_{(V-A)^{\text{adj}}_{\perp}}-\frac{1}{N_c}\lambda^2_{(V-A)^{\text{adj}}_{\perp}}\Big)l^{(\text{F})}_{\perp}(\tau,0,0)\ ,
\end{aligned}
$$

$$
\partial_t\lambda_{(S+P)_-} \;=\; 2\lambda_{(S+P)_-}+64v_4\Big(-\frac{1}{2}\lambda^2_{(\sigma\text{-}\pi)}+\lambda_{(\sigma\text{-}\pi)}\lambda_{(S+P)_-}+2\lambda^2_{(S+P)_-}+\frac{1}{2}\lambda_{(\sigma\text{-}\pi)}\lambda_{(V+A)_{\parallel}}
$$

$$
\begin{aligned}
&+2\lambda_{(S+P)_-}\lambda_{(V+A)_\parallel}-\frac{1}{2}\lambda_{(\sigma\text{-}\pi)}\lambda_{(V-A)_\parallel}+\lambda_{(\sigma\text{-}\pi)}\lambda_{(V+A)_\parallel^{\text{adj}}}\\
&+\frac{1}{4}\lambda_{(S+P)_-^{\text{adj}}}\lambda_{(V+A)_\parallel^{\text{adj}}}-\frac{1}{2}\lambda^2_{(V+A)_\parallel^{\text{adj}}}-\frac{1}{2}\lambda_{(\sigma\text{-}\pi)}\lambda_{(V+A)_\perp}+2\lambda_{(S+P)_-}\lambda_{(V+A)_\perp}\\
&+\lambda_{(S+P)_-^{\text{adj}}}\lambda_{(V+A)_\perp}+\frac{1}{2}\lambda_{(V+A)_\parallel^{\text{adj}}}\lambda_{(V+A)_\perp}-\frac{1}{2}\lambda_{(\sigma\text{-}\pi)}\lambda_{(V-A)_\perp}-\lambda_{(\sigma\text{-}\pi)}\lambda_{(V-A)_\perp^{\text{adj}}}\\
&+\frac{3}{2}\lambda_{(V-A)_\perp}\lambda_{(V-A)_\perp^{\text{adj}}}-\frac{3}{8}\lambda^2_{(V-A)_\perp^{\text{adj}}}+\frac{1}{2N_c^2}\lambda^2_{(S+P)_-^{\text{adj}}}-\frac{1}{4N_c^2}\lambda_{(S+P)_-^{\text{adj}}}\lambda_{(V+A)_\parallel^{\text{adj}}}\\
&-\frac{1}{N_c^2}\lambda_{(S+P)_-^{\text{adj}}}\lambda_{(V+A)_\perp}+\frac{3}{4N_c^2}\lambda^2_{(V-A)_\perp^{\text{adj}}}+\frac{1}{2N_c}\lambda^2_{(\sigma\text{-}\pi)}-\frac{1}{2N_c}\lambda_{(\sigma\text{-}\pi)}\lambda_{(S+P)_-^{\text{adj}}}\\
&-\frac{2}{N_c}\lambda_{(S+P)_-}\lambda_{(S+P)_-^{\text{adj}}}-\frac{1}{2N_c}\lambda^2_{(S+P)_-^{\text{adj}}}-\frac{1}{N_c}\lambda_{(\sigma\text{-}\pi)}\lambda_{(V+A)_\parallel^{\text{adj}}}-\frac{1}{2N_c}\lambda_{(S+P)_-}\lambda_{(V+A)_\parallel^{\text{adj}}}\\
&+\frac{1}{2N_c}\lambda^2_{(V+A)_\parallel^{\text{adj}}}+\frac{1}{N_c}\lambda_{(\sigma\text{-}\pi)}\lambda_{(V+A)_\perp}+\frac{2}{N_c}\lambda_{(S+P)_-}\lambda_{(V+A)_\perp}+\frac{1}{4N_c}\lambda_{(\sigma\text{-}\pi)}\lambda_{(V-A)_\perp^{\text{adj}}}\\
&-\frac{3}{2N_c}\lambda_{(V-A)_\perp}\lambda_{(V-A)_\perp^{\text{adj}}}-\frac{3}{4N_c}\lambda^2_{(V-A)_\perp^{\text{adj}}}+2N_c\lambda^2_{(S+P)_-}+N_c\lambda_{(S+P)_-}\lambda_{(S+P)_-^{\text{adj}}}\\
&+\frac{N_c}{2}\lambda_{(S+P)_-}\lambda_{(V+A)_\parallel^{\text{adj}}}+\frac{3N_c}{8}\lambda^2_{(V-A)_\perp^{\text{adj}}}-\lambda_{(\sigma\text{-}\pi)}\lambda_{\text{csc}}+\frac{1}{2}\lambda_{(S+P)_-^{\text{adj}}}\lambda_{\text{csc}}\\
&-\lambda_{(V+A)_\parallel}\lambda_{\text{csc}}+\lambda_{(V-A)_\parallel}\lambda_{\text{csc}}+\frac{1}{2}\lambda_{(V+A)_\parallel^{\text{adj}}}\lambda_{\text{csc}}-\frac{3}{2}\lambda_{(V-A)_\perp^{\text{adj}}}\lambda_{\text{csc}}\\
&-\frac{1}{2N_c^2}\lambda_{(V+A)_\parallel^{\text{adj}}}\lambda_{\text{csc}}+\frac{1}{N_c}\lambda_{(V+A)_\parallel}\lambda_{\text{csc}}-\frac{1}{N_c}\lambda_{(V-A)_\parallel}\lambda_{\text{csc}}+\frac{1}{4N_c}\lambda_{(V+A)_\parallel^{\text{adj}}}\lambda_{\text{csc}}\\
&+\frac{3}{4N_c}\lambda_{(V-A)_\perp^{\text{adj}}}\lambda_{\text{csc}}-N_c\lambda_{(S+P)_-}\lambda_{\text{csc}}-\frac{N_c}{2}\lambda_{(S+P)_-^{\text{adj}}}\lambda_{\text{csc}}-\frac{N_c}{4}\lambda_{(V+A)_\parallel^{\text{adj}}}\lambda_{\text{csc}}\\
&+\frac{3N_c}{4}\lambda_{(V-A)_\perp^{\text{adj}}}\lambda_{\text{csc}}-\frac{3}{2}\lambda^2_{\text{csc}}+\frac{1}{N_c}\lambda^2_{\text{csc}}+\frac{N_c}{2}\lambda^2_{\text{csc}}\Big)I^{(\text{F})}_\parallel(\tau,0,0)\\
&+64v_4\Big(-\frac{1}{2}\lambda^2_{(\sigma\text{-}\pi)}-2\lambda_{(\sigma\text{-}\pi)}\lambda_{(S+P)_-}-2\lambda^2_{(S+P)_-}-2\lambda_{(\sigma\text{-}\pi)}\lambda_{(S+P)_-^{\text{adj}}}-4\lambda_{(S+P)_-}\lambda_{(S+P)_-^{\text{adj}}}\\
&-\frac{1}{2}\lambda^2_{(S+P)_-^{\text{adj}}}+\frac{1}{2}\lambda_{(\sigma\text{-}\pi)}\lambda_{(V+A)_\parallel}-\frac{1}{2}\lambda_{(\sigma\text{-}\pi)}\lambda_{(V-A)_\parallel}-\lambda_{(S+P)_-}\lambda_{(V-A)_\parallel}-\frac{1}{2}\lambda_{(\sigma\text{-}\pi)}\lambda_{(V+A)_\perp}\\
&-\frac{1}{2}\lambda_{(V+A)_\parallel^{\text{adj}}}\lambda_{(V+A)_\perp}-\frac{1}{2}\lambda_{(\sigma\text{-}\pi)}\lambda_{(V-A)_\perp}-\lambda_{(S+P)_-}\lambda_{(V-A)_\perp}+\lambda_{(S+P)_-^{\text{adj}}}\lambda_{(V-A)_\perp}\\
&+\frac{1}{2}\lambda_{(\sigma\text{-}\pi)}\lambda_{(V-A)_\perp^{\text{adj}}}+\lambda_{(S+P)_-}\lambda_{(V-A)_\perp^{\text{adj}}}-\frac{1}{4}\lambda_{(S+P)_-^{\text{adj}}}\lambda_{(V-A)_\perp^{\text{adj}}}-\frac{3}{2}\lambda_{(V-A)_\perp}\lambda_{(V-A)_\perp^{\text{adj}}}\\
&+\frac{1}{2N_c^3}\lambda^2_{(S+P)_-^{\text{adj}}}+\frac{1}{2N_c^3}\lambda_{(S+P)_-^{\text{adj}}}\lambda_{(V-A)_\perp^{\text{adj}}}-\frac{1}{N_c^2}\lambda_{(\sigma\text{-}\pi)}\lambda_{(S+P)_-^{\text{adj}}}-\frac{2}{N_c^2}\lambda_{(S+P)_-}\lambda_{(S+P)_-^{\text{adj}}}
\end{aligned}
$$

$$
\begin{aligned}
&-\frac{5}{2N_c^2}\lambda^2_{(S+P)_-^{\rm adj}}\\
&-\frac{1}{N_c^2}\lambda_{(S+P)_-^{\rm adj}}\lambda_{(V-A)_\perp}-\frac{1}{2N_c^2}\lambda_{(\sigma\text{-}\pi)}\lambda_{(V-A)_\perp^{\rm adj}}-\frac{1}{N_c^2}\lambda_{(S+P)_-}\lambda_{(V-A)_\perp^{\rm adj}}\\
&+\frac{1}{4N_c^2}\lambda_{(S+P)_-^{\rm adj}}\lambda_{(V-A)_\perp^{\rm adj}}-\frac{3}{4N_c^2}\lambda^2_{(V-A)_\perp^{\rm adj}}+\frac{1}{2N_c}\lambda^2_{(\sigma\text{-}\pi)}+\frac{2}{N_c}\lambda_{(\sigma\text{-}\pi)}\lambda_{(S+P)_-}\\
&+\frac{2}{N_c}\lambda^2_{(S+P)_-}+\frac{3}{N_c}\lambda_{(\sigma\text{-}\pi)}\lambda_{(S+P)_-^{\rm adj}}+\frac{6}{N_c}\lambda_{(S+P)_-}\lambda_{(S+P)_-^{\rm adj}}+\frac{5}{2N_c}\lambda^2_{(S+P)_-^{\rm adj}}\\
&-\frac{1}{4N_c}\lambda_{(\sigma\text{-}\pi)}\lambda_{(V+A)_\parallel^{\rm adj}}+\frac{1}{N_c}\lambda_{(\sigma\text{-}\pi)}\lambda_{(V-A)_\perp}+\frac{2}{N_c}\lambda_{(S+P)_-}\lambda_{(V-A)_\perp}\\
&-\frac{1}{2N_c}\lambda_{(S+P)_-^{\rm adj}}\lambda_{(V-A)_\perp^{\rm adj}}+\frac{3}{2N_c}\lambda_{(V-A)_\perp}\lambda_{(V-A)_\perp^{\rm adj}}+\frac{3}{4N_c}\lambda^2_{(V-A)_\perp^{\rm adj}}\Big)l_\parallel^{(\rm F)}(\tau,0,0)\\
&+64v_4\Big(\frac{1}{2}\lambda^2_{(\sigma\text{-}\pi)}+\lambda_{(\sigma\text{-}\pi)}\lambda_{(S+P)_-}+2\lambda^2_{(S+P)_-}+\frac{1}{3}\lambda_{(\sigma\text{-}\pi)}\lambda_{(S+P)_-^{\rm adj}}\\
&+\frac{2}{3}\lambda_{(S+P)_-}\lambda_{(S+P)_-^{\rm adj}}-\frac{1}{6}\lambda_{(\sigma\text{-}\pi)}\lambda_{(V+A)_\parallel}+\frac{2}{3}\lambda_{(S+P)_-}\lambda_{(V+A)_\parallel}\\
&+\frac{1}{3}\lambda_{(S+P)_-^{\rm adj}}\lambda_{(V+A)_\parallel}-\frac{1}{6}\lambda_{(\sigma\text{-}\pi)}\lambda_{(V-A)_\parallel}-\frac{5}{6}\lambda_{(\sigma\text{-}\pi)}\lambda_{(V+A)_\parallel^{\rm adj}}\\
&+\frac{1}{3}\lambda_{(S+P)_-}\lambda_{(V+A)_\parallel^{\rm adj}}-\frac{1}{12}\lambda_{(S+P)_-^{\rm adj}}\lambda_{(V+A)_\parallel^{\rm adj}}+\frac{1}{6}\lambda_{(V+A)_\parallel}\lambda_{(V+A)_\parallel^{\rm adj}}+\frac{1}{2}\lambda^2_{(V+A)_\parallel^{\rm adj}}\\
&+\frac{1}{6}\lambda_{(\sigma\text{-}\pi)}\lambda_{(V+A)_\perp}+\frac{10}{3}\lambda_{(S+P)_-}\lambda_{(V+A)_\perp}+\frac{2}{3}\lambda_{(S+P)_-^{\rm adj}}\lambda_{(V+A)_\perp}\\
&+\frac{1}{3}\lambda_{(V+A)_\parallel^{\rm adj}}\lambda_{(V+A)_\perp}-\frac{1}{6}\lambda_{(\sigma\text{-}\pi)}\lambda_{(V-A)_\perp}-\frac{1}{3}\lambda_{(\sigma\text{-}\pi)}\lambda_{(V-A)_\perp^{\rm adj}}\\
&+\frac{1}{2}\lambda_{(V-A)_\parallel}\lambda_{(V-A)_\perp^{\rm adj}}-\lambda_{(V-A)_\perp}\lambda_{(V-A)_\perp^{\rm adj}}+\frac{1}{4}\lambda^2_{(V-A)_\perp^{\rm adj}}+\frac{1}{6N_c^3}\lambda_{(S+P)_-^{\rm adj}}\lambda_{(V+A)_\parallel^{\rm adj}}\\
&+\frac{1}{2N_c^2}\lambda^2_{(S+P)_-^{\rm adj}}-\frac{1}{3N_c^2}\lambda_{(S+P)_-^{\rm adj}}\lambda_{(V+A)_\parallel}-\frac{1}{6N_c^2}\lambda_{(\sigma\text{-}\pi)}\lambda_{(V+A)_\parallel^{\rm adj}}\\
&-\frac{1}{3N_c^2}\lambda_{(S+P)_-}\lambda_{(V+A)_\parallel^{\rm adj}}+\frac{1}{12N_c^2}\lambda_{(S+P)_-^{\rm adj}}\lambda_{(V+A)_\parallel^{\rm adj}}-\frac{2}{3N_c^2}\lambda_{(S+P)_-^{\rm adj}}\lambda_{(V+A)_\perp}\\
&-\frac{1}{2N_c^2}\lambda^2_{(V-A)_\perp^{\rm adj}}-\frac{1}{2N_c}\lambda^2_{(\sigma\text{-}\pi)}-\frac{1}{2N_c}\lambda_{(\sigma\text{-}\pi)}\lambda_{(S+P)_-^{\rm adj}}-\frac{2}{N_c}\lambda_{(S+P)_-}\lambda_{(S+P)_-^{\rm adj}}\\
&-\frac{5}{6N_c}\lambda^2_{(S+P)_-^{\rm adj}}+\frac{1}{3N_c}\lambda_{(\sigma\text{-}\pi)}\lambda_{(V+A)_\parallel}+\frac{2}{3N_c}\lambda_{(S+P)_-}\lambda_{(V+A)_\parallel}\\
&+\frac{1}{N_c}\lambda_{(\sigma\text{-}\pi)}\lambda_{(V+A)_\parallel^{\rm adj}}-\frac{1}{2N_c}\lambda_{(S+P)_-}\lambda_{(V+A)_\parallel^{\rm adj}}-\frac{1}{3N_c}\lambda_{(S+P)_-^{\rm adj}}\lambda_{(V+A)_\parallel^{\rm adj}}
\end{aligned}
$$

$$
\begin{aligned}
&-\frac{7}{12N_c}\lambda^2_{(V+A)^{\text{adj}}_{\parallel}}+\frac{2}{3N_c}\lambda_{(\sigma\text{-}\pi)}\lambda_{(V+A)_\perp}+\frac{4}{3N_c}\lambda_{(S+P)_-}\lambda_{(V+A)_\perp}\\
&+\frac{1}{12N_c}\lambda_{(\sigma\text{-}\pi)}\lambda_{(V-A)^{\text{adj}}_{\perp}}-\frac{1}{2N_c}\lambda_{(V-A)_\parallel}\lambda_{(V-A)^{\text{adj}}_{\perp}}+\frac{1}{N_c}\lambda_{(V-A)_\perp}\lambda_{(V-A)^{\text{adj}}_{\perp}}\\
&+\frac{1}{2N_c}\lambda^2_{(V-A)^{\text{adj}}_{\perp}}+2N_c\lambda^2_{(S+P)_-}+N_c\lambda_{(S+P)_-}\lambda_{(S+P)^{\text{adj}}_{-}}+\frac{N_c}{6}\lambda^2_{(S+P)^{\text{adj}}_{-}}\\
&+\frac{N_c}{2}\lambda_{(S+P)_-}\lambda_{(V+A)^{\text{adj}}_{\parallel}}+\frac{N_c}{6}\lambda_{(S+P)^{\text{adj}}_{-}}\lambda_{(V+A)^{\text{adj}}_{\parallel}}+\frac{N_c}{24}\lambda^2_{(V+A)^{\text{adj}}_{\parallel}}\\
&-\frac{N_c}{4}\lambda^2_{(V-A)^{\text{adj}}_{\perp}}-\frac{1}{3}\lambda_{(\sigma\text{-}\pi)}\lambda_{\text{csc}}+\frac{2}{3}\lambda_{(S+P)_-}\lambda_{\text{csc}}+\frac{1}{6}\lambda_{(S+P)^{\text{adj}}_{-}}\lambda_{\text{csc}}-\lambda_{(V+A)_\perp}\lambda_{\text{csc}}\\
&+\lambda_{(V-A)_\perp}\lambda_{\text{csc}}+\frac{1}{2}\lambda_{(V-A)^{\text{adj}}_{\perp}}\lambda_{\text{csc}}+\frac{1}{2N_c^2}\lambda_{(V-A)^{\text{adj}}_{\perp}}\lambda_{\text{csc}}-\frac{1}{3N_c}\lambda_{(S+P)^{\text{adj}}_{-}}\lambda_{\text{csc}}\\
&+\frac{1}{12N_c}\lambda_{(V+A)^{\text{adj}}_{\parallel}}\lambda_{\text{csc}}+\frac{1}{N_c}\lambda_{(V+A)_\perp}\lambda_{\text{csc}}-\frac{1}{N_c}\lambda_{(V-A)_\perp}\lambda_{\text{csc}}-\frac{3}{4N_c}\lambda_{(V-A)^{\text{adj}}_{\perp}}\lambda_{\text{csc}}\\
&-N_c\lambda_{(S+P)_-}\lambda_{\text{csc}}-\frac{N_c}{6}\lambda_{(S+P)^{\text{adj}}_{-}}\lambda_{\text{csc}}-\frac{N_c}{12}\lambda_{(V+A)^{\text{adj}}_{\parallel}}\lambda_{\text{csc}}-\frac{N_c}{4}\lambda_{(V-A)^{\text{adj}}_{\perp}}\lambda_{\text{csc}}\\
&-\frac{1}{3}\lambda^2_{\text{csc}}+\frac{N_c}{6}\lambda^2_{\text{csc}}\Big)l^{(\text{F})}_{\perp}(\tau,0,0)\\
&+64v_4\Big(\frac{1}{2}\lambda^2_{(\sigma\text{-}\pi)}+2\lambda_{(\sigma\text{-}\pi)}\lambda_{(S+P)_-}+2\lambda^2_{(S+P)_-}+\frac{1}{2}\lambda^2_{(S+P)^{\text{adj}}_{-}}-\frac{1}{6}\lambda_{(\sigma\text{-}\pi)}\lambda_{(V+A)_\parallel}\\
&-\frac{1}{6}\lambda_{(\sigma\text{-}\pi)}\lambda_{(V-A)_\parallel}-\frac{1}{3}\lambda_{(S+P)_-}\lambda_{(V-A)_\parallel}+\frac{1}{3}\lambda_{(S+P)^{\text{adj}}_{-}}\lambda_{(V-A)_\parallel}-\frac{1}{6}\lambda_{(V+A)_\parallel}\lambda_{(V+A)^{\text{adj}}_{\parallel}}\\
&+\frac{5}{6}\lambda_{(\sigma\text{-}\pi)}\lambda_{(V+A)_\perp}+\frac{1}{3}\lambda_{(V+A)^{\text{adj}}_{\parallel}}\lambda_{(V+A)_\perp}-\frac{5}{6}\lambda_{(\sigma\text{-}\pi)}\lambda_{(V-A)_\perp}-\frac{5}{3}\lambda_{(S+P)_-}\lambda_{(V-A)_\perp}\\
&+\frac{2}{3}\lambda_{(S+P)^{\text{adj}}_{-}}\lambda_{(V-A)_\perp}+\frac{1}{3}\lambda_{(\sigma\text{-}\pi)}\lambda_{(V-A)^{\text{adj}}_{\perp}}+\frac{2}{3}\lambda_{(S+P)_-}\lambda_{(V-A)^{\text{adj}}_{\perp}}-\frac{5}{12}\lambda_{(S+P)^{\text{adj}}_{-}}\lambda_{(V-A)^{\text{adj}}_{\perp}}\\
&-\frac{1}{2}\lambda_{(V-A)_\parallel}\lambda_{(V-A)^{\text{adj}}_{\perp}}-\lambda_{(V-A)_\perp}\lambda_{(V-A)^{\text{adj}}_{\perp}}-\frac{1}{2N_c^3}\lambda^2_{(S+P)^{\text{adj}}_{-}}+\frac{1}{3N_c^3}\lambda_{(S+P)^{\text{adj}}_{-}}\lambda_{(V-A)^{\text{adj}}_{\perp}}\\
&+\frac{1}{N_c^2}\lambda_{(\sigma\text{-}\pi)}\lambda_{(S+P)^{\text{adj}}_{-}}+\frac{2}{N_c^2}\lambda_{(S+P)_-}\lambda_{(S+P)^{\text{adj}}_{-}}+\frac{1}{2N_c^2}\lambda^2_{(S+P)^{\text{adj}}_{-}}-\frac{1}{3N_c^2}\lambda_{(S+P)^{\text{adj}}_{-}}\lambda_{(V-A)_\parallel}\\
&-\frac{2}{3N_c^2}\lambda_{(S+P)^{\text{adj}}_{-}}\lambda_{(V-A)_\perp}-\frac{1}{3N_c^2}\lambda_{(\sigma\text{-}\pi)}\lambda_{(V-A)^{\text{adj}}_{\perp}}-\frac{2}{3N_c^2}\lambda_{(S+P)_-}\lambda_{(V-A)^{\text{adj}}_{\perp}}\\
&+\frac{5}{12N_c^2}\lambda_{(S+P)^{\text{adj}}_{-}}\lambda_{(V-A)^{\text{adj}}_{\perp}}-\frac{1}{2N_c^2}\lambda^2_{(V-A)^{\text{adj}}_{\perp}}-\frac{1}{2N_c}\lambda^2_{(\sigma\text{-}\pi)}-\frac{2}{N_c}\lambda_{(\sigma\text{-}\pi)}\lambda_{(S+P)_-}-\frac{2}{N_c}\lambda^2_{(S+P)_-}\\
&-\frac{1}{N_c}\lambda_{(\sigma\text{-}\pi)}\lambda_{(S+P)^{\text{adj}}_{-}}-\frac{2}{N_c}\lambda_{(S+P)_-}\lambda_{(S+P)^{\text{adj}}_{-}}-\frac{1}{2N_c}\lambda^2_{(S+P)^{\text{adj}}_{-}}+\frac{1}{3N_c}\lambda_{(\sigma\text{-}\pi)}\lambda_{(V-A)_\parallel}
\end{aligned}
$$

$$
\begin{aligned}
&+\frac{2}{3N_c}\lambda_{(S+P)_-}\lambda_{(V-A)_\parallel}+\frac{1}{12N_c}\lambda_{(\sigma\text{-}\pi)}\lambda_{(V+A)_\parallel^{\text{adj}}}+\frac{1}{12N_c}\lambda^2_{(V+A)_\parallel^{\text{adj}}}\\
&+\frac{2}{3N_c}\lambda_{(\sigma\text{-}\pi)}\lambda_{(V-A)_\perp}+\frac{4}{3N_c}\lambda_{(S+P)_-}\lambda_{(V-A)_\perp}-\frac{1}{3N_c}\lambda_{(S+P)_-^{\text{adj}}}\lambda_{(V-A)_\perp^{\text{adj}}}\\
&+\frac{1}{2N_c}\lambda_{(V-A)_\parallel}\lambda_{(V-A)_\perp^{\text{adj}}}+\frac{1}{N_c}\lambda_{(V-A)_\perp}\lambda_{(V-A)_\perp^{\text{adj}}}+\frac{1}{2N_c}\lambda^2_{(V-A)_\perp^{\text{adj}}}\Big)l_\perp^{(\text{F})}(\tau,0,0)\ ,
\end{aligned}
$$

$$
\begin{aligned}
\partial_t\lambda_{(V+A)_\parallel} \;=\;& 2\lambda_{(V+A)_\parallel}+64v_4\Big(\frac{1}{2}\lambda^2_{(\sigma\text{-}\pi)}+2\lambda_{(\sigma\text{-}\pi)}\lambda_{(S+P)_-}+2\lambda^2_{(S+P)_-}+\frac{1}{2}\lambda_{(\sigma\text{-}\pi)}\lambda_{(S+P)_-^{\text{adj}}}\\
&+\lambda_{(S+P)_-}\lambda_{(S+P)_-^{\text{adj}}}+\lambda^2_{(S+P)_-^{\text{adj}}}+\frac{1}{2}\lambda^2_{(V+A)_\parallel}+2\lambda_{(\sigma\text{-}\pi)}\lambda_{(V-A)_\parallel}\\
&+\lambda_{(V+A)_\parallel}\lambda_{(V-A)_\parallel}+\frac{1}{8}\lambda^2_{(V+A)_\parallel^{\text{adj}}}+\frac{3}{2}\lambda^2_{(V+A)_\perp}-3\lambda_{(V+A)_\parallel}\lambda_{(V-A)_\perp}\\
&+\frac{3}{4}\lambda_{(\sigma\text{-}\pi)}\lambda_{(V-A)_\perp^{\text{adj}}}-\frac{1}{2N_c^2}\lambda^2_{(S+P)_-^{\text{adj}}}-\frac{1}{8N_c^2}\lambda^2_{(V+A)_\parallel^{\text{adj}}}-\frac{1}{N_c^2}\lambda_{(\sigma\text{-}\pi)}\lambda_{(V-A)_\perp^{\text{adj}}}\\
&-\frac{1}{2N_c}\lambda^2_{(S+P)_-^{\text{adj}}}-\frac{1}{2N_c}\lambda_{(V+A)_\parallel^{\text{adj}}}\lambda_{(V+A)_\perp}+\frac{2}{N_c}\lambda_{(\sigma\text{-}\pi)}\lambda_{(V-A)_\perp}\\
&+\frac{1}{N_c}\lambda_{(\sigma\text{-}\pi)}\lambda_{(V-A)_\perp^{\text{adj}}}+\frac{3}{2N_c}\lambda_{(V+A)_\parallel}\lambda_{(V-A)_\perp^{\text{adj}}}-4N_c\lambda_{(V+A)_\parallel}\lambda_{(V-A)_\parallel}\\
&-\frac{3N_c}{2}\lambda_{(V+A)_\parallel}\lambda_{(V-A)_\perp^{\text{adj}}}-\lambda_{(\sigma\text{-}\pi)}\lambda_{\text{csc}}-\lambda_{(S+P)_-}\lambda_{\text{csc}}+\frac{3}{2}\lambda_{(S+P)_-^{\text{adj}}}\lambda_{\text{csc}}\\
&-\lambda_{(V+A)_\parallel}\lambda_{\text{csc}}-\frac{1}{N_c^2}\lambda_{(S+P)_-^{\text{adj}}}\lambda_{\text{csc}}+\frac{2}{N_c}\lambda_{(\sigma\text{-}\pi)}\lambda_{\text{csc}}+\frac{2}{N_c}\lambda_{(S+P)_-}\lambda_{\text{csc}}\\
&-\frac{1}{2N_c}\lambda_{(S+P)_-^{\text{adj}}}\lambda_{\text{csc}}+N_c\lambda_{(V+A)_\parallel}\lambda_{\text{csc}}+\lambda^2_{\text{csc}}-\frac{1}{N_c}\lambda^2_{\text{csc}}\Big)l_\parallel^{(\text{F})}(\tau,0,0)\\
&+64v_4\Big(-\frac{1}{2}\lambda^2_{(\sigma\text{-}\pi)}-\frac{1}{2}\lambda^2_{(V+A)_\parallel}+\frac{1}{4}\lambda_{(\sigma\text{-}\pi)}\lambda_{(V+A)_\parallel^{\text{adj}}}-\frac{1}{8}\lambda^2_{(V+A)_\parallel^{\text{adj}}}-\frac{3}{2}\lambda^2_{(V+A)_\perp}\\
&+\frac{1}{8N_c^2}\lambda^2_{(V+A)_\parallel^{\text{adj}}}+\frac{2}{N_c}\lambda_{(\sigma\text{-}\pi)}\lambda_{(V+A)_\perp}+\frac{1}{2N_c}\lambda_{(V+A)_\parallel^{\text{adj}}}\lambda_{(V+A)_\perp}\Big)l_\parallel^{(\text{F})}(\tau,0,0)\\
&+64v_4\Big(\frac{1}{2}\lambda_{(\sigma\text{-}\pi)}\lambda_{(S+P)_-^{\text{adj}}}+\lambda_{(S+P)_-}\lambda_{(S+P)_-^{\text{adj}}}+\frac{1}{3}\lambda^2_{(S+P)_-^{\text{adj}}}-2\lambda_{(\sigma\text{-}\pi)}\lambda_{(V-A)_\parallel}\\
&-\lambda_{(V+A)_\parallel}\lambda_{(V-A)_\parallel}-\frac{1}{24}\lambda^2_{(V+A)_\parallel^{\text{adj}}}+\lambda_{(V+A)_\parallel}\lambda_{(V+A)_\perp}+\lambda^2_{(V+A)_\perp}\\
&+3\lambda_{(V+A)_\parallel}\lambda_{(V-A)_\perp}-\frac{3}{4}\lambda_{(\sigma\text{-}\pi)}\lambda_{(V-A)_\perp^{\text{adj}}}+\frac{1}{3N_c^2}\lambda^2_{(S+P)_-^{\text{adj}}}+\frac{1}{12N_c^2}\lambda^2_{(V+A)_\parallel^{\text{adj}}}\\
&+\frac{2}{3N_c^2}\lambda_{(\sigma\text{-}\pi)}\lambda_{(V-A)_\perp^{\text{adj}}}-\frac{1}{3N_c}\lambda_{(\sigma\text{-}\pi)}\lambda_{(S+P)_-^{\text{adj}}}-\frac{2}{3N_c}\lambda_{(S+P)_-}\lambda_{(S+P)_-^{\text{adj}}}
\end{aligned}
$$

$$
\begin{aligned}
&-\frac{1}{2N_c}\lambda^2_{(S+P)^{\text{adj}}_-}+\frac{2}{3N_c}\lambda_{(\sigma\text{-}\pi)}\lambda_{(V-A)_\parallel}-\frac{1}{6N_c}\lambda_{(V+A)_\parallel}\lambda_{(V+A)^{\text{adj}}_\parallel}\\
&-\frac{1}{3N_c}\lambda_{(V+A)^{\text{adj}}_\parallel}\lambda_{(V+A)_\perp}-\frac{4}{3N_c}\lambda_{(\sigma\text{-}\pi)}\lambda_{(V-A)_\perp}+\frac{1}{3N_c}\lambda_{(\sigma\text{-}\pi)}\lambda_{(V-A)^{\text{adj}}_\perp}\\
&-\frac{3}{2N_c}\lambda_{(V+A)_\parallel}\lambda_{(V-A)^{\text{adj}}_\perp}+4N_c\lambda_{(V+A)_\parallel}\lambda_{(V-A)_\parallel}+\frac{3N_c}{2}\lambda_{(V+A)_\parallel}\lambda_{(V-A)^{\text{adj}}_\perp}+\lambda_{(\sigma\text{-}\pi)}\lambda_{\text{csc}}\\
&+\lambda_{(S+P)_-}\lambda_{\text{csc}}+\frac{1}{6}\lambda_{(S+P)^{\text{adj}}_-}\lambda_{\text{csc}}+\lambda_{(V+A)_\parallel}\lambda_{\text{csc}}+\frac{1}{3N_c^2}\lambda_{(S+P)^{\text{adj}}_-}\lambda_{\text{csc}}\\
&-\frac{2}{3N_c}\lambda_{(\sigma\text{-}\pi)}\lambda_{\text{csc}}-\frac{2}{3N_c}\lambda_{(S+P)_-}\lambda_{\text{csc}}-\frac{1}{6N_c}\lambda_{(S+P)^{\text{adj}}_-}\lambda_{\text{csc}}-N_c\lambda_{(V+A)_\parallel}\lambda_{\text{csc}}\\
&-\frac{1}{6}\lambda^2_{\text{csc}}+\frac{1}{3N_c}\lambda^2_{\text{csc}}\Big)l^{(\text{F})}_\perp(\tau,0,0)\\
&+64v_4\Big(\frac{1}{4}\lambda_{(\sigma\text{-}\pi)}\lambda_{(V+A)^{\text{adj}}_\parallel}-\lambda_{(V+A)_\parallel}\lambda_{(V+A)_\perp}+\lambda^2_{(V+A)_\perp}-\frac{1}{3N_c^2}\lambda_{(\sigma\text{-}\pi)}\lambda_{(V+A)^{\text{adj}}_\parallel}\\
&-\frac{1}{12N_c^2}\lambda^2_{(V+A)^{\text{adj}}_\parallel}\\
&+\frac{2}{3N_c}\lambda_{(\sigma\text{-}\pi)}\lambda_{(V+A)_\parallel}+\frac{1}{6N_c}\lambda_{(V+A)_\parallel}\lambda_{(V+A)^{\text{adj}}_\parallel}\\
&-\frac{4}{3N_c}\lambda_{(\sigma\text{-}\pi)}\lambda_{(V+A)_\perp}-\frac{1}{3N_c}\lambda_{(V+A)^{\text{adj}}_\parallel}\lambda_{(V+A)_\perp}\Big)l^{(\text{F})}_\perp(\tau,0,0)\ ,
\end{aligned}
$$

$$
\begin{aligned}
\partial_t\lambda_{(V+A)_\perp} \;=\;& 2\lambda_{(V+A)_\perp}+64v_4\Big(-\frac{1}{2N_c}\lambda^2_{(S+P)^{\text{adj}}_-}+\frac{1}{2}\lambda^2_{(S+P)^{\text{adj}}_-}+\frac{1}{2}\lambda_{\text{csc}}\lambda_{(S+P)^{\text{adj}}_-}+\frac{1}{2}\lambda_{(\sigma\text{-}\pi)}\lambda_{(S+P)^{\text{adj}}_-}\\
&+\lambda_{(S+P)_-}\lambda_{(S+P)^{\text{adj}}_-}-\frac{1}{2N_c}\lambda_{\text{csc}}\lambda_{(S+P)^{\text{adj}}_-}+\lambda^2_{(V+A)_\perp}+\lambda_{\text{csc}}\lambda_{(\sigma\text{-}\pi)}+\lambda_{\text{csc}}\lambda_{(S+P)_-}\\
&-2\lambda_{(\sigma\text{-}\pi)}\lambda_{(V-A)_\perp}-\frac{1}{4}\lambda_{(\sigma\text{-}\pi)}\lambda_{(V-A)^{\text{adj}}_\perp}+\lambda_{\text{csc}}\lambda_{(V+A)_\perp}+\lambda_{(V-A)_\parallel}\lambda_{(V+A)_\perp}+\lambda_{(V-A)_\perp}\lambda_{(V+A)_\perp}\\
&+\lambda_{(V+A)_\parallel}\lambda_{(V+A)_\perp}-N_c\lambda_{\text{csc}}\lambda_{(V+A)_\perp}+4N_c\lambda_{(V-A)_\perp}\lambda_{(V+A)_\perp}+\frac{N_c}{2}\lambda_{(V-A)^{\text{adj}}_\perp}\lambda_{(V+A)_\perp}\\
&+\frac{1}{N_c}\lambda_{(\sigma\text{-}\pi)}\lambda_{(V-A)^{\text{adj}}_\perp}-\frac{1}{2N_c}\lambda_{(V-A)^{\text{adj}}_\perp}\lambda_{(V+A)_\perp}-\frac{1}{2N_c}\lambda_{(V+A)^{\text{adj}}_\parallel}\lambda_{(V+A)_\perp}\Big)l^{(\text{F})}_\parallel(\tau,0,0)\\
&+64v_4\Big(\lambda^2_{(V+A)_\perp}-\lambda_{(V+A)_\parallel}\lambda_{(V+A)_\perp}+\frac{1}{2N_c}\lambda_{(V+A)^{\text{adj}}_\parallel}\lambda_{(V+A)_\perp}+\frac{1}{4}\lambda_{(\sigma\text{-}\pi)}\lambda_{(V+A)^{\text{adj}}_\parallel}\Big)l^{(\text{F})}_\parallel(\tau,0,0)\\
&+64v_4\Big(\frac{1}{6}\lambda^2_{\text{csc}}+\frac{1}{3}\lambda_{(\sigma\text{-}\pi)}\lambda_{\text{csc}}+\frac{1}{3}\lambda_{(S+P)_-}\lambda_{\text{csc}}+\frac{1}{2}\lambda_{(S+P)^{\text{adj}}_-}\lambda_{\text{csc}}+\frac{1}{3}\lambda_{(V+A)_\perp}\lambda_{\text{csc}}\\
&-\frac{N_c}{3}\lambda_{(V+A)_\perp}\lambda_{\text{csc}}-\frac{1}{6N_c}\lambda_{(S+P)^{\text{adj}}_-}\lambda_{\text{csc}}+\frac{1}{6}\lambda^2_{(\sigma\text{-}\pi)}+\frac{2}{3}\lambda^2_{(S+P)_-}+\frac{1}{2}\lambda^2_{(S+P)^{\text{adj}}_-}+\frac{1}{6}\lambda^2_{(V+A)_\parallel}
\end{aligned}
$$

$$
\begin{aligned}
&+\frac{7}{6}\lambda^2_{(V+A)_\perp}+\frac{2}{3}\lambda_{(\sigma\text{-}\pi)}\lambda_{(S+P)_-}+\frac{1}{2}\lambda_{(\sigma\text{-}\pi)}\lambda_{(S+P)_-^{\rm adj}}+\lambda_{(S+P)_-}\lambda_{(S+P)_-^{\rm adj}}\\
&-\frac{2}{3}\lambda_{(\sigma\text{-}\pi)}\lambda_{(V-A)_\perp}-\frac{1}{12}\lambda_{(\sigma\text{-}\pi)}\lambda_{(V-A)_\perp^{\rm adj}}+\frac{1}{3}\lambda_{(V-A)_\parallel}\lambda_{(V+A)_\perp}\\
&+\frac{1}{3}\lambda_{(V-A)_\perp}\lambda_{(V+A)_\perp}+\frac{2}{3}\lambda_{(V+A)_\parallel}\lambda_{(V+A)_\perp}\\
&+\frac{4}{3}N_c\lambda_{(V-A)_\perp}\lambda_{(V+A)_\perp}+\frac{N_c}{6}\lambda_{(V-A)_\perp^{\rm adj}}\lambda_{(V+A)_\perp}-\frac{1}{2N_c}\lambda^2_{(S+P)_-^{\rm adj}}\\
&-\frac{1}{3N_c}\lambda_{(\sigma\text{-}\pi)}\lambda_{(S+P)_-^{\rm adj}}-\frac{2}{3N_c}\lambda_{(S+P)_-}\lambda_{(S+P)_-^{\rm adj}}+\frac{1}{3N_c}\lambda_{(\sigma\text{-}\pi)}\lambda_{(V-A)_\perp^{\rm adj}}\\
&-\frac{1}{6N_c}\lambda_{(V+A)_\parallel}\lambda_{(V+A)_\parallel^{\rm adj}}-\frac{1}{6N_c}\lambda_{(V-A)_\perp^{\rm adj}}\lambda_{(V+A)_\perp}-\frac{1}{3N_c}\lambda_{(V+A)_\parallel^{\rm adj}}\lambda_{(V+A)_\perp}\\
&+\frac{1}{6N_c^2}\lambda^2_{(S+P)_-^{\rm adj}}+\frac{1}{24N_c^2}\lambda^2_{(V+A)_\parallel^{\rm adj}}\Big)l_\perp^{(\rm F)}(\tau,0,0)\\
&+64v_4\Big(-\frac{1}{6}\lambda^2_{(\sigma\text{-}\pi)}-\frac{1}{12}\lambda_{(V+A)_\parallel^{\rm adj}}\lambda_{(\sigma\text{-}\pi)}-\frac{1}{6}\lambda^2_{(V+A)_\parallel}-\frac{1}{24}\lambda^2_{(V+A)_\parallel^{\rm adj}}\\
&-\frac{7}{6}\lambda^2_{(V+A)_\perp}+\frac{2}{3}\lambda_{(V+A)_\parallel}\lambda_{(V+A)_\perp}+\frac{1}{6N_c}\lambda_{(V+A)_\parallel}\lambda_{(V+A)_\parallel^{\rm adj}}\\
&-\frac{1}{3N_c}\lambda_{(V+A)_\parallel^{\rm adj}}\lambda_{(V+A)_\perp}-\frac{1}{24N_c^2}\lambda^2_{(V+A)_\parallel^{\rm adj}}\Big)l_\perp^{(\rm F)}(\tau,0,0)\,,\\
\partial_t\lambda_{(V-A)_\parallel} \;=\;& 2\lambda_{(V-A)_\parallel}+64v_4\Big(\frac{1}{2}N_c\lambda^2_{\rm csc}-\frac{1}{2}\lambda^2_{\rm csc}-\lambda_{(V-A)_\parallel}\lambda_{\rm csc}-\frac{3}{2}\lambda_{(V-A)_\perp^{\rm adj}}\lambda_{\rm csc}\\
&+N_c\lambda_{(V-A)_\parallel}\lambda_{\rm csc}+\frac{3}{2}N_c\lambda_{(V-A)_\perp^{\rm adj}}\lambda_{\rm csc}-\frac{1}{2}\lambda^2_{(\sigma\text{-}\pi)}+\frac{3}{2}\lambda^2_{(V-A)_\parallel}+\frac{3}{2}\lambda^2_{(V-A)_\perp}\\
&-\frac{1}{2}\lambda^2_{(V+A)_\parallel^{\rm adj}}-3\lambda_{(V-A)_\parallel}\lambda_{(V-A)_\perp}+\frac{3}{2}\lambda_{(V-A)_\perp}\lambda_{(V-A)_\perp^{\rm adj}}+2\lambda_{(\sigma\text{-}\pi)}\lambda_{(V+A)_\parallel}\\
&+\lambda_{(\sigma\text{-}\pi)}\lambda_{(V+A)_\parallel^{\rm adj}}-2N_c\lambda^2_{(V-A)_\parallel}+\frac{3}{8}N_c\lambda^2_{(V-A)_\perp^{\rm adj}}-2N_c\lambda^2_{(V+A)_\parallel}-\\
&\frac{3}{2}N_c\lambda_{(V-A)_\parallel}\lambda_{(V-A)_\perp^{\rm adj}}-\frac{3}{4N_c}\lambda^2_{(V-A)_\perp^{\rm adj}}+\frac{1}{2N_c}\lambda^2_{(V+A)_\parallel^{\rm adj}}+\frac{3}{2N_c}\lambda_{(V-A)_\parallel}\lambda_{(V-A)_\perp^{\rm adj}}\\
&-\frac{3}{2N_c}\lambda_{(V-A)_\perp}\lambda_{(V-A)_\perp^{\rm adj}}-\frac{1}{N_c}\lambda_{(\sigma\text{-}\pi)}\lambda_{(V+A)_\parallel^{\rm adj}}+\frac{3}{8N_c^2}\lambda^2_{(V-A)_\perp^{\rm adj}}\Big)l_\parallel^{(\rm F)}(\tau,0,0)\\
&+64v_4\Big(-\frac{3}{2}\lambda^2_{(\sigma\text{-}\pi)}-6\lambda_{(S+P)_-}\lambda_{(\sigma\text{-}\pi)}-3\lambda_{(S+P)_-^{\rm adj}}\lambda_{(\sigma\text{-}\pi)}+\frac{3}{N_c}\lambda_{(S+P)_-^{\rm adj}}\lambda_{(\sigma\text{-}\pi)}\\
&-6\lambda^2_{(S+P)_-}-\frac{3}{2}\lambda^2_{(S+P)_-^{\rm adj}}-\frac{1}{2}\lambda^2_{(V-A)_\parallel}-\frac{3}{2}\lambda^2_{(V-A)_\perp}-\frac{3}{8}\lambda^2_{(V-A)_\perp^{\rm adj}}\\
&-6\lambda_{(S+P)_-}\lambda_{(S+P)_-^{\rm adj}}-\frac{3}{2}\lambda_{(V-A)_\perp}\lambda_{(V-A)_\perp^{\rm adj}}+\frac{3}{N_c}\lambda^2_{(S+P)_-^{\rm adj}}+\frac{3}{4N_c}\lambda^2_{(V-A)_\perp^{\rm adj}}
\end{aligned}
$$

$$
\begin{aligned}
&+\frac{6}{N_c}\lambda_{(S+P)_-}\lambda_{(S+P)_-^{\rm adj}}+\frac{3}{2N_c}\lambda_{(V-A)_\perp}\lambda_{(V-A)_\perp^{\rm adj}}-\frac{3}{2N_c^2}\lambda^2_{(S+P)_-^{\rm adj}}\\
&-\frac{3}{8N_c^2}\lambda^2_{(V-A)_\perp^{\rm adj}}\Big)l^{(\rm F)}_{\parallel}(\tau,0,0)\\
&+64v_4\Big(\frac{1}{2}\lambda^2_{(\sigma\text{-}\pi)}-2\lambda_{(V+A)_\parallel}\lambda_{(\sigma\text{-}\pi)}-\lambda_{(V+A)_\parallel^{\rm adj}}\lambda_{(\sigma\text{-}\pi)}+\frac{1}{N_c}\lambda_{(V+A)_\parallel^{\rm adj}}\lambda_{(\sigma\text{-}\pi)}-\lambda^2_{(V-A)_\parallel}\\
&-\lambda^2_{(V-A)_\perp}+\frac{1}{2}\lambda^2_{(V+A)_\parallel^{\rm adj}}+\lambda_{\rm csc}\lambda_{(V-A)_\parallel}+4\lambda_{(V-A)_\parallel}\lambda_{(V-A)_\perp}+\lambda_{\rm csc}\lambda_{(V-A)_\perp^{\rm adj}}\\
&+\frac{1}{2}\lambda_{(V-A)_\parallel}\lambda_{(V-A)_\perp^{\rm adj}}-\lambda_{(V-A)_\perp}\lambda_{(V-A)_\perp^{\rm adj}}+2N_c\lambda^2_{(V-A)_\parallel}-\frac{N_c}{4}\lambda^2_{(V-A)_\perp^{\rm adj}}+2N_c\lambda^2_{(V+A)_\parallel}\\
&-N_c\lambda_{\rm csc}\lambda_{(V-A)_\parallel}-N_c\lambda_{\rm csc}\lambda_{(V-A)_\perp^{\rm adj}}+\frac{3}{2}N_c\lambda_{(V-A)_\parallel}\lambda_{(V-A)_\perp^{\rm adj}}+\frac{1}{2N_c}\lambda^2_{(V-A)_\perp^{\rm adj}}\\
&-\frac{1}{2N_c}\lambda^2_{(V+A)_\parallel^{\rm adj}}-\frac{2}{N_c}\lambda_{(V-A)_\parallel}\lambda_{(V-A)_\perp^{\rm adj}}+\frac{1}{N_c}\lambda_{(V-A)_\perp}\lambda_{(V-A)_\perp^{\rm adj}}\\
&-\frac{1}{4N_c^2}\lambda^2_{(V-A)_\perp^{\rm adj}}\Big)l^{(\rm F)}_{\perp}(\tau,0,0)\\
&+64v_4\Big(\frac{1}{2}\lambda^2_{(\sigma\text{-}\pi)}+2\lambda_{(S+P)_-}\lambda_{(\sigma\text{-}\pi)}+\lambda_{(S+P)_-^{\rm adj}}\lambda_{(\sigma\text{-}\pi)}-\frac{1}{N_c}\lambda_{(S+P)_-^{\rm adj}}\lambda_{(\sigma\text{-}\pi)}+2\lambda^2_{(S+P)_-}\\
&+\frac{1}{2}\lambda^2_{(S+P)_-^{\rm adj}}-\lambda^2_{(V-A)_\perp}-\frac{1}{4}\lambda^2_{(V-A)_\perp^{\rm adj}}+2\lambda_{(S+P)_-}\lambda_{(S+P)_-^{\rm adj}}-\lambda_{(V-A)_\parallel}\lambda_{(V-A)_\perp}\\
&-\frac{1}{2}\lambda_{(V-A)_\parallel}\lambda_{(V-A)_\perp^{\rm adj}}-\lambda_{(V-A)_\perp}\lambda_{(V-A)_\perp^{\rm adj}}-\frac{1}{N_c}\lambda^2_{(S+P)_-^{\rm adj}}+\frac{1}{2N_c}\lambda^2_{(V-A)_\perp^{\rm adj}}\\
&-\frac{2}{N_c}\lambda_{(S+P)_-}\lambda_{(S+P)_-^{\rm adj}}+\frac{1}{2N_c}\lambda_{(V-A)_\parallel}\lambda_{(V-A)_\perp^{\rm adj}}+\frac{1}{N_c}\lambda_{(V-A)_\perp}\lambda_{(V-A)_\perp^{\rm adj}}+\frac{1}{2N_c^2}\lambda^2_{(S+P)_-^{\rm adj}}\\
&-\frac{1}{4N_c^2}\lambda^2_{(V-A)_\perp^{\rm adj}}\Big)l^{(\rm F)}_{\perp}(\tau,0,0)\,,
\end{aligned}
$$

$$
\begin{aligned}
\partial_t\lambda_{(V-A)_\perp} \;=\;& 2\lambda_{(V-A)_\perp}+64v_4\Big(\frac{N_c}{2}\lambda^2_{\rm csc}+\frac{1}{N_c}\lambda^2_{\rm csc}-\frac{3}{2}\lambda^2_{\rm csc}+\lambda_{(V-A)_\perp}\lambda_{\rm csc}-\frac{3}{2}\lambda_{(V-A)_\perp^{\rm adj}}\lambda_{\rm csc}\\
&-N_c\lambda_{(V-A)_\perp}\lambda_{\rm csc}+\frac{N_c}{2}\lambda_{(V-A)_\perp^{\rm adj}}\lambda_{\rm csc}+\frac{1}{N_c}\lambda_{(V-A)_\perp^{\rm adj}}\lambda_{\rm csc}-\frac{1}{2}\lambda^2_{(\sigma\text{-}\pi)}-\frac{5}{8}\lambda^2_{(V-A)_\perp^{\rm adj}}\\
&-\frac{1}{2}\lambda^2_{(V+A)_\parallel^{\rm adj}}+2\lambda_{(V-A)_\parallel}\lambda_{(V-A)_\perp}+\frac{3}{2}\lambda_{(V-A)_\perp}\lambda_{(V-A)_\perp^{\rm adj}}+\lambda_{(\sigma\text{-}\pi)}\lambda_{(V+A)_\parallel^{\rm adj}}\\
&-2\lambda_{(\sigma\text{-}\pi)}\lambda_{(V+A)_\perp}+2N_c\lambda^2_{(V-A)_\perp}+\frac{3}{8}N_c\lambda^2_{(V-A)_\perp^{\rm adj}}+2N_c\lambda^2_{(V+A)_\perp}\\
&+\frac{N_c}{2}\lambda_{(V-A)_\perp}\lambda_{(V-A)_\perp^{\rm adj}}+\frac{1}{N_c}\lambda^2_{(\sigma\text{-}\pi)}-\frac{3}{4N_c}\lambda^2_{(V-A)_\perp^{\rm adj}}+\frac{1}{2N_c}\lambda^2_{(V+A)_\parallel^{\rm adj}}
\end{aligned}
$$

$$
\begin{aligned}
&-\frac{2}{N_c}\lambda_{(V-A)_\perp}\lambda_{(V-A)^{\rm adj}_\perp}-\frac{1}{N_c}\lambda_{(\sigma\text{-}\pi)}\lambda_{(V+A)^{\rm adj}_\parallel}+\frac{1}{N_c^2}\lambda^2_{(V-A)^{\rm adj}_\perp}\Big)l^{(\rm F)}_\parallel(\tau,0,0)\\
&+64v_4\Big(\frac{1}{N_c}\lambda^2_{(\sigma\text{-}\pi)}-\frac{1}{2}\lambda^2_{(\sigma\text{-}\pi)}-2\lambda_{(S+P)_-}\lambda_{(\sigma\text{-}\pi)}-\lambda_{(S+P)^{\rm adj}_-}\lambda_{(\sigma\text{-}\pi)}\\
&+\frac{4}{N_c}\lambda_{(S+P)_-}\lambda_{(\sigma\text{-}\pi)}\\
&+\frac{3}{N_c}\lambda_{(S+P)^{\rm adj}_-}\lambda_{(\sigma\text{-}\pi)}-\frac{2}{N_c^2}\lambda_{(S+P)^{\rm adj}_-}\lambda_{(\sigma\text{-}\pi)}-2\lambda^2_{(S+P)_-}-\frac{1}{2}\lambda^2_{(S+P)^{\rm adj}_-}\\
&-\lambda^2_{(V-A)_\perp}-\frac{1}{4}\lambda^2_{(V-A)^{\rm adj}_\perp}-2\lambda_{(S+P)_-}\lambda_{(S+P)^{\rm adj}_-}-\lambda_{(V-A)_\parallel}\lambda_{(V-A)_\perp}\\
&-\frac{3}{2}\lambda_{(V-A)_\perp}\lambda_{(V-A)^{\rm adj}_\perp}+\frac{4}{N_c}\lambda^2_{(S+P)_-}+\frac{2}{N_c}\lambda^2_{(S+P)^{\rm adj}_-}+\frac{3}{4N_c}\lambda^2_{(V-A)^{\rm adj}_\perp}\\
&+\frac{6}{N_c}\lambda_{(S+P)_-}\lambda_{(S+P)^{\rm adj}_-}+\frac{3}{2N_c}\lambda_{(V-A)_\perp}\lambda_{(V-A)^{\rm adj}_\perp}-\frac{5}{2N_c^2}\lambda^2_{(S+P)^{\rm adj}_-}\\
&-\frac{1}{2N_c^2}\lambda^2_{(V-A)^{\rm adj}_\perp}-\frac{4}{N_c^2}\lambda_{(S+P)_-}\lambda_{(S+P)^{\rm adj}_-}+\frac{1}{N_c^3}\lambda^2_{(S+P)^{\rm adj}_-}\Big)l^{(\rm F)}_\parallel(\tau,0,0)\\
&+64v_4\Big(-\frac{1}{3N_c}\lambda^2_{\rm csc}+\frac{1}{3}\lambda^2_{\rm csc}+\frac{1}{3}\lambda_{(V-A)_\perp}\lambda_{\rm csc}+\lambda_{(V-A)^{\rm adj}_\perp}\lambda_{\rm csc}-\frac{N_c}{3}\lambda_{(V-A)_\perp}\lambda_{\rm csc}\\
&-\frac{N_c}{3}\lambda_{(V-A)^{\rm adj}_\perp}\lambda_{\rm csc}-\frac{2}{3N_c}\lambda_{(V-A)^{\rm adj}_\perp}\lambda_{\rm csc}+\frac{1}{2}\lambda^2_{(\sigma\text{-}\pi)}+\frac{1}{6}\lambda^2_{(V-A)_\parallel}+\frac{3}{2}\lambda^2_{(V-A)_\perp}\\
&+\frac{13}{24}\lambda^2_{(V-A)^{\rm adj}_\perp}+\frac{1}{2}\lambda^2_{(V+A)^{\rm adj}_\parallel}-\frac{1}{3}\lambda_{(V-A)_\parallel}\lambda_{(V-A)_\perp}+\frac{1}{2}\lambda_{(V-A)_\parallel}\lambda_{(V-A)^{\rm adj}_\perp}\\
&-\lambda_{(V-A)_\perp}\lambda_{(V-A)^{\rm adj}_\perp}-\lambda_{(\sigma\text{-}\pi)}\lambda_{(V+A)^{\rm adj}_\parallel}-\frac{2}{3}\lambda_{(\sigma\text{-}\pi)}\lambda_{(V+A)_\perp}+\frac{2}{3}N_c\lambda^2_{(V-A)_\perp}\\
&-\frac{N_c}{4}\lambda^2_{(V-A)^{\rm adj}_\perp}+\frac{2}{3}N_c\lambda^2_{(V+A)_\perp}+\frac{N_c}{6}\lambda_{(V-A)_\perp}\lambda_{(V-A)^{\rm adj}_\perp}\\
&-\frac{1}{3N_c}\lambda^2_{(\sigma\text{-}\pi)}+\frac{1}{2N_c}\lambda^2_{(V-A)^{\rm adj}_\perp}-\frac{1}{2N_c}\lambda^2_{(V+A)^{\rm adj}_\parallel}-\frac{1}{2N_c}\lambda_{(V-A)_\parallel}\lambda_{(V-A)^{\rm adj}_\perp}\\
&+\frac{5}{6N_c}\lambda_{(V-A)_\perp}\lambda_{(V-A)^{\rm adj}_\perp}+\frac{1}{N_c}\lambda_{(\sigma\text{-}\pi)}\lambda_{(V+A)^{\rm adj}_\parallel}-\frac{19}{24N_c^2}\lambda^2_{(V-A)^{\rm adj}_\perp}\Big)l^{(\rm F)}_\perp(\tau,0,0)\\
&+64v_4\Big(-\frac{1}{3N_c}\lambda^2_{(\sigma\text{-}\pi)}+\frac{1}{6}\lambda^2_{(\sigma\text{-}\pi)}+\frac{2}{3}\lambda_{(S+P)_-}\lambda_{(\sigma\text{-}\pi)}+\frac{1}{3}\lambda_{(S+P)^{\rm adj}_-}\lambda_{(\sigma\text{-}\pi)}\\
&-\frac{4}{3N_c}\lambda_{(S+P)_-}\lambda_{(\sigma\text{-}\pi)}-\frac{1}{N_c}\lambda_{(S+P)^{\rm adj}_-}\lambda_{(\sigma\text{-}\pi)}+\frac{2}{3N_c^2}\lambda_{(S+P)^{\rm adj}_-}\lambda_{(\sigma\text{-}\pi)}\\
&+\frac{2}{3}\lambda^2_{(S+P)_-}+\frac{1}{6}\lambda^2_{(S+P)^{\rm adj}_-}-\frac{1}{6}\lambda^2_{(V-A)_\parallel}-\frac{7}{6}\lambda^2_{(V-A)_\perp}-\frac{7}{24}\lambda^2_{(V-A)^{\rm adj}_\perp}
\end{aligned}
$$

$$
\begin{aligned}
&+\frac{2}{3}\lambda_{(S+P)_-}\lambda_{(S+P)_-^{\rm adj}}-\frac{2}{3}\lambda_{(V-A)_\parallel}\lambda_{(V-A)_\perp}-\frac{1}{2}\lambda_{(V-A)_\parallel}\lambda_{(V-A)_\perp^{\rm adj}}\\
&-\lambda_{(V-A)_\perp}\lambda_{(V-A)_\perp^{\rm adj}}-\frac{4}{3N_c}\lambda^2_{(S+P)_-}-\frac{2}{3N_c}\lambda^2_{(S+P)_-^{\rm adj}}+\frac{1}{2N_c}\lambda^2_{(V-A)_\perp^{\rm adj}}\\
&-\frac{2}{N_c}\lambda_{(S+P)_-}\lambda_{(S+P)_-^{\rm adj}}+\frac{1}{2N_c}\lambda_{(V-A)_\parallel}\lambda_{(V-A)_\perp^{\rm adj}}+\frac{1}{N_c}\lambda_{(V-A)_\perp}\lambda_{(V-A)_\perp^{\rm adj}}\\
&+\frac{5}{6N_c^2}\lambda^2_{(S+P)_-^{\rm adj}}-\frac{5}{24N_c^2}\lambda^2_{(V-A)_\perp^{\rm adj}}+\frac{4}{3N_c^2}\lambda_{(S+P)_-}\lambda_{(S+P)_-^{\rm adj}}\\
&-\frac{1}{3N_c^3}\lambda^2_{(S+P)_-^{\rm adj}}\Big)l_\perp^{(\rm F)}(\tau,0,0)\,,
\end{aligned}
$$

$$
\begin{aligned}
\partial_t\lambda_{(V+A)_\parallel^{\rm adj}} \;=\;& 2\lambda_{(V+A)_\parallel^{\rm adj}}+64v_4\Big(2N_c\lambda_{\rm csc}\lambda_{(S+P)_-^{\rm adj}}-\frac{2}{N_c}\lambda_{\rm csc}\lambda_{(S+P)_-^{\rm adj}}+N_c\lambda^2_{\rm csc}-\frac{2}{N_c}\lambda_{(\sigma\text{-}\pi)}\lambda_{(V-A)_\perp^{\rm adj}}\\
&+N_c\lambda^2_{(S+P)_-^{\rm adj}}-\frac{2}{N_c}\lambda^2_{(S+P)_-^{\rm adj}}+\frac{3}{2N_c}\lambda_{(V-A)_\perp^{\rm adj}}\lambda_{(V+A)_\parallel^{\rm adj}}+\frac{N_c}{4}\lambda^2_{(V+A)_\parallel^{\rm adj}}-\frac{1}{2N_c}\lambda^2_{(V+A)_\parallel^{\rm adj}}\\
&+4\lambda_{\rm csc}\lambda_{(\sigma\text{-}\pi)}+4\lambda_{\rm csc}\lambda_{(S+P)_-}-2\lambda_{\rm csc}\lambda_{(S+P)_-^{\rm adj}}-\lambda_{\rm csc}\lambda_{(V+A)_\parallel^{\rm adj}}-2\lambda^2_{\rm csc}+2\lambda_{(\sigma\text{-}\pi)}\lambda_{(S+P)_-^{\rm adj}}\\
&+4\lambda_{(\sigma\text{-}\pi)}\lambda_{(V-A)_\perp}+2\lambda_{(\sigma\text{-}\pi)}\lambda_{(V-A)_\perp^{\rm adj}}+4\lambda_{(S+P)_-}\lambda_{(S+P)_-^{\rm adj}}+\lambda_{(V-A)_\parallel}\lambda_{(V+A)_\parallel^{\rm adj}}\\
&-3\lambda_{(V-A)_\perp}\lambda_{(V+A)_\parallel^{\rm adj}}+\lambda_{(V+A)_\parallel}\lambda_{(V+A)_\parallel^{\rm adj}}-\lambda_{(V+A)_\parallel^{\rm adj}}\lambda_{(V+A)_\perp}\Big)l_\parallel^{(\rm F)}(\tau,0,0)\\
&+64v_4\Big(\frac{1}{2N_c}\lambda^2_{(V+A)_\parallel^{\rm adj}}+4\lambda_{(\sigma\text{-}\pi)}\lambda_{(V+A)_\perp}-\lambda_{(V+A)_\parallel}\lambda_{(V+A)_\parallel^{\rm adj}}+\lambda_{(V+A)_\parallel^{\rm adj}}\lambda_{(V+A)_\perp}\Big)l_\parallel^{(\rm F)}(\tau,0,0)\\
&+64v_4\Big(-\frac{2}{3}N_c\lambda_{\rm csc}\lambda_{(S+P)_-^{\rm adj}}+\frac{2}{3N_c}\lambda_{\rm csc}\lambda_{(S+P)_-^{\rm adj}}-\frac{N_c}{3}\lambda^2_{\rm csc}+\frac{4}{3N_c}\lambda_{(\sigma\text{-}\pi)}\lambda_{(V-A)_\perp^{\rm adj}}\\
&-\frac{N_c}{3}\lambda^2_{(S+P)_-^{\rm adj}}+\frac{2}{3N_c}\lambda^2_{(S+P)_-^{\rm adj}}-\frac{3}{2N_c}\lambda_{(V-A)_\perp^{\rm adj}}\lambda_{(V+A)_\parallel^{\rm adj}}-\frac{N_c}{12}\lambda^2_{(V+A)_\parallel^{\rm adj}}+\frac{1}{6N_c}\lambda^2_{(V+A)_\parallel^{\rm adj}}\\
&-\frac{4}{3}\lambda_{\rm csc}\lambda_{(\sigma\text{-}\pi)}-\frac{4}{3}\lambda_{\rm csc}\lambda_{(S+P)_-}+\frac{2}{3}\lambda_{\rm csc}\lambda_{(S+P)_-^{\rm adj}}+\lambda_{\rm csc}\lambda_{(V+A)_\parallel^{\rm adj}}+\frac{2}{3}\lambda^2_{\rm csc}-\frac{2}{3}\lambda_{(\sigma\text{-}\pi)}\lambda_{(S+P)_-^{\rm adj}}\\
&+\frac{4}{3}\lambda_{(\sigma\text{-}\pi)}\lambda_{(V-A)_\parallel}-\frac{8}{3}\lambda_{(\sigma\text{-}\pi)}\lambda_{(V-A)_\perp}+\frac{2}{3}\lambda_{(\sigma\text{-}\pi)}\lambda_{(V-A)_\perp^{\rm adj}}-\frac{4}{3}\lambda_{(S+P)_-}\lambda_{(S+P)_-^{\rm adj}}\\
&-\lambda_{(V-A)_\parallel}\lambda_{(V+A)_\parallel^{\rm adj}}+3\lambda_{(V-A)_\perp}\lambda_{(V+A)_\parallel^{\rm adj}}-\frac{1}{3}\lambda_{(V+A)_\parallel}\lambda_{(V+A)_\parallel^{\rm adj}}\\
&+\frac{1}{3}\lambda_{(V+A)_\parallel^{\rm adj}}\lambda_{(V+A)_\perp}\Big)l_\perp^{(\rm F)}(\tau,0,0)\\
&+64v_4\Big(-\frac{2}{3N_c}\lambda_{(\sigma\text{-}\pi)}\lambda_{(V+A)_\parallel^{\rm adj}}-\frac{1}{6N_c}\lambda^2_{(V+A)_\parallel^{\rm adj}}+\frac{4}{3}\lambda_{(\sigma\text{-}\pi)}\lambda_{(V+A)_\parallel}-\frac{8}{3}\lambda_{(\sigma\text{-}\pi)}\lambda_{(V+A)_\perp}\\
&+\frac{1}{3}\lambda_{(V+A)_\parallel}\lambda_{(V+A)_\parallel^{\rm adj}}-\frac{5}{3}\lambda_{(V+A)_\parallel^{\rm adj}}\lambda_{(V+A)_\perp}\Big)l_\perp^{(\rm F)}(\tau,0,0)\,,
\end{aligned}
$$

$$
\begin{aligned}
\partial_t \lambda_{(V-A)_\perp^{\rm adj}} \;=\;& 2\lambda_{(V-A)_\perp^{\rm adj}} + 64 v_4 \Big(-2N_c \lambda_{\rm csc} \lambda_{(V-A)_\perp^{\rm adj}} - N_c \lambda_{\rm csc}^2 - \frac{5}{4} N_c \lambda_{(V-A)_\perp^{\rm adj}}^2 \\
& + \frac{2}{N_c} \lambda_{(V-A)_\perp^{\rm adj}}^2 + 3\lambda_{\rm csc} \lambda_{(V-A)_\perp^{\rm adj}} + 2\lambda_{\rm csc}^2 - 2\lambda_{(\sigma\text{-}\pi)} \lambda_{(V+A)_\parallel^{\rm adj}} + 2\lambda_{(\sigma\text{-}\pi)}^2 \\
& + 2\lambda_{(V-A)_\parallel} \lambda_{(V-A)_\perp^{\rm adj}} - 4\lambda_{(V-A)_\perp} \lambda_{(V-A)_\perp^{\rm adj}} + \lambda_{(V-A)_\perp^{\rm adj}}^2 + \lambda_{(V+A)_\parallel^{\rm adj}}^2 \Big) l_\parallel^{(\rm F)}(\tau,0,0) \\
& + 64 v_4 \Big(-\frac{4}{N_c} \lambda_{(\sigma\text{-}\pi)} \lambda_{(S+P)_-^{\rm adj}} - \frac{8}{N_c} \lambda_{(S+P)_-} \lambda_{(S+P)_-^{\rm adj}} - \frac{4}{N_c} \lambda_{(S+P)_-^{\rm adj}}^2 \\
& + \frac{2}{N_c^2} \lambda_{(S+P)_-^{\rm adj}}^2 - \frac{1}{2N_c} \lambda_{(V-A)_\perp^{\rm adj}}^2 + 8\lambda_{(\sigma\text{-}\pi)} \lambda_{(S+P)_-} + 4\lambda_{(\sigma\text{-}\pi)} \lambda_{(S+P)_-^{\rm adj}} \\
& + 2\lambda_{(\sigma\text{-}\pi)}^2 + 8\lambda_{(S+P)_-} \lambda_{(S+P)_-^{\rm adj}} + 8\lambda_{(S+P)_-}^2 + 2\lambda_{(S+P)_-^{\rm adj}}^2 - \lambda_{(V-A)_\parallel} \lambda_{(V-A)_\perp^{\rm adj}} \\
& + \lambda_{(V-A)_\perp} \lambda_{(V-A)_\perp^{\rm adj}} \Big) l_\parallel^{(\rm F)}(\tau,0,0) \\
& + 64 v_4 \Big(\frac{4}{3} N_c \lambda_{\rm csc} \lambda_{(V-A)_\perp^{\rm adj}} + \frac{N_c}{3} \lambda_{\rm csc}^2 + \frac{13}{12} N_c \lambda_{(V-A)_\perp^{\rm adj}}^2 - \frac{7}{3N_c} \lambda_{(V-A)_\perp^{\rm adj}}^2 \\
& - \lambda_{\rm csc} \lambda_{(V-A)_\perp^{\rm adj}} - \frac{2}{3} \lambda_{\rm csc}^2 + 2\lambda_{(\sigma\text{-}\pi)} \lambda_{(V+A)_\parallel^{\rm adj}} - \frac{2}{3} \lambda_{(\sigma\text{-}\pi)}^2 \\
& - \frac{4}{3} \lambda_{(V-A)_\parallel} \lambda_{(V-A)_\perp^{\rm adj}} + \frac{14}{3} \lambda_{(V-A)_\perp} \lambda_{(V-A)_\perp^{\rm adj}} + \frac{1}{3} \lambda_{(V-A)_\perp^{\rm adj}}^2 \\
& - \lambda_{(V+A)_\parallel^{\rm adj}}^2 \Big) l_\perp^{(\rm F)}(\tau,0,0) \\
& + 64 v_4 \Big(\frac{4}{3N_c} \lambda_{(\sigma\text{-}\pi)} \lambda_{(S+P)_-^{\rm adj}} + \frac{8}{3N_c} \lambda_{(S+P)_-} \lambda_{(S+P)_-^{\rm adj}} + \frac{4}{3N_c} \lambda_{(S+P)_-^{\rm adj}}^2 \\
& - \frac{2}{3N_c^2} \lambda_{(S+P)_-^{\rm adj}}^2 + \frac{1}{6N_c} \lambda_{(V-A)_\perp^{\rm adj}}^2 - \frac{8}{3} \lambda_{(\sigma\text{-}\pi)} \lambda_{(S+P)_-} - \frac{4}{3} \lambda_{(\sigma\text{-}\pi)} \lambda_{(S+P)_-^{\rm adj}} \\
& - \frac{2}{3} \lambda_{(\sigma\text{-}\pi)}^2 - \frac{8}{3} \lambda_{(S+P)_-} \lambda_{(S+P)_-^{\rm adj}} - \frac{8}{3} \lambda_{(S+P)_-}^2 - \frac{2}{3} \lambda_{(S+P)_-^{\rm adj}}^2 \\
& + \frac{1}{3} \lambda_{(V-A)_\parallel} \lambda_{(V-A)_\perp^{\rm adj}} - \frac{1}{3} \lambda_{(V-A)_\perp} \lambda_{(V-A)_\perp^{\rm adj}} \Big) l_\perp^{(\rm F)}(\tau,0,0) \,.
\end{aligned}
$$

D. Threshold functions

In Chapter 3 the following flow equation was derived for the mass parameter within a simple truncation of the ϕ^4-theory

$$\partial_t m_k^2 = -\frac{\lambda_k}{2} \int \frac{d^4p}{(2\pi)^4} \frac{\partial_t R_k(p)}{\left(p^2 + m_k^2 + R_k(p)\right)^2} \tag{3.28}$$

The regulator can still be chosen. One can introduce threshold functions that absorb the regulator dependence and the integral, leading to simpler expressions for the flow equations such as the one above. Depending on the chosen regulator the involved integrations can either be carried out analytically yielding exact expressions for them, and if not one can at least evaluate them numerically and tabulate the values. When solving a set of flow equations for a given truncation the performance is improved when the solver does not have to perform the momentum integration involving the regulator at each RG step.

D.1. Threshold functions for the Litim regulator

Here we show the threshold functions that appear in the flow equations of Chapter 4. This section is based on the Appendix N of [48].

For the eQCD code the 3d Litim regulator was chosen. The fermionic, mesonic and gluonic regulators read

$$R_k^q(q_0, \boldsymbol{q}) = Z_{q,k} i\boldsymbol{\gamma} \cdot \boldsymbol{q}\, r_F(\boldsymbol{q}^2/k^2) \tag{D.1}$$

$$R_k^\phi(q_0, \boldsymbol{q}) = Z_{\phi,k} \boldsymbol{q}^2 r_B(\boldsymbol{q}^2/k^2) \tag{D.2}$$

$$(R_k^A)_{\mu\nu}(q_0, \boldsymbol{q}) = Z_{A,k} \boldsymbol{q}^2 r_B(\boldsymbol{q}^2/k^2)\Big(\delta_{\mu\nu} - \frac{q_\mu q_\nu}{q^2}\Big) + \frac{\boldsymbol{q}^2}{\xi} r_B(\boldsymbol{q}^2/k^2)\Big(\frac{q_\mu q_\nu}{q^2}\Big) \tag{D.3}$$

with the regulator shape functions

$$r_F(x) = \Big(\frac{1}{\sqrt{x}} - 1\Big)\Theta(1-x) \tag{D.4}$$

$$r_B(x) = \Big(\frac{1}{x} - 1\Big)\Theta(1-x) \tag{D.5}$$

and where the Landau gauge $\xi = 0$ is chosen.

The involvement of the Heaviside step function in expressions such as Eq. (3.28) lead to a simple expression of the integral and the momentum integration can be carried out. The Matsubara sum still remains, and the resulting expressions still contain sums of the bosonic and fermionic propagators

$$G_b(q, m^2) = \frac{1}{\tilde{q}_0^2 + 1 + m^2} \qquad \text{with} \qquad q_0 = 2n\pi T, n \in \mathbb{Z} \tag{D.6}$$

$$G_f(q, m^2) = \frac{1}{\tilde{q}_0^2 + 1 + m^2} \qquad \text{with} \qquad q_0 = (2n+1)\pi T, n \in \mathbb{Z} \tag{D.7}$$

with $\tilde{q}_0 = q_0/k$.

The following functions are defined

$$\mathcal{F}_{(n)}(m^2; T) = \frac{T}{k} \sum_{n_q} \Big(G_f(q, m^2)\Big)^n \tag{D.8}$$

$$\mathcal{B}_{(n)}(m^2; T) = \frac{T}{k} \sum_{n_q} \Big(G_b(q, m^2)\Big)^n . \tag{D.9}$$

which fulfill the recursion relations

$$\mathcal{F}_{(n+1)}(m^2; T) = -\frac{1}{n} \frac{\partial}{\partial m^2} \mathcal{F}_{(n)}(m^2; T) \tag{D.10}$$

$$\mathcal{B}_{(n+1)}(m^2; T) = -\frac{1}{n} \frac{\partial}{\partial m^2} \mathcal{B}_{(n)}(m^2; T) \tag{D.11}$$

Evaluation of the sum for the case $n = 1$ gives

$$\begin{aligned} \mathcal{F}_{(1)}(m^2; T) &= \frac{1}{\sqrt{1+m^2}} \Big(\frac{1}{2} - n_F(m^2; T)\Big) \\ \mathcal{B}_{(1)}(m^2; T) &= \frac{1}{\sqrt{1+m^2}} \Big(\frac{1}{2} + n_B(m^2; T)\Big) \end{aligned} \tag{D.12}$$

with the distribution functions

$$n_F(m^2; T) = \frac{1}{\exp\Big\{\frac{k}{T}\Big(1+m^2\Big)^{1/2}\Big\} + 1} . \tag{D.13}$$

$$n_B(m^2;T) = \frac{1}{\exp\left\{\frac{k}{T}\left(1+m^2\right)^{1/2}\right\}-1}\,. \tag{D.14}$$

where the fermionic distribution function will get modified according to Eq. (4.10) when a non-trivial Polyakov loop expectation value is present.

In terms of these newly defined functions, we can now give expressions for the threshold functions appearing in e.g. Eq. (4.11)

$$l_0^{(B,d)}(m^2,\eta;T) = \frac{2}{d-1}\Big(1-\frac{\eta}{d+1}\Big)\mathcal{B}_{(1)}(m^2;T) \tag{D.15}$$

$$l_0^{(F,d)}(m^2,\eta;T) = \frac{2}{d-1}\Big(1-\frac{\eta}{d}\Big)\mathcal{F}_{(1)}(m^2;T)\,. \tag{D.16}$$

Similarly, we have the functions describing mixed loops

$$\mathcal{BB}_{(n_1,n_2)}(m_1^2,m_2^2;T) = \frac{T}{k}\sum_{n_q}\Big(G_b(q,m_1^2)\Big)^{n_1}\Big(G_b(q,m_2^2)\Big)^{n_2} \tag{D.17}$$

$$\mathcal{FB}_{(n_f,n_b)}(m_f^2,m_b^2;T,p_0) = \frac{T}{k}\sum_{n_q}\Big(G_f(q,m_f^2)\Big)^{n_f}\Big(G_b(q-p,m_b^2)\Big)^{n_b} \tag{D.18}$$

$$\mathcal{FBB}_{(n_f,n_{b1},n_{b2})}(m_f^2,m_{b1}^2,m_{b2}^2) = \frac{T}{k}\sum_{n_q}\Big(G_f(q,m_f^2)\Big)^{n_f}\Big(G_b(q-p,m_{b1}^2)\Big)^{n_{b1}}\Big(G_b(q-p,m_{b2}^2)\Big)^{n_{b2}} \tag{D.19}$$

$$\mathcal{FF}_{(n_{f_1},n_{f_2})}(m_{f_1}^2,m_{f_2}^2;T,p_0,\boldsymbol{p}) = \frac{T}{k}\sum_{n_q}\Big(G_f(q,m_{f_1}^2)\Big)^{n_f}\Big(G'_f(q-p,m_{f_2}^2)\Big)^{n_b} \tag{D.20}$$

where for some the external momentum was not set to zero, as required for e.g. the anomalous dimension.

For the expression of the flow of the Yukawa coupling Eq. (4.49) additionally the function

$$L^{(d)}_{(1,1)}(m_f^2,m_b^2,\eta_f,\eta_b;T,p_0) = \tag{D.21}$$

$$\frac{2}{d-1}\left[\Big(1-\frac{\eta_b}{d+1}\Big)\mathcal{FB}_{(1,2)}(m_f^2,m_b^2;T,p_0)+\Big(1-\frac{\eta_f}{d}\Big)\mathcal{FB}_{(2,1)}(m_f^2,m_b^2;T,p_0)\right] \tag{D.22}$$

is needed.

D.2. Threshold functions for the exponential regulator

For the threshold functions required in Appendix C, used to calculate the results of Chapter 5, the exponential regulator is used instead. The details are laid out in Appendix C of [80] and Appendix A of [73] and repeated here for the special case of $\mu = 0$.

The regulator reads

$$R_k^{\psi} = -\not{p}\, r_\psi \tag{D.23}$$

with the regulator shape function

$$r_\psi = \frac{1}{\sqrt{1 - e^{-\bar{\omega}^2}}} - 1 \tag{D.24}$$

where $\bar{\omega} = \omega/k$ and $\omega^2 = p_0^2 + \boldsymbol{p}^2$.

With the propagator

$$\tilde{G}_\psi(y_0, y, \omega) = \frac{1}{(y_0 + y)(1 + r_\psi)^2 + \omega} \tag{D.25}$$

and the Matsubara frequencies $\tilde{\nu}_n = (2n + 1)\pi\tau$ for the dimensionless temperature $\tau = T/k$, the threshold functions read

$$l_{\parallel}^{(\mathrm{F})}(\tau, \omega, 0) = -\frac{\tau}{2} \sum_{n=-\infty}^{+\infty} \int_0^\infty dy\, y^{\frac{1}{2}} \tilde{\partial}_t \left[\tilde{\nu_n}^2 (1 + r_\psi)^2 \left(\tilde{G}_\psi(\tilde{\nu_n}^2, y, \omega) \right)^2 \right] \tag{D.26}$$

$$l_{\perp}^{(\mathrm{F})}(\tau, \omega, 0) = -\frac{\tau}{2} \sum_{n=-\infty}^{+\infty} \int_0^\infty \mathrm{d}y\, y^{\frac{1}{2}} \tilde{\partial}_t \left[\left(y(1 + r_\psi)^2 + \omega \right) \left(\tilde{G}_\psi(\tilde{\nu_n}^2, y, \omega) \right)^2 \right] \tag{D.27}$$

with the formal derivative

$$\tilde{\partial}_t = (\partial_t r_\psi) \frac{\partial}{\partial r_\psi} = \frac{(y_0 + y)\mathrm{e}^{-(y_0+y)}}{(1 - \mathrm{e}^{-(y_0+y)})^{\frac{3}{2}}} \frac{\partial}{\partial r_\psi}. \tag{D.28}$$

Bibliography

[1] R. D. Pisarski and F. Wilczek, *Remarks on the chiral phase transition in chromodynamics*, Physical Review D **29**, 338 (1984).

[2] M. Gell-Mann, *A schematic model of baryons and mesons*, Physics Letters **8**, 214 (1964).

[3] D. J. Gross and F. Wilczek, *Ultraviolet Behavior of Non-Abelian Gauge Theories*, Physical Review Letters **30**, 1343 (1973).

[4] D. J. Griffiths, *Introduction to Elementary Particles* (Wiley, 2004).

[5] D. Rosenblüh, *Transport Coefficients in Yang-Mills Theory*, unpublished, Masters Thesis (University of Heidelberg, 2017).

[6] N. Glendenning, *Compact Stars: Nuclear Physics, Particle Physics and General Relativity*, 2nd (Springer, 2000).

[7] M. E. Peskin and D. V. Schroeder, *An Introduction to Quantum Field Theory* (Westview Press, 1995).

[8] T. Matsubara, *A New Approach to Quantum-Statistical Mechanics*, Progress of Theoretical Physics **14**, 351 (1955).

[9] M. Laine and A. Vuorinen, *Basics of Thermal Field Theory: A Tutorial on Perturbative Computations* (Springer International Publishing, 2016).

[10] A. Das, *Finite Temperature Field Theory* (World Scientific, 1997).

[11] Y. Nambu, *Axial Vector Current Conservation in Weak Interactions*, Phys. Rev. Lett. **4**, 380 (1960).

[12] S. L. Adler, *Axial-Vector Vertex in Spinor Electrodynamics*, Phys. Rev. **177**, 2426 (1969).

[13] J. S. Bell and R. Jackiw, *A PCAC puzzle: $\pi^0 \to \gamma\gamma$ in the σ-model*, Nuovo Cimento A Serie **60**, 47 (1969).

[14] K. Fujikawa, *Path-Integral Measure for Gauge-Invariant Fermion Theories*, Physical Review Letters **42**, 1195 (1979).

[15] G. 't Hooft, *How instantons solve the U(1) problem*, Physics Reports **142**, 357 (1986).

[16] H. Forkel, *A Primer on Instantons in QCD*, 2002.

[17] D. Tong, *Gauge Theory*, Lecture notes, DAMTP Cambridge **10**, 8 (2018).

[18] A. Belavin, A. Polyakov, A. Schwartz, and Y. Tyupkin, *Pseudoparticle solutions of the Yang-Mills equations*, Physics Letters B **59**, 85 (1975).

[19] G. 't Hooft, *Symmetry Breaking through Bell-Jackiw Anomalies*, Phys. Rev. Lett. **37**, 8 (1976).

[20] N. Goldenfeld, *Lectures on Phase Transitions and the Renormalization Group* (CRC Press, 1992).

[21] L. Onsager, *Crystal Statistics. I. A Two-Dimensional Model with an Order-Disorder Transition*, Phys. Rev. **65**, 117 (1944).

[22] J. F. Melo, *Introduction to Renormalisation*, arXiv:1909.11099 [hep-th] (2019).

[23] A. C. D. van Enter, R. Fernández, and A. D. Sokal, *Regularity properties and pathologies of position-space renormalization-group transformations: Scope and limitations of Gibbsian theory*, Journal of Statistical Physics **72**, 879 (1993).

[24] C.-H. Chang, V. Dommes, R. S. Erramilli, A. Homrich, P. Kravchuk, A. Liu, M. S. Mitchell, D. Poland, and D. Simmons-Duffin, *Bootstrapping the 3d Ising Stress Tensor*, arXiv:2411.15300 [hep-th] (2024).

[25] D. J. Amit and V. Martin-Mayor, *Field Theory, the Renormalization Group, and Critical Phenomena*, 3rd (World Scientific, 2005).

[26] Y. Nambu and G. Jona-Lasinio, *Dynamical Model of Elementary Particles Based on an Analogy with Superconductivity. I*, Physical Review **122**, 345 (1961).

[27] Y. Nambu and G. Jona-Lasinio, *Dynamical Model of Elementary Particles Based on an Analogy with Superconductivity. II*, Physical Review **124**, 246 (1961).

[28] R. D. Pisarski and F. Rennecke, *Conjectures about the Chiral Phase Transition in QCD from Anomalous Multi-Instanton Interactions*, Physical Review Letters **132** (2024).

[29] R. D. Pisarski and D. L. Stein, *The renormalisation group and global G×G' theories about four dimensions*, Journal of Physics A: Mathematical and General **14**, 3341 (1981).

[30] J. Berges, N. Tetradis, and C. Wetterich, *Non-perturbative renormalization flow in quantum field theory and statistical physics*, Physics Reports **363**, 223 (2002).

[31] A. Sciarra, *The QCD phase diagram at purely imaginary chemical potential from the lattice*, PhD thesis (2016).

[32] R. Vértesi, T. Csörgő, and J. Sziklai, *Significant in-medium η' mass reduction in $\sqrt{s_{NN}} = 200$ GeV Au + Au collisions at the BNL Relativistic Heavy Ion Collider*, Physical Review C **83**, 054903 (2011).

[33] T. Csörgő, R. Vértesi, and J. Sziklai, *Indirect Observation of an In-Medium η' Mass Reduction in $\sqrt{s_{NN}} = 200$ GeV Au + Au Collisions*, Physical Review Letters **105**, 182301 (2010).

[34] S. P. Klevansky, *The Nambu—Jona-Lasinio model of quantum chromodynamics*, Rev. Mod. Phys. **64**, 649 (1992).

[35] T. Hatsuda and T. Kunihiro, *QCD phenomenology based on a chiral effective Lagrangian*, Physics Reports **247**, 221 (1994).

[36] R. Machleidt and D. R. Entem, *Chiral effective field theory and nuclear forces*, Physics Reports **503**, 1 (2011).

[37] D.-U. Jungnickel and C. Wetterich, *Effective action for the chiral quark-meson model*, Physical Review D **53**, 5142 (1996).

[38] J. Berges, D.-U. Jungnickel, and C. Wetterich, *Two flavor chiral phase transition from nonperturbative flow equations*, Physical Review D **59**, 034010 (1999).

[39] B.-J. Schaefer and J. Wambach, *The phase diagram of the quark–meson model*, Nuclear Physics A **757**, 479 (2005).

[40] C. Wetterich, *Exact evolution equation for the effective potential*, Physics Letters B **301**, 90 (1993).

[41] M. Shaposhnikov and C. Wetterich, *Asymptotic safety of gravity and the Higgs boson mass*, Phys. Lett. B **683**, 196 (2010).

[42] H. Gies, *Introduction to the functional RG and applications to gauge theories*, ECT* School: Renormalization Group and Effective Field Theory Approaches to Many-Body Systems (2006).

[43] I. Boettcher, J. M. Pawlowski, and S. Diehl, *Ultracold atoms and the Functional Renormalization Group*, Nuclear Physics B - Proceedings Supplements **228**, 63 (2012).

[44] D. F. Litim, *Optimized renormalization group flows*, Physical Review D **64**, 105007 (2001).

[45] H. Gies and C. Wetterich, *Renormalization flow of bound states*, Physical Review D **65**, 065001 (2002).

[46] J. Braun and B. Klein, *Scaling functions for the $O(4)$ model in $d = 3$ dimensions*, Phys. Rev. D **77**, 096008 (2008).

[47] J. Braun, B. Klein, and H. J. Pirner, *Volume dependence of the pion mass in the quark-meson model*, Phys. Rev. D **71**, 014032 (2005).

[48] W.-j. Fu, J. M. Pawlowski, and F. Rennecke, *QCD phase structure at finite temperature and density*, Physical Review D **101**, 054032 (2020).

[49] A. K. Cyrol, M. Mitter, J. M. Pawlowski, and N. Strodthoff, *Nonperturbative quark, gluon, and meson correlators of unquenched QCD*, Phys. Rev. D **97**, 054006 (2018).

[50] J. Braun, L. Fister, J. M. Pawlowski, and F. Rennecke, *From quarks and gluons to hadrons: Chiral symmetry breaking in dynamical QCD*, Phys. Rev. D **94**, 034016 (2016).

[51] W. H. Press, S. A. Teukolsky, W. T. Vetterling, and B. P. Flannery, *Numerical Recipes*, Third Edition (Cambridge University Press, 2007).

[52] H.-T. Ding, P. Hegde, O. Kaczmarek, F. Karsch, A. Lahiri, S.-T. Li, S. Mukherjee, H. Ohno, P. Petreczky, C. Schmidt, and P. Steinbrecher, *Chiral phase transition temperature in $(2+1)$-flavor QCD*, Physical Review Letters **123**, 062002 (2019).

[53] B. Widom, *Equation of State in the Neighborhood of the Critical Point*, The Journal of Chemical Physics **43**, 3898 (1965).

[54] R. Guida and J. Zinn-Justin, *Critical exponents of the N-vector model*, J. Phys. A **31**, 8103 (1998).

[55] K. Kanaya and S. Kaya, *Critical exponents of a three-dimensional $O(4)$ spin model*, Phys. Rev. D **51**, 2404 (1995).

[56] M. Hasenbusch, *Eliminating leading corrections to scaling in the three-dimensional $O(N)$ symmetric ϕ^4 model: $N = 3$ and $N = 4$*, J. Phys. A **34**, 8221 (2001).

[57] N. Tetradis and C. Wetterich, *Critical exponents from effective average action*, Nucl. Phys. B **422**, 541 (1994).

[58] A. Bonanno and D. Zappala, *Towards an accurate determination of the critical exponents with the renormalization group flow equations*, Phys. Lett. B **504**, 181 (2001).

[59] D. F. Litim and D. Zappala, *Ising exponents from the functional renormalisation group*, Phys. Rev. D **83**, 085009 (2011).

[60] I. Balog, H. Chaté, B. Delamotte, M. Marohnic, and N. Wschebor, *Convergence of Nonperturbative Approximations to the Renormalization Group*, Phys. Rev. Lett. **123**, 240604 (2019).

[61] J. Braun, W.-j. Fu, J. M. Pawlowski, F. Rennecke, D. Rosenblüh, and S. Yin, *Chiral susceptibility in $(2+1)$-flavor QCD*, Phys. Rev. D **102**, 056010 (2020).

[62] J. Braun, B. Klein, and P. Piasecki, *On the scaling behavior of the chiral phase transition in QCD in finite and infinite volume*, Eur. Phys. J. C **71**, 1576 (2011).

[63] J. Braun, B. Klein, H.-J. Pirner, and A. H. Rezaeian, *Volume and quark mass dependence of the chiral phase transition*, Phys. Rev. D **73**, 074010 (2006).

[64] J. Braun, M. Leonhardt, J. M. Pawlowski, and D. Rosenblüh, *Chiral and effective $U(1)_{\mathrm{A}}$ symmetry restoration in QCD*, arXiv:2012.06231 [hep-ph] (2020).

[65] M. Leonhardt, *Phase structure and equation of state of dense strong-interaction matter*, en, PhD thesis (Technische Universität, Darmstadt, 2019).

[66] J. Braun, M. Leonhardt, and M. Pospiech, *Fierz-complete NJL model study. III. emergence from quark-gluon dynamics*, Physical Review D **101**, 036004 (2020).

[67] H. Gies and C. Wetterich, *Universality of spontaneous chiral symmetry breaking in gauge theories*, Physical Review D **69**, 025001 (2004).

[68] J. Braun and H. Gies, *Running coupling at finite temperature and chiral symmetry restoration in QCD*, Physics Letters B **645**, 53 (2007).

[69] J. F. Nieves and P. B. Pal, *Generalized Fierz identities*, American Journal of Physics **72**, 1100 (2004).

[70] M. Q. Huber and J. Braun, *Algorithmic derivation of functional renormalization group equations and Dyson–Schwinger equations*, Computer Physics Communications **183**, 1290 (2012).

[71] M. Q. Huber, A. K. Cyrol, and J. M. Pawlowski, *DoFun 3.0: Functional equations in Mathematica*, Computer Physics Communications **248**, 107058 (2020).

[72] A. K. Cyrol, M. Mitter, and N. Strodthoff, *Formtracer. a mathematica tracing package using form*, Computer Physics Communications **219**, 346 (2017).

[73] J. Braun, M. Leonhardt, and M. Pospiech, *Fierz-complete NJL model study. II. Toward the fixed-point and phase structure of hot and dense two-flavor QCD*, Phys. Rev. D **97**, 076010 (2018).

[74] J. Braun and H. Gies, *Chiral phase boundary of QCD at finite temperature*, Journal of High Energy Physics, 024 (2006).

[75] H. Gies, J. Jaeckel, and C. Wetterich, *Towards a renormalizable standard model without a fundamental Higgs scalar*, Physical Review D **69**, 105008 (2004).

[76] J. M. Pawlowski, *Exact flow equations and the $U(1)$ problem*, Phys. Rev. D **58**, 045011 (1998).

[77] A. Koenigstein, M. J. Steil, N. Wink, E. Grossi, J. Braun, M. Buballa, and D. H. Rischke, *Numerical fluid dynamics for FRG flow equations: Zero-dimensional QFTs as numerical test cases. I. The $O(N)$ model*, Phys. Rev. D **106**, 065012 (2022).

[78] A. Koenigstein, M. J. Steil, N. Wink, E. Grossi, and J. Braun, *Numerical fluid dynamics for FRG flow equations: Zero-dimensional QFTs as numerical test cases. II. Entropy production and irreversibility of RG flows*, Phys. Rev. D **106**, 065013 (2022).

[79] M. J. Steil and A. Koenigstein, *Numerical fluid dynamics for FRG flow equations: Zero-dimensional QFTs as numerical test cases. III. Shock and rarefaction waves in RG flows reveal limitations of the $N \to \infty$ limit in $O(N)$-type models*, Phys. Rev. D **106**, 065014 (2022).

[80] J. Braun, M. Leonhardt, and M. Pospiech, *Fierz-complete NJL model study: Fixed points and phase structure at finite temperature and density*, Physical Review D **96**, 076003 (2017).